ALMA MATER STUDIORUM
UNIVERSITÀ DEGLI STUDI DI BOLOGNA
Facoltà di Scienze Matematiche Fisiche e Naturali

Dottorato di Ricerca in Geofisica
XXIII Ciclo

Settore scientifico disciplinare di afferenza: GEO/10

Structure of the Southern Tyrrhenian Subduction System: Insights from seismological analysis of anisotropy and attenuation

Ph.D. Thesis of:
Paola Baccheschi

Tutor:
Dr. ssa Lucia Margheriti

Supervisor:
Prof. Enzo Boschi

Coordinator:
Prof. Michele Dragoni

Academic Year 2010- 2011

To mommy and daddy,

and myself

CONTENTS

Abstract

The Southern Tyrrhenian subduction system shows a complex interaction among asthenospheric flow, subducting slab and overriding plate. To shed light on the deformations and mechanical properties of the slab and surrounding mantle, I investigated seismic anisotropy and attenuation properties through the subduction region. I used both teleseisms and slab earthquakes, analyzing shear-wave splitting on SKS and S phases, respectively. The fast polarization directions φ, and the delay time, δt, were retrieved using the method of Silver and Chan [1991. SKS and S φ reveal a complex anisotropy pattern across the subduction zone. SKS-rays sample primarily the sub-slab region showing rotation of fast directions following the curved shape of the slab and very strong anisotropy. S-rays sample mainly the slab, showing variable φ and a smaller δt. SKS and S splitting reveals a well developed toroidal flow at SW edge of the slab, while at its NE edge the pattern is not very clear. This suggests that the anisotropy is controlled by the slab rollback, responsible for about 100 km slab parallel φ in the sub-slab mantle. The slab is weakly anisotropic, suggesting the asthenosphere as main source of anisotropy. To investigate the physical properties of the slab and surrounding regions, I analyzed the seismic P and S wave attenuation. By inverting high-quality S-waves $t*$ from slab earthquakes, 3D attenuation models down to 300 km were obtained. Attenuation results image the slab as low-attenuation body, but with heterogeneous Q_S and Q_P structure showing spot of high attenuation , between 100-200 km depth, which could be due dehydration associated to the slab metamorphism. A low Q_S anomaly is present in the mantle wedge beneath the Aeolian volcanic arc and could indicate mantle melting and slab dehydration.

Introduction

Subduction zones have always been a challenging topic of Earth sciences since they are responsible for the formation of accretionary prisms and mountain ranges at convergent margins, drive the migration of fluids in the mantle that are responsible for the generation of arc volcanism, and are the locus where the largest earthquakes on Earth are generated.

The Southern Tyrrhenian Subduction System is one of the most complicated and intriguing subduction settings in the world. It is widely accept that the geodynamic setting of the Southern Italy Subduction System results from the southeast retrograde motion of the northwestward subducting Western Mediterranean slab. The retrograde motion of the slab was responsible for the creation of the backarc extensional Tyrrhenian basin and of the building of the Southern Apennines and Calabrian arcuate orogenic belts. Albeit the Southern Tyrrhenian Subduction system shows the common geometries of many subduction zones, such as a backarc basin (the Tyrrhenian Sea), a magmatic arc (the volcanic Eolian Islands), a subaerial thrust belt(the Calabrian Arc) and an offshore accretionary wedge, nonetheless it presents some controversial features that needed to be addressed. Undeniably, an important role in shaping the Tyrrhenian Sea basin and the counterpart Calabrian Arc orogen, is played by the interaction among the asthenospheric flow, occurring in the upper mantle wedge above the sinking oceanic slab and in the mantle below the slab, and the retreating Ionian slab. Moreover, the subduction dynamics is strictly influenced by both the slab-derived fluid and volatile content, and variations in kind and degree of melting.

The aim of this PhD Thesis is to gain insights into the deformation status of the Ionian slab and of the surrounding mantle, trying to describe a comprehensive geodynamical model that takes account the heterogeneity of strain in the mantle and lithosphere. To do this, I analyzed the information provided by several earthquakes using two different techniques: the study of seismic anisotropy due to the shear wave splitting and the study of seismic attenuation of P- and S-waves.

This PhD thesis is therefore subdivided in two main parts. The first part is devoted to the study of the anisotropic pattern beneath the Southern Tyrrhenian Subduction System. Due to the relationships between seismic anisotropy and the past and present deformation of the medium crossed by shear waves, seismic anisotropy has becoming extensively used in studying dynamic processes in subduction system. Previous shear wave splitting studies in the Southern Tyrrhenian Sea related the observed pattern of anisotropy to the retrograde motion of the Ionian

retreating slab. The slab rollback is responsible for the activation of a toroidal flow around its edges, flowing throughout the slab windows. Moreover, previous study identifies such a toroidal flow only at the southwestern edge of the slab, while none of similar circular mantle flow are satisfactory retrieved also around the its northeastern edge. In addition, previous studies retrieved the pattern of seismic anisotropy in the sub-slab region, while the nature of seismic anisotropy within both the mantle wedge and of the slab itself has been barely defined. To shed new light on these arguments, I defined the anisotropic pattern of the study region using several teleseisms and local deep earthquakes. The analysis has been performed with the method of Silver and Chan [1991]. The two different dataset used have allowed to distinguish, for the first time, the different sources of the anisotropy in the Southern Italy subduction system. Indeed, the results obtained by the analysis of the teleseisms have allowed me to better constrain the large scale anisotropic structure of the region structure, providing much more details on the sub-slab mantle region. Moreover, the unique events-stations distribution relative to the geometry of the subduction itself induces most of the S rays coming from the deep local earthquake travel for almost their entire ray-path inside the slab. The anisotropic parameters obtained with the analysis of local earthquakes gave me the opportunity to describe in better details the anisotropic structure of the mantle wedge and of the slab itself.

The second part of this study address the study of the seismic anelastic attenuation properties of the Southern Tyrrhenian Sea. In subduction zones the studies of seismic attenuation can help to better constrain the spatial relationship between melt production and volatile content in the mantle wedge, to clarify the physical nature of the slab, its water content and the metamorphic reactions that follow subduction processes. Recently, several models of attenuation tomography of the study area have been evaluated using either teleseisms and the P-waves of the local deep earthquakes. Anyway, the properties and the behavior of the mantle and of the slab, along with the nature of the magmatism, can be better constrained using also the information from S-waves. In this study, therefore, along with the 3D attenuation tomography performed on the P-waves, the attenuation properties have also been explored using several S-waves from earthquakes located within the descending slab I have performed the 3D attenuation tomography on several P- and S- wave generated by slab earthquakes using the damped least squared technique of Thurber [1993] as modified for attenuation by Rietbrock [2001].

This allowed me to better constrain the geometry and anelastic structure of the slab-asthenosphere, which results enabled me to hypothesized the relationship among attenuation properties of the subduction system, the Eolian volcanism, and the intermediate to deep earthquakes of the Ionian slab.

CHAPTER ONE

The Southern Tyrrhenian Subduction System

The Southern Tyrrhenian Subduction System results from several phases of fragmentation of the former, continuous Western Mediterranean subduction zone. It is presently enclosed in the central Mediterranean area and is part of the complex tectonic boundary between the two major plates, Africa and Eurasia. The boundary between Africa and Eurasia is composed of small, narrow and arcuate trenches, reflecting the complexity of the inherited geodynamic evolution. Indeed, the present-day tectonic setting of the Southern Tyrrhenian Subduction System results from several partly synchronous processes that involved the Central Mediterranea region: oceanic subduction, continental collision, slab rollback, and back-arc basin formation [Malinverno and Ryan, 1986; Faccenna et al., 2004; Stampfli and Borel, 2002; Jolivet et al., 2008]. The synchronism between the spreading of the Tyrrhenian Sea and the eastward migration of the Apennines belt as well as the coexistence of compression and extension structures suggest that they are the results of the eastward retreat of the Ionian– Adriatic slab [Patacca et al., 1990, Faccenna et al., 2001; Guillaume et al., 2010]. The combination of such different tectonic styles in a very narrow area is still a discussed feature of the region and requires a more complex model of geodynamic evolution. Despite these complexities, the Southern Tyrrhenian Subduction System is a natural laboratory to investigate the style of subduction processes

1.1 Geodynamics of the Southern Italy Subduction System

The Southern Tyrrhenian Subduction System is located along the fragmented convergent margin between Africa and Eurasia and it develops in a geodynamic setting characterized by N-S convergent relative motion between these two major plates. Despite the fact that the slow N-S convergent motion between Africa and Eurasia has always been invoked as the primary tectonic process in the Mediterranean area [Wortel and Spackman, 2000], the existence of large basins with E-W extensional tectonics, such as the Tyrrhenian Sea, along with compressional arcuate mountain belts, such as the Apennines and Alps, implies the existence of forces and processes independent of the Africa-Eurasia collision [Dewey et al., 1989; Jolivet and Faccenna, 2000]. Moreover, the rate of convergence between these two plates is on the order of 1-2 cm/yr [Faccenna et al., 2004], which is far slower than the rate (5-7 cm/yr) of both the opening of the

1

Tyrrhenian back-arc basin and of the building of the Apenninic and Calabrian mountains [Malinverno and Ryan, 1986; Patacca et al., 1990]. With these perspective, numerous authors [i.e., Gueguen et al, 1998; Carminati et al, 1998a, 1998b; Doglioni et al., 1999 and references therein; Rosenbaum and Lister, 2004; Rosenbaum et al., 2008] explain the geodynamic setting of the Tyrrhenian Sea-Calabrian Arc System as resulting from the southeast retrograde motion of the northwestward subducting Western Mediterranean slab and the associated arc migration. The rollback of the slab provided the driving force for the creation of the backarc, extensional Tyrrhenian Sea and the building of the Southern Apennines and Calabrian arcuate orogenic belts.
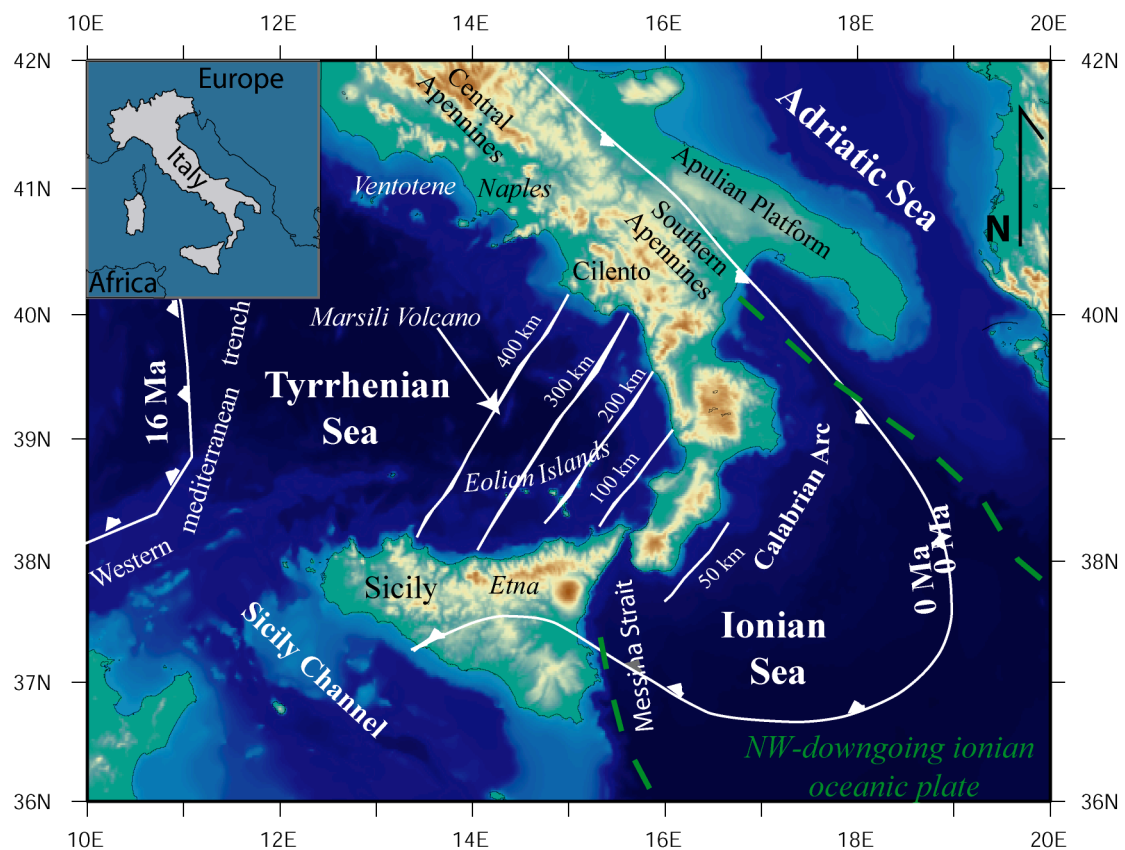
Figure 1.1 Tectonic frame of the Western Mediterranean region.White lines and triangles indicate the actual position of the thrust front of the Western Mediterranean subduction zone.

The present configuration of the Southern Tyrrhenian Subduction System has been achieved ca. 1-0.7 Ma, when the plate boundary system reorganized to accommodate the Africa-Eurasia convergence [Goes et al., 2004] Indeed, 35 Ma ago the western Mediterranean area was characterized by an active trench oriented NE-SW and dipping to the NW. The trench extended continuously from the southern Iberia to the Ligurian region [Dewey et al., 1989] (Fig. 1). From

30 to 23 Ma, an increment of the E-SE retrograde motion of the western Mediterranean trench caused the opening of several back-arc extensional basins, the Liguro-Provençal basin first and the Valencia and Alboran basins afterwards [Malinverno and Ryan, 1986; Beccaluva et al., 1989; Carminati et al, 1998; Jolivet and Faccenna, 2000]. Between 10 and 5 Ma the spreading migrated eastwards toward the Tyrrhenian Sea where occurred with the opening of the Vavilov basin first (~ 5-4 Ma) and then the Marsili basin (~2-1 Ma) and with a decrease of the subduction width [Guillaume et al., 2010]. The spreading of the oceanic Marsili basin, located at the center of the Tyrrhenian Sea, occurs at the rate of about 19 cm/yr and was synchronous with the southeastward drift of the Calabrian Arc, northeastward nappe stacking in the Southern Apennines [Menardi Noguera and Rea, 2000], and southward shortening in the Sicilian Maghrebides [Lickorish et al., 1999; Mattei et al., 2004]. Overall, from 5 Ma onward, the continuity of the old western Mediterranean trench was broken, and the extensional velocity of the Tyrrhenian basin increased (up to 19 cm/y) during the break of the slab along the Sicily Channel. The lateral tearing of the subduction front from its western prolongation beneath north Africa favored the rotation of the Apenninic-Calabrian plate [Carminati et al., 1998; Faccenna et al., 2004; Nicolosi et al., 2006]. Once the Apenninic-Calabrian trench encountered the Adriatic continental lithosphere to the east, a new slab break-off took place in the northern part of the trench causing the separation of the Apenninic front into two main arcs, the Northern Apennines Arc to the north and the Calabrian Arc to the south [Patacca et al., 1990]. The subduction migrated southeastward and remained active only off-shore Calabria [Doglioni et al., 1999; Wortel and Spackman, 2000]. To accomodate the remaining active portion of the slab beneath Calabria [D'Agostino and Selvaggi, 2004; Goes et al., 2004; Billi et al., 2006], a diffuse transform zone formed in northeastern Sicily and the northwestern Ionian region
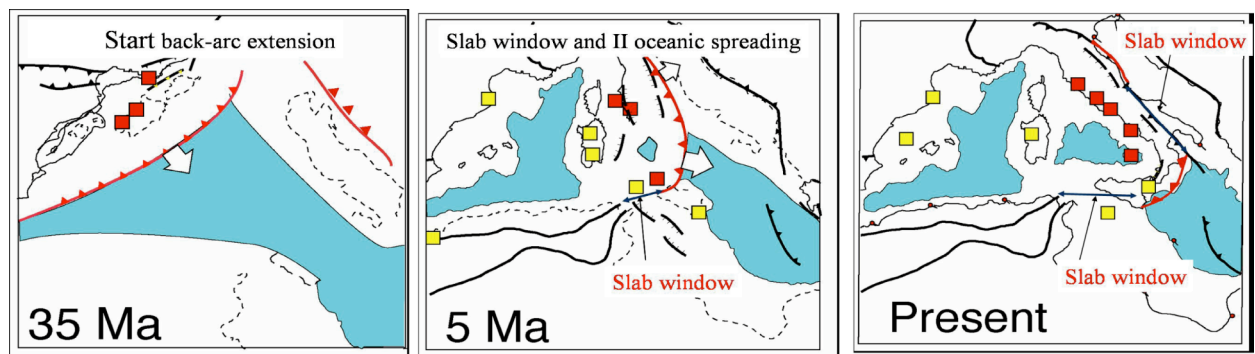
Figure 1.2 Reconstruction of the geodynamic evolution of the Mediterranean region from 35 Ma to present-day in relative. The deep basin domains are colored in blue. The reconstruction considered the Eurasia plate fixed [from Faccenna et al., 2004].

Despite the Calabrian Arc slab experienced more than 800 km rapid rollback to E-SE, the trench should have stopped its retrograde motion and, during the late Pleistocene, rollback and subduction slowed down, likely proceeding at less than 1 cm/y [D'Agostino and Selvaggi, 2004]. Indeed, geodetic data showed that today the Calabrian Arc is not retreating and that back-arc extension is not active [Hollenstein et al, 2003] However, Nicolosi et al. [2006] by unraveling magnetic anomalies in the young Tyrrhenian Sea oceanic crust, suggest that back arc spreading was always episodic and, thus, the present day configuration can be followed by a definitive stop or a new acceleration of the process.

1.2 Seismological evidence of the slab

Beneath the Calabrian Arc are many seismological features suggest the presence of subducted oceanic Ionian lithosphere. The actual existence of the slab is defined by the occurrence of many shallow and deep earthquakes concentrated along the Calabrian Arc and in the southeastern sector of the Tyrrhenian basin respectively (Fig. 2a). The subducting slab consists of a 200 km wide and 500 km deep Wadati-Benioff zone [Anderson and Jackson, 1987; Giardini and Velonà, 1991; Selvaggi and Chiarabba, 1995; Chiarabba et al., 2005; Billi et al., 2010] dipping toward the northwest at about 70° (Fig. 1.3). The distribution of earthquakes in vertical sections depicts the slab extending from the Ionian foreland in front of the Calabrian Arc to the central sector of the Tyrrhenian backarc basin (Fig. 1.3 A, B, C, D). At shallow depth, the seismicity images a sub-horizontal seismic plane that could be interpreted as the upper portion of the subducting Ionian lithosphere [Frepoli et al., 1996; Selvaggi 2001; Chiarabba et al., 2005; Pondrelli et al., 2004].

Beneath the northern sector of the Calabrian Arc, the seismicity has a gap between 100 and 200 km depth, but it forms a continuous body at greater depth. The lateral extent of this slab, as delineated by seismicity and tomography, is very narrow, no wider than 250 km. Several seismic tomography studies [Piromallo and Morelli, 2003; Spakman et al., 1993; Cimini, 1999; Lucente et al., 1999; Montuori et al., 2007; Cimini and De Gori, 2001; Neri et al., 2009] describe the present-day shape and extent of the slab going beyond the imaging obtained by seismicity alone Fig. 1.4).

These studies agree on several features. A vertical section (Fig 1.4) reveals that a high velocity anomaly is present only where the deep seismicity is located. At about 100 km depth, the high velocity is present only along the southern portion of the Tyrrhenian coast of Calabria. The

adjacent Tyrrhenian Sea, Sicily, the Southern Apennines and the Adriatic Sea are characterized by low velocity anomalies. At greater depth, the fast velocity anomaly broadens its size lying
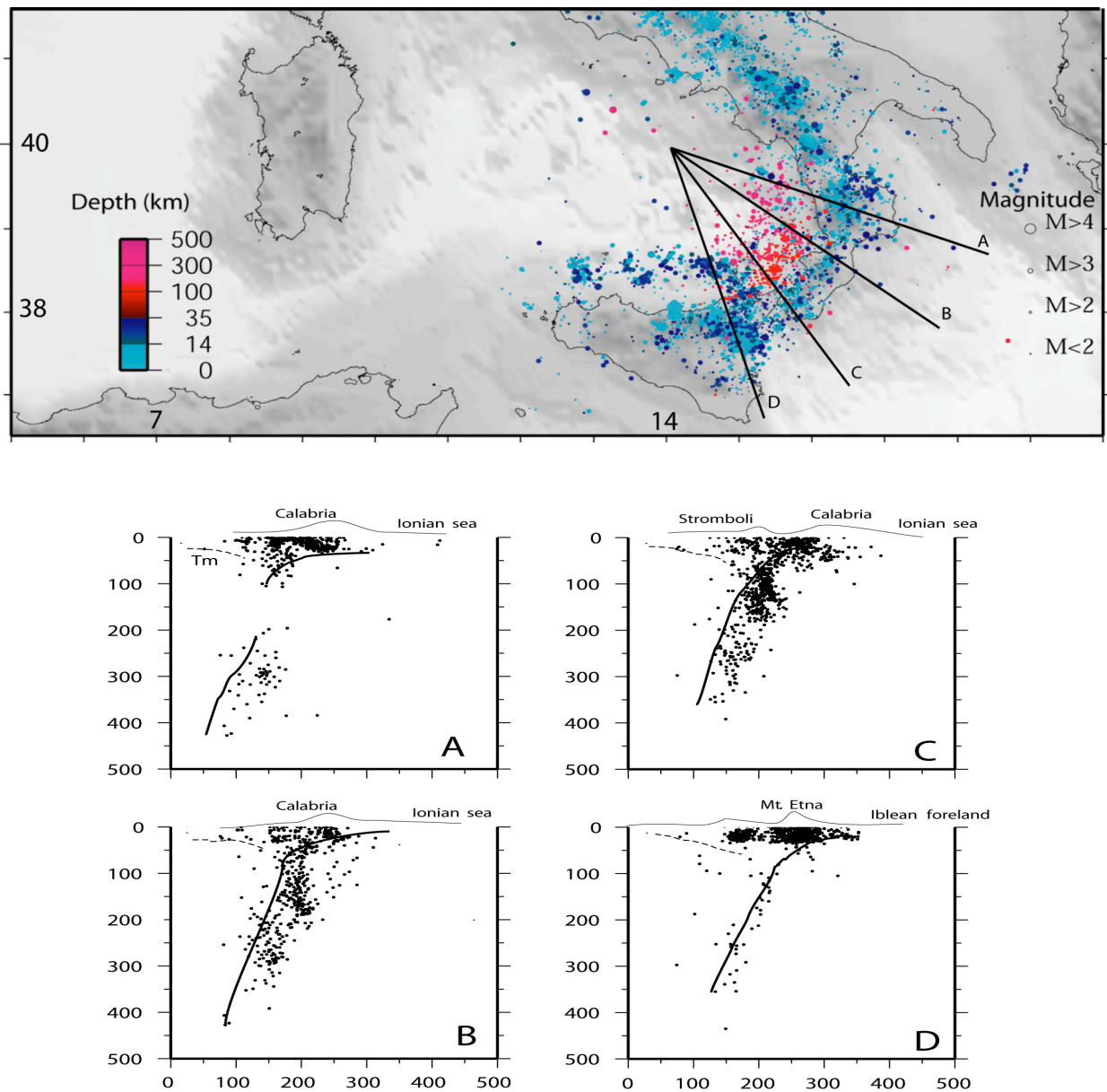
Figure 1.3 a) Hypocentral distributions of earthquakes characterizing the Southern Tyrrhenian Calabrian Arc System [Chiarabba et al., 2005]. The different hypocentral depth (km) of the events is given by the color scale indicated on the lower left corner. The distribution of events shows the lithosphere subducted beneath the Calabrian Arc and the progressive increase of slab depth toward the central sector of the Tyrrhenian Sea. The intermediate-depth earthquakes (blues circles) are confined to the front of the Tyrrhenian Calabrian coast, east of the Aeolian Islands, while the deeper events are mainly concentrated offshore in the Tyrrhenian Sea (red circles). b) Vertical sections oriented NW–SE across the Ionian slab from the north sector of Calabrian arc to north-eastern sector of Sicily. The lines indicates the geometry of the Tyrrhenian Moho (dashed line) and the top of the Ionian slab (solid line) as inferred from deep earthquakes

beneath the whole Calabrian Arc. At about 300km depth, the high velocity anomaly is a continuous body running from the Southern Apennines in the NE to the Sicily-Maghrebides in the SW, and extending from the Calabrian Arc to SE sector of the Tyrrhenian Sea. This high velocity anomaly is interpreted as the subducting lithosphere [Piromallo and Morelli, 2003]. Thus, the slab is horizontal in its shallow portion on the Ionian side, it is steeply dipping (about 70°) to NW down to 400 km and then it bends towards horizontal in the transition zone, lying flat on the upper mantle-lower mantle boundary (660 km depth) [Lucente et al., 1999; Piromallo and Morelli, 2003; Chiarabba et al., 2008; Monna et al., 2009; Piana Agostinetti et al., 2009].
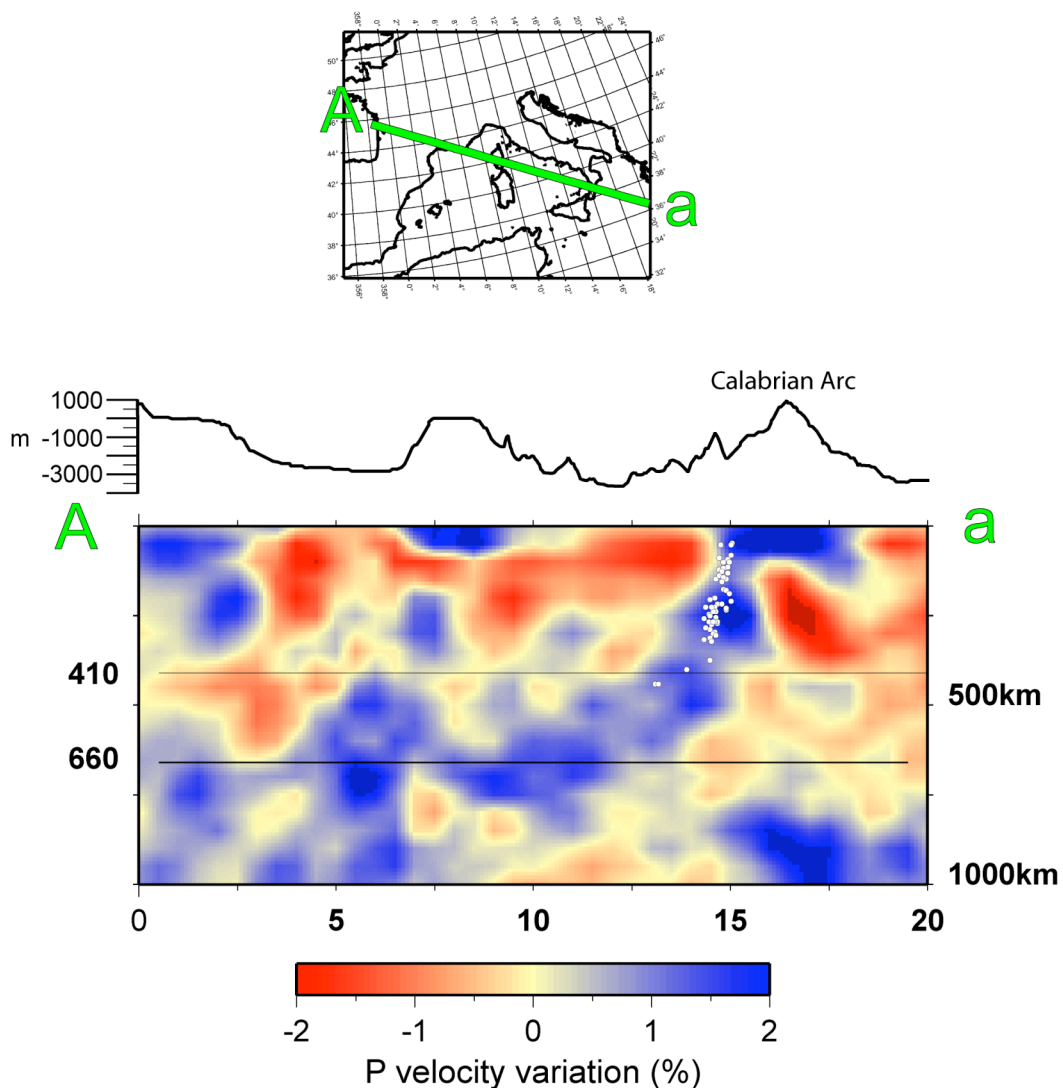
Figure 1.4 Cross section of P-wave tomography image at 150 km depth of the Calabrian subduction zone [Piromallo and Morelli, 2003]. There is a well defined high velocity body, interpreted as the sinking slab, which can be followed from its shallow horizontal portion beneath Calabria, then steeply dipping (~70°) toward the Tyrrhenian Sea into the upper mantle and finally lying almost horizontal on the 660 km discontinuity. The white solid circles are the intermediate and deep earthquakes localized in correspondence with the high velocity anomaly.

There is still an open debate whether the subducting Ionian microplate oceanic or not. One of the arguments in favour of the oceanic nature of the Ionian crust is the low heat flow of the Ionian Sea and its deep bathymetry (3000-5000 m depth). Refraction of the Ionian Sea crust south of Calabria shows a typical oceanic crustal structure [de Voogd et al., 1992]. Moreover, the subducted lithosphere beneath the southern Tyrrhenian Sea has clear oceanic seismic characteristics: high *Vp*, high *Qp* and low *Vp/Vs* anomalies [Chiarabba et al., 2008]. According to some authors it is a remnant of the Mesozoic neo-Tethys Ocean and thus one of the oldest oceanic crusts in the world [Catalano et al., 2001].

1.3 Geological features

The actual tectonic setting the surface tectonics of the area analyzed in this study (Fig. 1.5) can be simplified by identifying three main outcropping regions: the Calabrian Arc, the Southern Apennines and its foreland: the Apulia Platform. The Calabrian Arc foreland is the crust present below the Ionian Sea. The Calabrian Arc fold and thrust belt is part of the accretionary wedge resulting from the subduction.
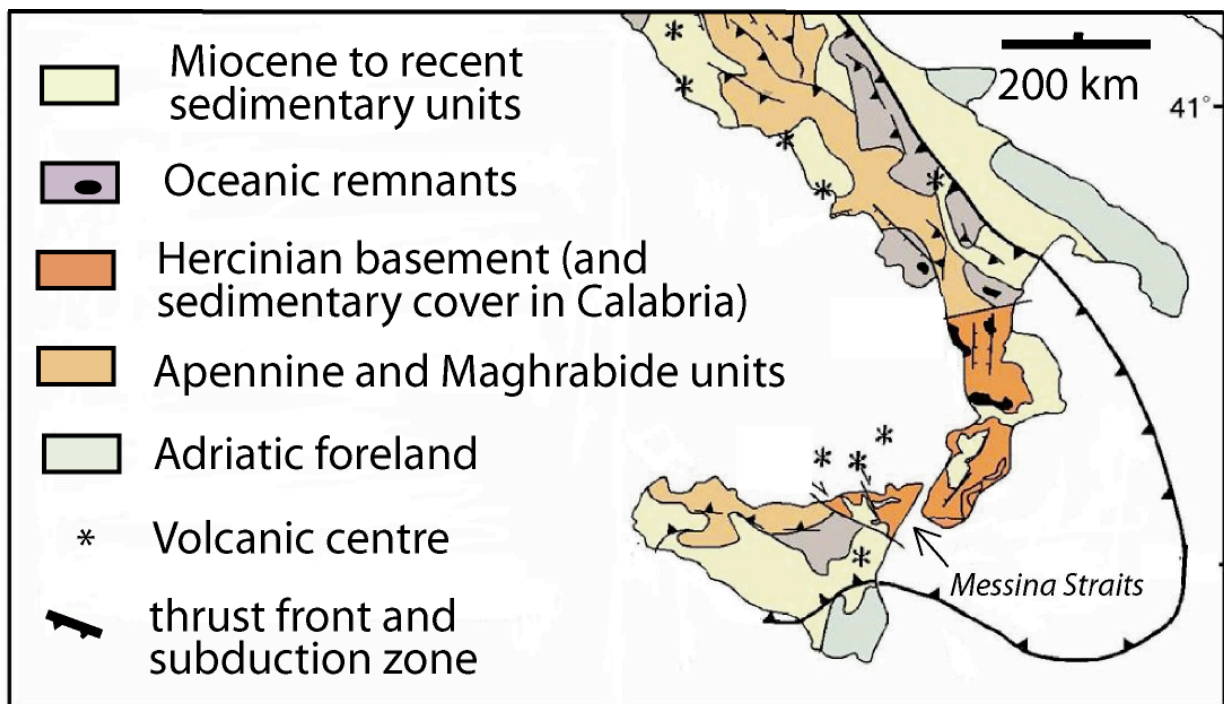
Figure 1.5 Geological map of the study region where surface geological differences between the Calabrian Arc, the Southern Apennines and the Apulian Platform are shown [from Rosenbaum et al., 2002].

The Calabrian terrane is a fragment of a preexisting Alpine–Apennine chain located east of Sardinia in pre-late Miocene times [Alvarez et al., 1974] and moved to the present-day location by the southeastern slab-roll-back. The top of the thrust stack in the Calabrian Arc is composed of metamorphic basement slices. These exposed Paleozoic crystalline rocks suggest that this part of Calabrian Arc is a remnant of the Europe-Iberia plate [Rossetti et al., 2004] that migrated southward with the subduction system [Gueguen et al., 1998].

A different structural style defines the Southern Apennines fold and thrust belt, resulted from the sinking of the Ionian lithosphere and from the collision with the Adriatic microplate [Patacca and Scandone, 1989]. The Southern Apennines fold and thrust belt is part of the accretionary wedge, constructed by the imbrication of a succession of carbonate platforms and pelagic basins. The most external of these domains is the Apulia Platform, which constitutes the foreland of the orogen [Patacca et al., 2000]. The Apulia Platform, along with the underlying basement, is partly involved in the orogenic wedge and partly forms the foreland lying below the outer front of the Apenninic chain [Patacca et al., 2000]. The foreland is formed by a rather uniform structure characterized by crystalline basement an about 6 km thick of Mesozoic sedimentary cover [Doglioni et al., 1994]. The Apulian Platform is part of the Adriatic microplate considered by some authors as an African promontory [Rosenbaum and Lister, 2004] and by others [Battaglia et al., 2004] as an independent microplate. The Adriatic microplate subducted below the Eurasian plate between the Cretaceous and the Tertiary forming the SW-vergent Dinarides [Aubouin et al., 1972] and, during the Tertiary, the NE-vergent Apennines.

The top of the thrust stack in the C.A. is composed of metamorphic basement slices, absent in the S.A., indicating that the C.A. is a remnant of the European plate [Rossetti et al., 2004] that migrated southward with the subduction system [Gueguen et al., 1998]. The differences between C.A. and S.A. extend beyond their crust; the Benioff plane below C.A. (Figure 2) is well defined down to 600 km [Chiarabba et al., 2005, and references therein] while no intermediate earthquakes occur below S.A.

CHAPTER TWO

Seismic Anisotropy and Attenuation

Before embarking on the study of deformation occurred at depth inside the mantle and on how seismic anisotropy and attenuation have been used to study the Southern Italy Subduction System, it is worth briefly outlining some of the general concepts regarding seismic anisotropy and attenuation. Undeniably, the Southern Italy Subduction zone is a complicated subduction and several aspects, among the others the interaction between sinking slab and the surrounding mantle flow field and the structure of the slab itself, remain still poorly understood. These two seismological observables, anisotropy and attenuation have represented a powerful tool to address questions such as the evolution of the complicated western Mediterranean subduction zone, the role of the mantle rheology, the structure of the Ionian descending plate and the causes and consequences of trench rollback.

2.1 Seismic anisotropy

The study of seismic anisotropy has a long history, but only recently it has become one of the central features of geophysics. Indeed, the observation that seismic waves propagate with different speeds depending on the propagation direction, that is seismic anisotropy, was done starting in 1960s; nevertheless in most studies, the Earth is usually assumed to be isotropic for mathematical convenience.

Most of seismological modelling, in fact, assume that the Earth is isotropic, with seismic velocities that do not vary with direction. A plausible reason for this is the growing computational complexity required for anisotropic calculations, but also the difficulty in inverting data for a greater number of elastic constants. Nonetheless, it has been broadly observed that crystals and most common materials are intrinsically anisotropic, with seismic wave velocities varying for different propagation and polarization directions. In addition, an ever-growing number of seismic data from different region show one of the most clear manifestation of anisotropy, that is the shear wave splitting.

Anisotropy is observed in different parts of the Earth, at different depths and at different scale; it can be observed within the crust [Crampin, 1994], the upper mantle [Long and Becker, 2010 and reference therein], the transition zone and the lower mantle [Trampert and van Heijst, 2002;

Beghein and Trampert, 2004, Karato, 2008, Cordier et al., 2004], the D'' layer [Kendall and Silver, 1998; Lay et al. 1998; Karato 1998; Yamazaki and Karato, 2007] , and the inner core [Beghein and Trampert, 2003], and it arises from a wide variety of different mechanisms [e.g., Maupin and Park, 2007]. Among these different parts of the Earth, the crust and the upper mantle are those that, more than the others ones, have been extensively studied in terms of seismic anisotropy and there is a large amount of experimental constraints on the relations between deformation and anisotropic structure in these two regions of the Earth [Savage, 1999; Mainprice, 2007; Mainprice et al., 2005; Karato et al., 2008 and reference therein]. In this study I have focused the attention on the mantle strain and therefore I have investigated the upper mantle anisotropy.

A material can be described as anisotropic when it has physical properties which depend on the direction. When a seismic wave enters an anisotropic medium, the wave velocities vary with propagation direction, that is travel with different velocities as a function of its propagation and polarization direction. In the crust the most likely mechanism responsible for the anisotropy is the presence of parallel, aligned fluid filled cracks or alternating isotropic layers with different elastic properties. In the mantle the most likely mechanism responsible for the anisotropy is the lattice preferred orientation (LPO), in which the anisotropy arises from a preferred orientation of intrinsically anisotropic crystals [Zhang and Karato, 1995; Ben Ismail and Mainprice, 1998; Savage, 1999]. In the upper mantle, the most abundant crystal is the olivine; it has an intrinsic anisotropic property of ~ 18% [Mainprice, 2007] and, therefore, the largest contribution to the upper mantle anisotropy can be ascribe to the olivine lattice preferred orientation. In general, the seismically fast axes of the olivine tend to align parallel to the stress field or flow field due to the finite strain [Ribe and Yu, 1991]; in other words, the *a*-axis are in the plane of the flow, with the *a*-axis, the fastest direction, pointing in the direction of flow (Figure 2.1).
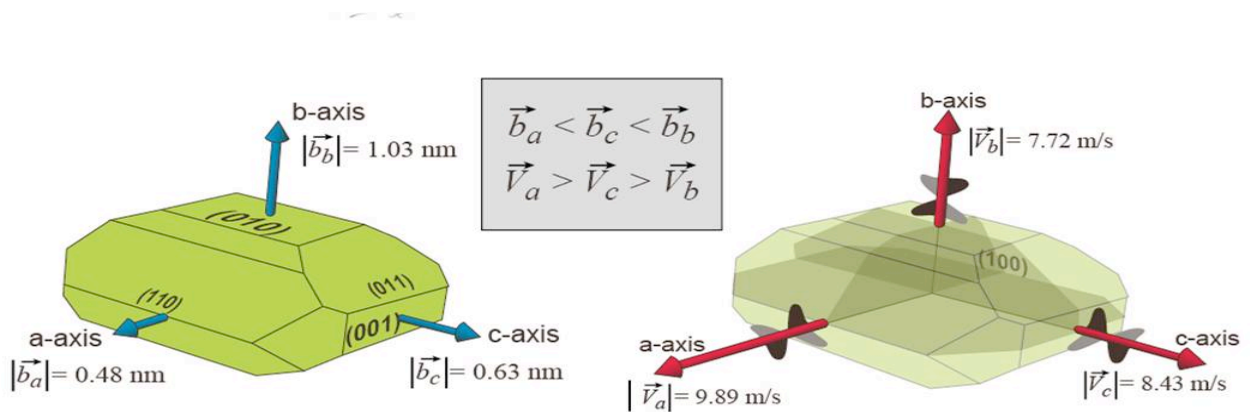
Figure 2.1 An olivine crystal and the orientation of three a-, b- and c-axes along with the corresponding velocity.

In the mantle, the rocks undergo two type of deformation: diffusion creep and dislocation creep. The diffusion creep is the solid-state diffusion between grain boundaries or across crystal lattice and occurs at relatively low stress and/or small grain size.; it does not develop LPO, and the resulting deformed material is isotropic. On the contrary, the olivine LPO, and thus anisotropy, is favoured when the mantle rock are deformed in regime of dislocation creep. The dislocation creep is the motion of crystalline dislocation within grains and occurs with high stress and/or large grain size [Nicolas and Christensen, 1987; Karato and Wu, 1993]. For large strain, the fast axis of olivine tends to align with the maximum shear [Christensen, 1984; Zhang and Karato, 1995].

The olivine LPO, and thus the anisotropy, is conditioned by the temperature, pressure, the partial melt and water content. The high pressure and high temperature ($\geq$ 900 °C) are favourable conditions for developing LPO in oriented grains [Mainprice and Nicolas, 1989; Mainprice et al., 2008], while below 900 °C the olivine crystals are not easily reoriented [Estey and Douglas, 1986]. The partial melting can alter olivine LPO development, changing by 90° the relationship between the shear direction and the fast splitting direction [Holtzman et al., 2003]. Similar effect is carried out by the water content: significant amount of water and high shear stress tend to align the olivine *a*-axis 90° away from the direction of maximum stress, thus becoming perpendicular to the mantle flow direction [Jung & Karato 2001]. This geometry of olivine aggregates is called as "B-type" and requires high stress, low temperature and presence of water [Kneller et al., 2005; Karato et al., 2008]. High water content but low stress conditions are suitable for produce C- and E-type olivine, which determine flow parallel fast directions, while the LPO generated under low stress and low water content is known as A-type [Katayama et al., 2004]. These different geometries of olivine aggregates have been proposed to explain the diverse anisotropic structure in subduction zone, as flow-parallel fast direction in the backarc region, and flow-perpendicular fast direction in the mantle wedge above the slab [Nakajima and Hasegawa, 2004; Long et al., 2007b; Kneller et al., 2008; Jung et al., 2009; Smith et al., 2001; Hoernle et al., 2008].

2.1.1 Shear-wave splitting

The clearest evidence of the presence of seismic anisotropy in a medium is the splitting of the shear waves, a phenomenon that is analogous to optical birefringence under polarized light (Figure 2.1). When a shear wave, with an initial linear polarization, travels through an anisotropic medium it splits into two components, known as the fast and the slow shear waves

which have polarization orientation normal to each other and propagate with different velocities [Savage, 1999; Bowman and Ando, 1987]. Consider, now, two media, one isotropic and the other one anisotropic, and the P and S elastic waves propagating through it, as shown in Figure 2.2. In the isotropic medium, the compressional P-wave has linear particle motion parallel to the propagation direction, while the shear S-wave has particle motion perpendicular to propagation and with two component oriented in the horizontal plane (SH) and in the vertical plane (SV). On the contrary, in the anisotropic medium, the P- and S-waves are neither purely perpendicular nor parallel to the direction of propagation; we identify, thus, a quasi-P wave (qP), with linear particle motion that is not quite parallel to the propagation direction, and two-quasi-S wave (qS$_1$ and qS$_2$) with polarizations parallel and perpendicular to the fast direction.
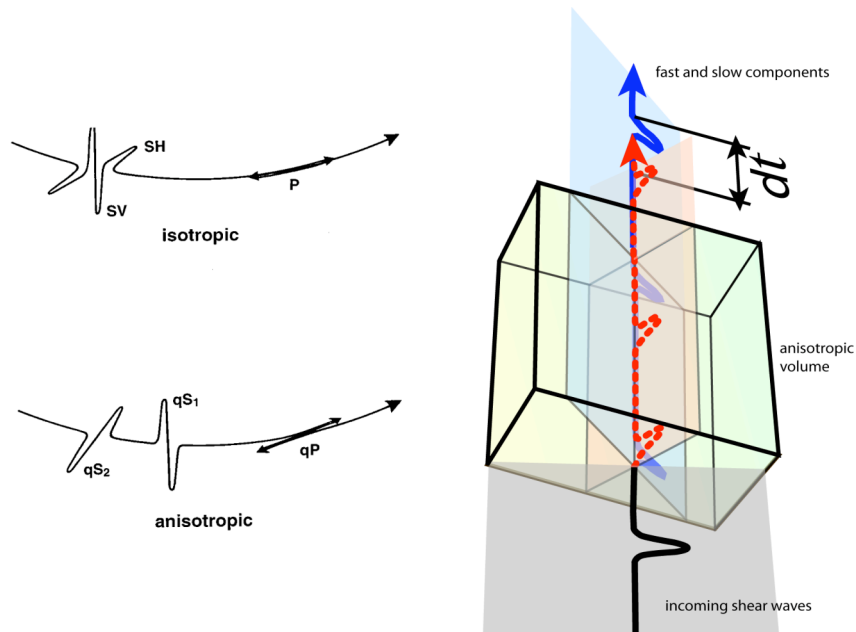
Figure 2.2 (Left) Comparison between propagation of the P-and S-waves in an isotropic and anisotropic medium [Savage, 1999] (Right) Schematic diagram showing the shear wave splitting phenomenon. An incoming shear wave, linearly polarized, enters the anisotropic volume and it splits into two components, one polarized parallel to the fast direction (blue) and one with perpendicular polarization (red) The fast and slow components traveling at different speed accumulate a delay time while propagate through the anisotropic medium (modified after http://garnero.asu.edu/research_images)

The seismic anisotropy of a medium can characterized by two parameters, φ and δt. The parameter φ, or fast axis direction, is the polarization azimuth of the fast shear wave and it corresponds to the alignment of fast axes of anisotropic minerals or fractures. Nevertheless, the initial shear wave, before entering the anisotropic medium, might be polarized parallel to either

the fast or slow direction of anisotropy. In this case, no splitting is observed because only the fast shear wave (for a fast initial polarization) or the slow shear wave (for a slow initial polarization) occurs. These kind of measurements are often referred as nulls and it does not necessarily mean that anisotropy is absent, but also that, if anisotropy is present, the fast direction is either parallel or perpendicular to the polarization of the shear wave. The other parameter describing the anisotropy is the δt: it represents the delay time between the fast and slow S waves. Indeed, as the two quasi-S waves propagate through the anisotropic region at different speeds, they accumulate a time delay, which depends on both the path length in the anisotropic medium and the difference in speed between qS_1 and qS_2. It is, therefore, a measure of the intensity of the anisotropy and/or of the thickness of the anisotropic layer. The fast polarization direction φ and delay time δt contain information about the geometry and the strength of the anisotropic volume. These splitting parameters are the direct expression of the internal structure of mantle and crustal rocks and, thus, are the expressions of the tectonic deformation that they have undergone.

Shear wave splitting measurement are assessed using a variety of shear phases that propagate through the mantle (Figure 2.3). Moreover, the most popular phases that are commonly used for surveying anisotropic structure in the upper mantle are the SKS phases. Within the last 10 years the SKS phases have been extensively used in probing anisotropy since the splitting analysis on SKS phases is simpler than for other phases. There exist several advantages in using them: due to SKS waves passing through the liquid core, all source-side anisotropy is removed. The P-S conversion at the core-mantle boundary provides a known polarization direction; they are polarized on the radial component. Therefore, the presence of energy on the transverse component indicates that the SKS waves have travelled through the anisotropic region on the receiver side [Silver and Chan, 1991]. Another advantage is that SKS is an isolated phase for epicentral distances ranging between 86° and 106° [Silver, 1996].

Other shear phases with almost the same properties are also useful to detect anisotropy such as the PKS, SKKS and PKKS. Phases such as the ScS, that reflect off the core-mantle boundary (CMB), and the Sdiff, that are diffracted around the CMB, are used to detect anisotropy within the D" region. Finally, also the direct local S phases, for example from earthquake generated within the slab, are particularly useful to better constrain the anisotropy in subduction zones.

2.2 The technique to retrieve anisotropic parameters

In my PhD Thesis, to diagnostic the anisotropy I used the well known and broadly used method of Silver and Chan [1991]. This method is based on the principles that when a shear wave pass
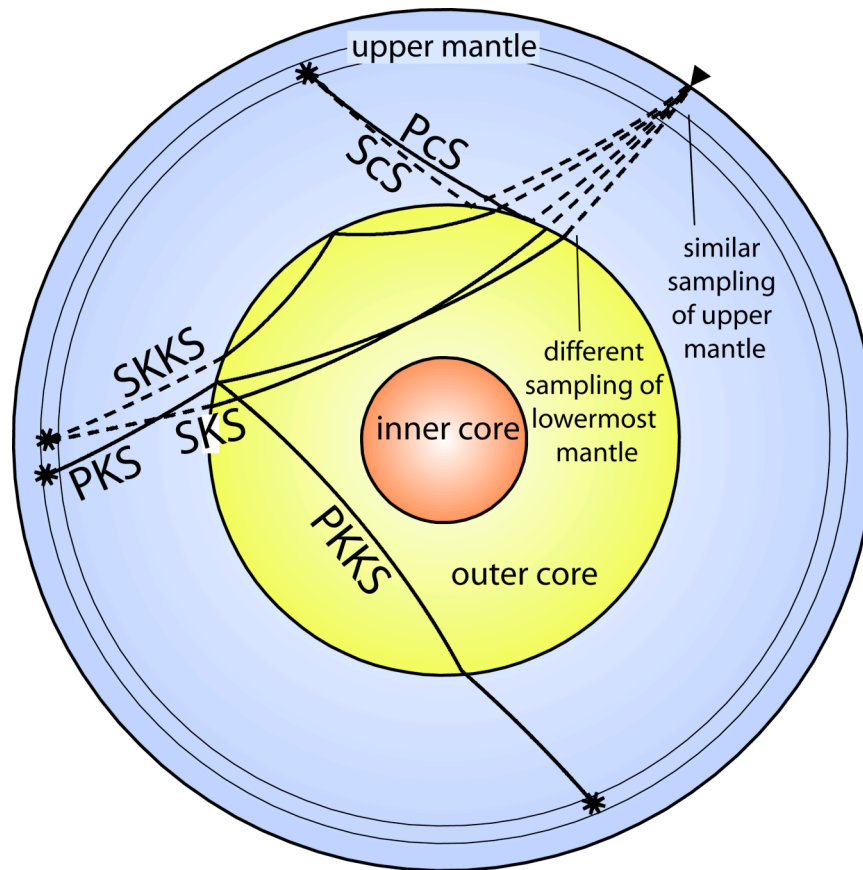
Figure 2.3 The most common rays used to probe anisotropy in the diverse region of the Earth (from http://garnero.asu.edu/research_images)

trough an isotropic medium is linearly polarized, but when the shear wave travels through an anisotropic medium there will exist a significant energy also on the horizontal transverse component, that results in elliptical particle motion. The presence of the elliptical particle motion is a diagnostic feature of the shear wave splitting, and thus of the anisotropy. The method corrects for anisotropy rotating and shifting the two horizontal components making a grid search to over all possible and reasonable values of φ and δt to find the pair of splitting parameters that better linearizes the shear wave polarization and minimizes the effect of the anisotropy. The code assume that the shear wave pass through a medium with homogeneous anisotropy and with a horizontal fast axis. It is generally used a range of φ between -90° and 90° and of δt between 0 and 4 sec.

The two parameters that describe an anisotropic volume, φ and δt, are found by computing the two-dimensional covariance matrix of particle motions in the horizontal plane, since its eigenvalue can be used as a measure of polarization linearity. The covariance matrix c_{ij} is

defined for any two orthogonal components of ground motions, which make angles φ and φ+π/2 with the original polarization direction for a time interval δt:

$$c_{ij}(\varphi,\delta t) = \int_{-\infty}^{+\infty} c_i(t)c_j(t-\delta t)dt \qquad \text{i,j} = 2,1 \qquad (2.1)$$

In absence of anisotropy, we will have a linear particle motion for the two horizontal components: the covariance matrix will, therefore, posses one nonzero eigenvalue [λ_1] and the corresponding eigenvector represent the direction of the linear particle motion. In presence of anisotropy, the covariance matrix will have two nonzero eigenvalues [λ_1 and λ_2], unless φ = π/2 or δt is zero. In presence of anisotropy the pair of splitting parameters that best resolve for the anisotropy correspond to that which produces the best linearized particle motion, that is the pair, which minimizes the smaller eigenvalue (λ_2) of the covariance matrix. What has just been described is the Eigenvalue Minimization Method that is applied when the initial polarization of the shear wave is unknown. This is generally the case of the direct S waves. Thus, the two horizontal components are rotated and time-shifted for each possible combinations of splitting pairs and the linearization of the particle motion of the two horizontal seismogram components is achieved by minimizing λ_2. The error associated in the correction for the anisotropy is a contour plot for all possible pairs of splitting parameters: the 95% confidence contour of the best fitting parameters for each measurement corresponds to the minimum of this contour plot. A slight variation on the Eigenvalue Minimization Method is the Transverse Component Minimization Method. This method is straightforward for estimation of splitting parameters and can be applied to that shear waves that are radially polarized. This is the case of the SKS and SKKS phases since the polarization direction is well known and correspond to the backazimuth. The method do not performs a minimization of the smaller eigenvalue of the corrected covariance matrix, but compute a minimization of the transverse component energy, that is:

$$E_t = \int_{-\infty}^{+\infty} \grave{u}_t^2(t)dt \qquad (2.2)$$

where $\grave{u}_t^2$ is the corrected transversal seismogram.

The two horizontal components are rotates and time-shift to find the pair of φ and δt that best minimize the amount of energy on the corrected transverse component, that is that best

linearizes the corrected particle motion. The best fitting parameters are shown on a contour plot of the transverse component energy and correspond to the minimum of this contour plot.

2.3 Attenuation

In the last section, I consider the Earth as an anisotropic elastic medium and I describe the effect of the anisotropy on the seismic waves as they pass through such a medium. Anyway, the real Earth is not perfectly elastic and do not responds elastically during wave propagation. For this reason, consider now another process, the anelasticity, a mechanism which can explains why the seismic waves attenuate. Attenuation means that when a seismic wave propagate throughout a medium they undergo a general decrease in their amplitude with distance from the wave source. Hence, small anelastic losses occur that progressively attenuate the wave energy. This phenomenon affects the shape and spectral content of seismic signals. The observed reduction in amplitude of the seismic wave can be ascribed to four processes: the geometrical spreading, the scattering, the multipathing and the anelasticity. The first three are elastic processes in which the integrated energy in the total propagating wavefield remains constant; for example, in the case of scattering attenuation, the amplitudes in the main seismic arrivals are reduced by scattering off small-scale heterogeneities, but the energy in the propagating wavefield is conserved. On the contrary, the anelasticity is the conversion of the kinetic energy of the elastic wave to heat by permanent deformation of the medium. Therefore there is a real dissipation of energy from elastic waves. The anelasticity is usually described as internal friction. Indeed, one of the major mechanisms of the anelasticity, and thus of internal friction, is due to various energy-loss or absorption, or frictional-loss, mechanisms in dry rocks due to relative movements along mineral dislocations or shear heating at grain boundaries, that taper the wave energy [Jackson et al., 1992]. In particular, intrinsic attenuation primarily results from the viscous damping by pore fluid motion and grain frictional sliding effects in a fluid saturated elastic solid [Berryman, 2002; Winkler and Murphy, 1995]. Moreover, attenuation can also be controlled by water content, temperature, and porosity of material [Aizawa et al., 2008].

The energy loss through nonelastic processes is usually measured by the intrinsic attenuation and parameterized with Q, the quality factor. Q is defined as a dimensionless quantity and express the fractional loss of energy per cycle of oscillation. In other word, Q represent the dissipation of seismic energy in the Earth. Q is inversely proportional to the damping factor, or coefficient of friction, therefore the smaller the damping, the greater Q is. For no damping, Q is infinite, the amplitude does not decay with time. As damping increase, Q decrease, so the

amplitude decays faster. Large values of Q imply small attenuation and, as Q approaches zero, attenuation is very strong. Q increases with material density and velocity. For a constant value of Q a high-frequency wave will attenuate more rapidly than a low-frequency wave. This is because for a given distance the high-frequency wave will go through more oscillations than a low-frequency wave will. Q for P waves in the Earth is systematically larger than Q for S waves.

In laboratory studies, Q is found to be dependent on frequency [Karato and Spetzler, 1990]. In general, the frequency dependence is described as $Q = Q_0 * f^{\alpha}$, where Q_0 is the frequency independent Q, and α quantifies the frequency dependence [Atkinson, 1995] At mantle depths, there seem to be a weak frequency dependence, consistent with long-period variation in Q at mantle depth [Jackson et al., 2002; Warren and Shearer, 2000,]. On the contrary, strong frequency dependence, for a frequency dependent factor $\alpha > 0.5$, is shown by crustal studies using Lg and coda waves (1-20 Hz) [Benz et al., 1997; McNamara, 2000] or body waves in continental crust (1-25 Hz) [Sarker and Abers, 1998a]. The physical mechanism of such strong frequency is still unclear, but it seems to be due to the presence and deformation of cracks or pores [O'Connell and Budiansky, 1977; Winkler and Nur, 1979].Albeit attenuation mechanism show some frequency dependent behaviour, most measurements of Q with body wave typically fixed $\alpha = 0$, assuming therefore a frequency independent Q. This is usually because frequency dependence cannot be resolved over limited frequency ranges [Schlotterbeck and Abers, 2001; Takanami et al., 2000].

Seismic wave attenuation is strongly dependent by the presence of fluids and gas. Indeed, different fluid conditions can lead to a strong variation in Q. The presence of gas in sandstone increases the P-wave attenuation but had negligible effect on the S-wave conditions [Winkler and Nur, 1979]. Partial water saturation significantly increases the attenuation of both compressional (P) and shear (S) waves relative to that in dry rock, resulting in greater P-wave than S-wave attenuation. Conversely, water-saturated conditions maximizes S-wave attenuation but causes a reduction in P-wave attenuation. These effects can be interpreted in terms of wave induced pore fluid flow. In the experiments the effects of confining pressure, pore pressure, degree of saturation, strain amplitude, and frequency were studied [Mavko, 1980; Mizutani and Kanamori, 1988; Klimentos, 1995]. Like elastic parameters, the ratio of compressional to shear attenuation better describe the fluid saturation and the physical state of fluids. is found to be a more sensitive and reliable indicator of partial gas saturation than is the corresponding velocity ratio [Winkler and Nur, 1979]. Low QP/QS ratio values are related to a partially saturated condition of the crustal volume investigated. Conversely, Q_P/Q_S might indicate a complete fluid

saturation, or dry rocks; both alternative features similarly explain the large reduction of shear rather than bulk attenuation [Hauksson and Shearer, 2006]

2.4 The estimation of attenuation

The attenuation of a seismic waves between the source *j* and the receiver *i* can be estimated from the amplitude spectrum $S_j(f)$, which can be describe by [Scherbaum, 1990; Rietbrock, 2001]:

$$A_{ij}(f) = S_i(f) \cdot I_j(f) \cdot R_j(f) \cdot B_{ij}(f) \qquad (2.3)$$

where *f* is the frequency, $S_i(f)$ is the source spectrum. In addition to the influence of attenuation *Bij(f)* along the ray path between the event *i* and the station j, the observed spectrum A_{ij} is affected by the instrumental response, $I_j(f,)$ and by the local site effect, $R_j(f)$.

The far-field source amplitude spectrum id defined as:

$$S_i(f) = \Omega_0 \frac{f_c^{\gamma}}{f_c^y + f^{\gamma}} \qquad (2.4)$$

where Ω_0, the seismic moment, describes the long-period plateau value, f_c is the source corner frequency, and *γ* the high-frequency decay factor, *f* the frequency.

Assuming the whole path attenuation, the attenuation spectrum B_{ij} is given by:

$$B_{ij} = \exp\left[-\left(\pi f\, t*_{ij}\right)\right] = \exp\left[-\pi f\left(T_{ij} / Q_{ij}\right)\right] \qquad (2.5)$$

Where t* is the whole path attenuation operator, T_{ij} the travel time, Q_{ij} the quality factor.

In this study of attenuation they have been followed some assumption: 1) the observed amplitude of the instrument spectra has been modeling in the passband of the seismometer, therefore the transfer function has been set to 1. In addition, it has been determined the high frequency decay rate, that give the opportunity to describe the local site effects by a station constant t* operator [Anderson and Hough, 1984]. Thus:

$$R_j(f) = \exp\left[-\pi f \, t^*_{station}\right] \tag{2.6}$$

In addition, posing $\gamma=2$, that is equivalent to a Brune type ω^2 source model [Brune, 1970] and combining the equations (2.4) and (2.6), the equation (2.3) become:

$$A_{ij}(f) = \Omega_0 f_c^{\gamma}/\left(f_c^{\gamma} + f^{\gamma}\right)\exp\left[-\pi f\left(t^*_{ij} + t^*_{station}\right)\right] \tag{2.7}$$

t* can also be expressed as the projection of $1/(Q(s){\cdot}v(s))$ along the ray path [Wittlinger et al., 1983], thus:

$$t^* = \int_{raypath} \frac{1}{Q(s){\cdot}v(s)} ds + t^*_{site}$$

(2.8)

where v is the velocity of P or S seismic waves and ds is the integration along the ray path. If ray are traced using a well known velocity model, then the t* only depends on $1/Q$ values along the ray path. Therefore, the term t*site accounts for the attenuation near the recording site that may have influence the observed spectrum. This allow to consider the equation (2. 8) similar to the travel time tomography using shots with known origin time. The sufficient number of t* observations along different ray path allow to construct a set of obtained t* which are then used to reconstruct the three-dimension Q structure.

2.3.1 t* operator

Body wave attenuation is often characterized by the parameter t*. If a ray travels through a volume with constant Q, t* is defined as:

$$t^* = \frac{t}{Q} = \frac{traveltime}{qualityfactor} \tag{2.9}$$

19

that take into account for the whole path attenuation term, $1/Q$, in the amplitude decay. Moreover, Q varies within the different region of the Earth, and is a function of the depth and frequency; thus t* can be expressed as the integrated value of $1/Q$ along the ray path, that is:

$$t^* = \int_{path} \frac{dt}{Q} = \sum_{i=1}^{N} \frac{\Delta t_i}{Q_i} \tag{2.10}$$

where Δt_i and Q_i are the travel time and the quality factor value for the ith segment of the ray path. Hence, t* is the total travel time divided by the path-average value of Q and is much larger for S waves than for P waves. This means that the S waves attenuate more rapidly with distance.

CHAPTER THREE

Focused mantle flow around the Calabrian slab as revealed by SKS seismic anisotropy

Throughout the last chapter I have illustrated the general concepts and principles governing the anisotropy and I have described the phenomenon of shear wave splitting, the unambiguous indicator of anisotropy. We are thus now able to explore the anisotropic structure of the Southern Tyrrhenian Subduction system.

In this chapter I start showing the results obtained using teleseismic shear waves to give the large scale picture of the anisotropic structure. I have analyzed a large number of events increasing the number of splitting measurements for Southern Italy; I will discuss the splitting results together with the previous presented in previous studies in the region [Baccheschi et al., 2007; Civello and Margheriti, 2004]. This has allowed me to better reveal the variations in the anisotropic parameters between three different geological and anisotropic domains: the highly deformed Southern Apennines and Calabrian Arc mountain belts and the weakly deformed Apulia Platform. Also, new evidence of anisotropy in the southernmost part of the Apulian Platform are found. I describe the range of splitting behaviour over the study region. There are areas where splitting patterns are generally consistent with a simple anisotropic model, and other places where I see evidence for complexity in the anisotropic fabric. I try to relate these differences to tectonic features and to the upper mantle structure.

3.1 Dataset used

I have calculated splitting parameters for 15 teleseisms (Figure 3.1) with high signal to noise ratio recorded from December 2003 to March 2006 at the 40 CAT/SCAN (Calabrian-Apennine-Tyrrhenian/Subduction-Collision-Accretion Network) stations (http://www.ldeo.columbia.edu/res/pi/catscan) (Figure 3.2).

I selected earthquakes with magnitude greater than 6.0 and epicentral distance $\Delta°$ ranging from 87° to 112°. The earthquakes span all back-azimuth, but are primarily concentrated in the E to NE and in the W (Figure 3.1). To obtain the best signal to noise ratio, all teleseisms are band-pass filtered with a Butterworth filter to frequencies between 0.03-0.3 Hz. I considered as good measurements only the events with waveforms that exhibit both SKS energy on the transverse

component and elliptical particle motion before anisotropy correction and, those, after the correction for anisotropy, show a clear energy reduction on transverse component, rectilinear polarization of the horizontal particle motions, and a good correlation between the fast and slow waves.
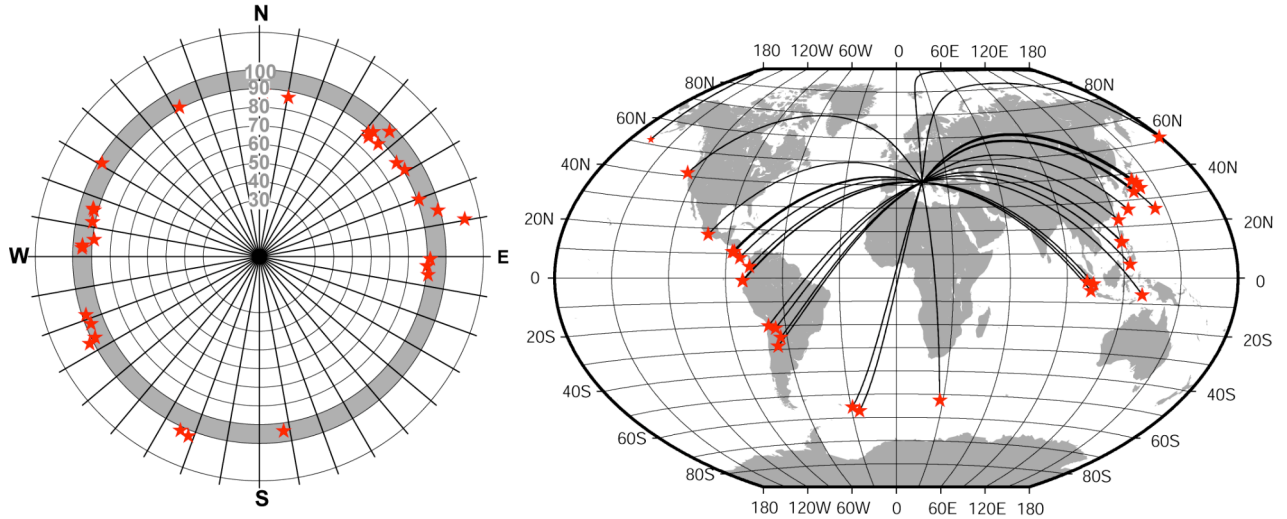
Figure 3.1 Distribution of the epicentres of the teleseisms used in this study added to those from Baccheschi et al., [2007] plotted as a function of the back-azimuth and of the epicentral distance (left). Map location of the events (right).
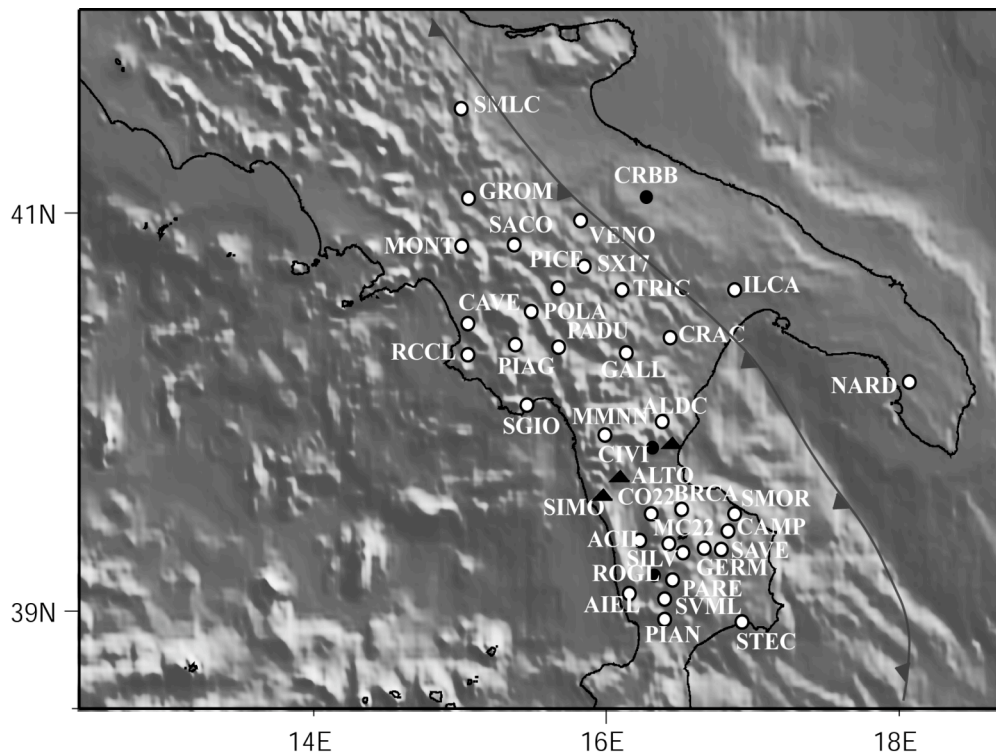
Figure 3.2 Map of the 40 CAT/SCAN temporary stations used for the splitting analysis. Black solid circles: stations used as examples in Figure 3.2. Black triangles: stations at which the 90% of seismograms are either complex and did not give a clear splitting result or gave null results.

The final collection of splitting results includes also null measurements. I considered as nulls those measurements in which the original seismograms do not show energy on the transverse component. I did not include in the results complex waveforms not resolvable by the splitting code to avoid the ambiguity between these two different results [Levin et al., 2006]. A null direction does not necessarily mean that anisotropy is absent beneath the station, but could also mean that the shear wave is initially polarized parallel to either the fast or slow direction. This second possibility is the most likely if null directions are obtained along with non-null measurements at the same station. In Figure 3.3, I show an example of null measurement, an example of a well-constrained result, and an example of complex waveform for which no results are found.

3.2 Results: geographical variations in splitting parameters

The final collection consists of 185 new SKS high quality measurements, 43 of which are nulls. For each event I report the complete list of individual shear wave splitting parameters along with station and event parameters (Table 1, Baccheschi et al., 2008). Results are mapped in Figure 3.4 and interpreted in the followings along with the splitting results obtained in the previous studies [Margheriti et al 2003; Civello and Margheriti, 2004; Lucente et al 2006; Baccheschi et al., 2007] to get a general picture of the anisotropy in the region.

I analyze and discuss the new splitting parameters results together with the results presented in Baccheschi et al. [2007]. At most of the stations used, I obtained both null and non-null results. The delay time varies between 0.6 s and 3.0 s with an average value of about 1.8 s. The value of δt is in agreement with the large delay time between fast and slow components found by other authors in the Mediterranean region [Schmid et al., 2004; Salimbeni et al., 2008] and in other subduction zones [Audoine et al., 2004; Anderson et al., 2004; Russo and Silver 1994]. Considering an average anisotropy of about 5%, then a delay time of 1.8 s would correspond to an anisotropic layer ~ 200 km thick [Mainprice et al, 2000]. In subduction zone environments, anisotropy has been inferred to exist at depths as great as 400 km or perhaps deeper [Fouch and Fischer, 1996; Fischer and Wiens, 1996]. I found the largest δt (up to 3.0 s) along the crest of the Southern Apennine chain and along the highest sector of the Calabrian Arc. It is evident that the orientation of φ is variable and changes moving from Calabrian Arc to the Southern Apennines and to the Apulian Platform. A clear separation is present in the transition zone between the Calabrian Arc and the Southern Apennines where not only the fast polarization
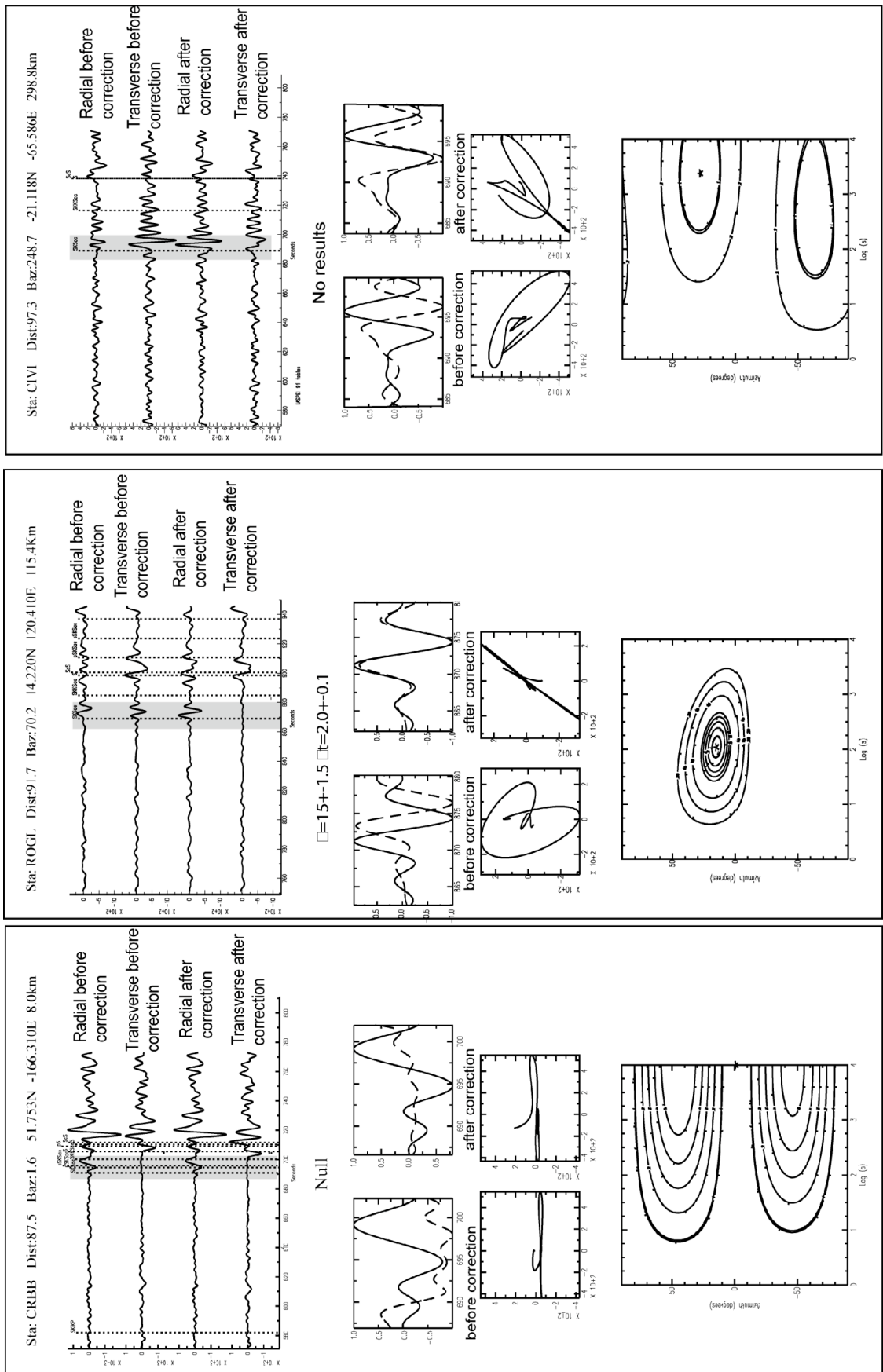
direction changes, but there is also a lack of measurements that is not related to the absence of stations and therefore of data.

At these stations (black triangles in Figure 3.2) 90% of the analyzed seismograms are either complex, and do not give clear and simple splitting results (as the CIVI example in Figure 3.3), or gave a null measurements. The Calabrian Arc and Southern Apennines show a pattern of trench-parallel fast axes. In the Calabrian Arc, fast directions are prevalently oriented NE-SW parallel to the slab strike. Moving toward the Southern Apennines, especially on its Tyrrhenian side, the fast directions rotate to follow the curved contour of the slab and are oriented NNW-SSE. Toward the Apulian Platform the orientation of φ exhibits a clear rotation from N-S in the northern sector to NNE-SSW toward the central-southern sector. The splitting results in the southernmost sector of the Apulian Platform, with fast directions oriented ENE-WSW, testify to the presence of an anisotropic mantle, whereas previous studies [Baccheschi et al., 2007] identified only nulls. In each of the studied regions, I have found some good measurements with orientation of fast directions that differs from the prevalent trend. In the following paragraphs I try to investigate the causes of the variability of the splitting parameters. I have separated the well-constrained SKS measurements in three groups: the Calabrian Arc, the Southern Apennines and the Apulia Platform; each of these corresponds to a region with a different geological and geodynamic history.

Figure 3.3 Examples of measurements: a null (left), a well-constrained splitting measurement (centre), an analysis where report no result (right). The upper panels show four traces: the radial and transverse seismograms as recorded, and the radial and transverse components after correction for the anisotropy (lower two traces). The null is evident due to the absence on the transverse component of SKS energy both before and after correction. For the well-constrained measurements SKS energy is clearly present on the transverse trace before correction and it is removed after the correction. In the no result analysis, SKS energy is clearly present on the transverse trace before and after the correction for anisotropy. The time window used for the splitting analysis is shown in grey. The four middle panels show the analysis window rotated in the fast (continuous line) and slow (dashed line) components (uncorrected (left) and corrected (right) and their respective particle motion (lower row). For the null measurement, the particle motion is linear before and after the correction; for the well-determined measurement, it is elliptical before and is linearized by the correction. The last panel displays the contour plot of energy on the corrected transverse component showing the minimum value (star symbol) of φ and δt for which the effect of stations anisotropy is best removed. The stations used in those analyses are highlighted as black solid circles in Figure 3.2.
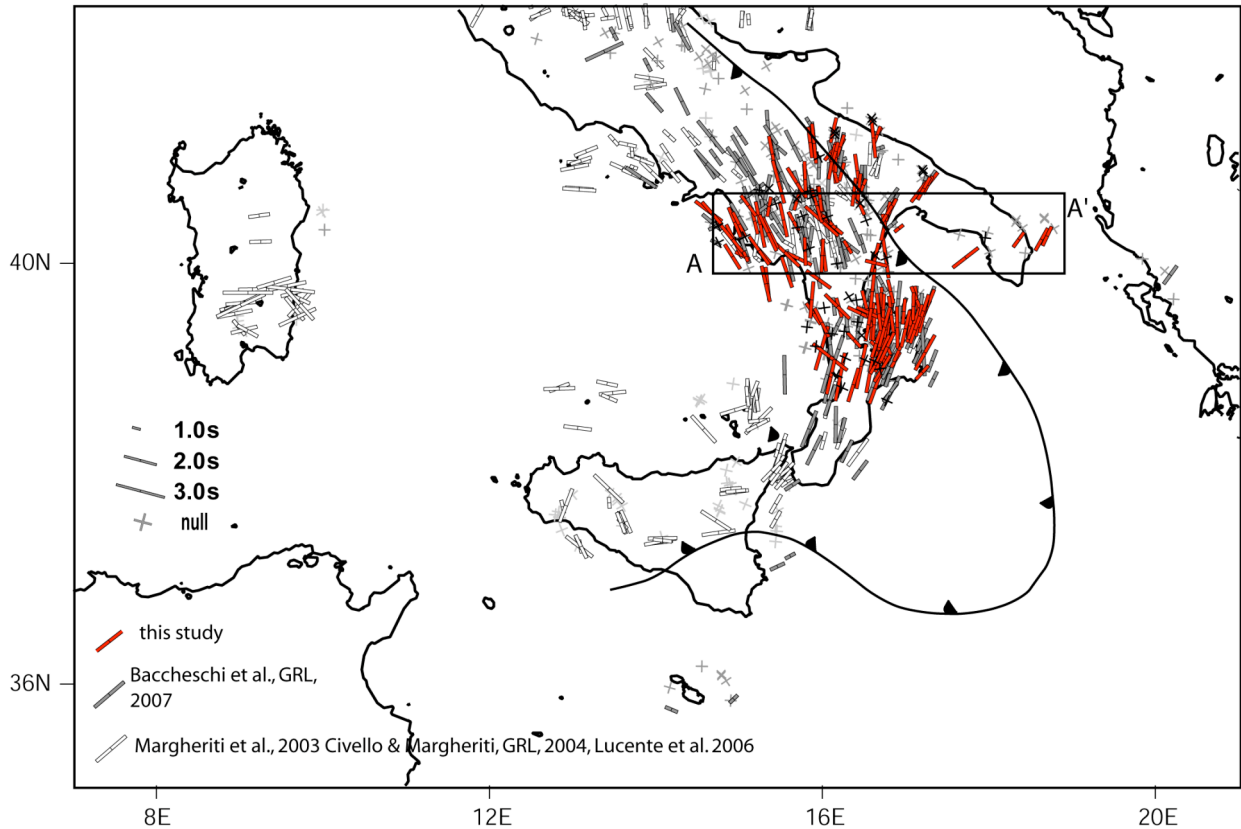
Figure 3.4 Map of SKS splitting results displayed as single measurements for individual station-earthquake pairs and plotted at the surface projection of the 150 km depth SKS ray piercing point; this depth enable us to visually separate measurements of events coming from various back-azimuths and different incidence angles. Each measurement is represented as solid bars oriented in the φ direction with a length proportional to the delay time, δt. Null measurements are displayed with two crossing-bars, one parallel to and one normal to the backazimuth. The thrust front is drawn as a solid black line.

I have made frequency plots of φ for each sector (Figure 3.5), obtaining 121 measurements for the Southern Apennines, 118 measurements for the Calabrian Arc and 37 measurements for the Apulia Platform. The rose diagrams show that the fast directions are quite stable in the Southern Apennines and Calabrian Arc, showing a prevalent trench-parallel direction. This trend suggests the existence of an anisotropic volume with uniform characteristics for each one. In the Apulia Platform, fast directions are less homogeneous and might reflect a more complicated anisotropic structure.
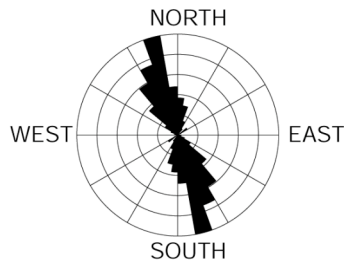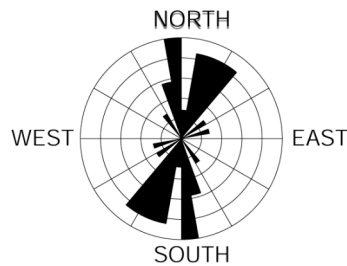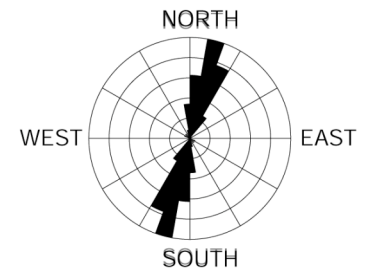
Figure 3.5 Rose frequency plots for the three different geological domains. The trend of each petal represents the azimuth φ of the fast split shear wave and the length is proportional to the number of measurements in the same interval of φ (at 10° intervals) weighted by the delay times of the measurements.

The prevalent φ is N-S, but NNE-SSW and ENE-WSW directions are also common. The N-S direction prevails in the northern sector of the Apulia Platform, while the NNE-SSW and ENE-WSW φ are found farther south together with several null measurements. The existence of regions each one with uniform anisotropic pattern, suggest a lateral variation in anisotropic structure. Even if I cannot exclude the existence of a volume with inclined fast axis, I prefer to interpret the variation in anisotropic parameters in terms of lateral or vertical variation of anisotropic volumes with horizontal fast axis following the initial hypothesis corresponding to the Silver and Chan (1991) method used.

3.2.1 Splitting parameters variability versus back-azimuth

In order to check for possible dependence between the back-azimuth and the anisotropic parameters I have grouped the stations of each anisotropic domain and I plot fast directions and delay times versus back-azimuths (Figure 3.6). The results obtained in this study are combined with the splitting measurements in Baccheschi et al. [2007]. Analyses of several events coming from different back-azimuth are needed to clarify the complex fabric of the anisotropic structures at depth [Levin et al. 2006; Long and van der Hilst, 2005]. Consideration of the distributions of φ and δt versus the back-azimuth on the diagrams (Figure 3.6) should be viewed with caution since each plot includes a large number of stations. I discuss the plots for the Southern Apennines and for the Calabrian Arc, while for the Apulian platform the number
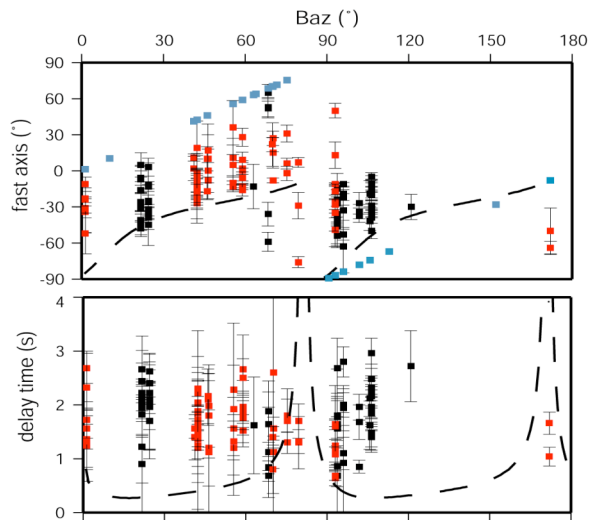
SOUTHERN APENNINES

lower layer: **f** = -65; **dt** = 0.5
upper layer: **f** = -20; **dt** = 0.7
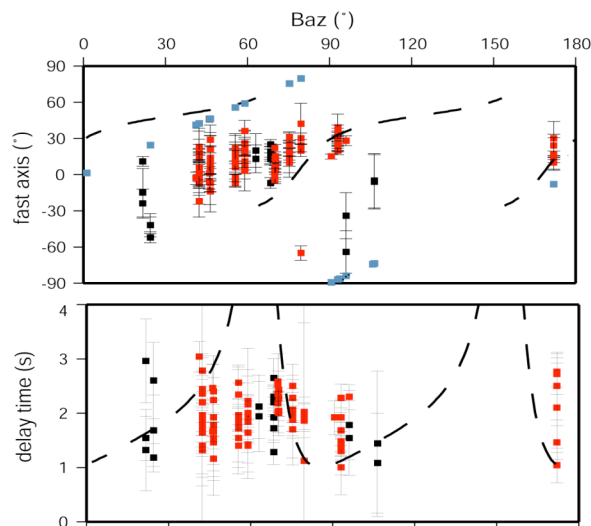
CALABRIAN ARC

lower layer: **f** = 85; **dt** = 1.5
upper layer: **f** = 20; **dt** = 1.0
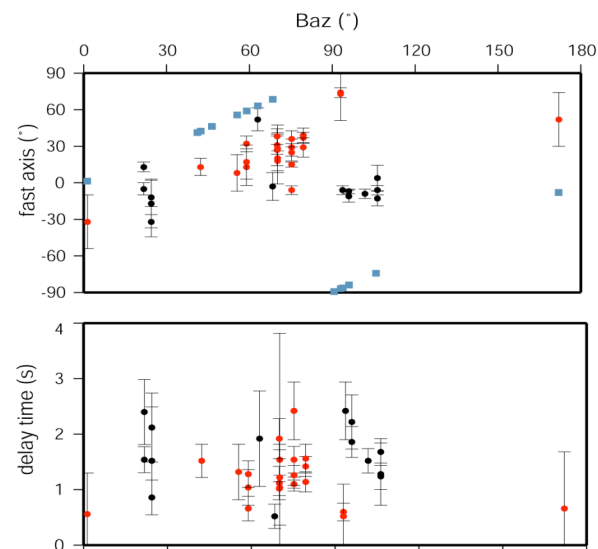
APULIAN PLATFORM

W° = black solid circles
E° = red solid circles
NULLS = blue square

of non-null measurements is not sufficient for such analysis. In Southern Apennines and in Calabrian Arc the measurements show a uniform pattern, suggesting that the anisotropic structure beneath the stations should be quite homogeneous. It is interesting to note that the measures that deviate from the most common fast direction are found for specific back-azimuth: measurements in the Southern Apennines with back-azimuths of about 70° and 70° +180° are much more scattered than the other measurements. In the Calabrian arc measurements coming from back-azimuth of about 20° and 20°+180° have values different from the most common. This may imply the presence of a layered anisotropic structure beneath the stations [Rumpker et al., 1999; Silver and Savage, 1994]. For each of those two domains I have investigated the possible depth-dependent anisotropy by computing a large number of two-layer models trying to fit the observed measurements but none of the model fit the data sufficiently suggesting that the anisotropic structure in the investigated regions is more complicated than a two-horizontal-layer model.

3.2.2 Splitting parameter variability along an E-W transect

The pattern of SKS splitting for the Southern Italy show a change of the fast axes orientation moving from the Southern Apennines to the Apulian Platform. To constrain the position of where this change take place, I have displayed the value of φ and δt along an E-W transect (Figure 3.7) running from the Tyrrhenian Sea to the Adriatic Sea at about latitude 40° (box AA' in Figure 3.4). The fast axes rotate from NW in the Southern Apennines to NE in the Apulian Platform. I observe two groups of fast directions; one with values between -50° and 20° related to the Southern Apennines domain; the other with values of φ between 30° and 70° related to the Apulia Platform domain. The rotation of fast directions takes place almost at the surface tectonic boundary between those different tectonic domains and corresponds to a distance along the profile of about 130 km.

Figure 3.6 Plots of the fast directions and delay times (with their errors) versus the backazimuth of each analyzed events are presented for each of the three different domains. Red solid squares indicate the events coming from east (rays that on average sample the sub-slab mantle); black solid squares indicate the events coming from west (rays that on average sample the slab). Null measurements are represented by blue squares and plotted as a function of back-azimuth.
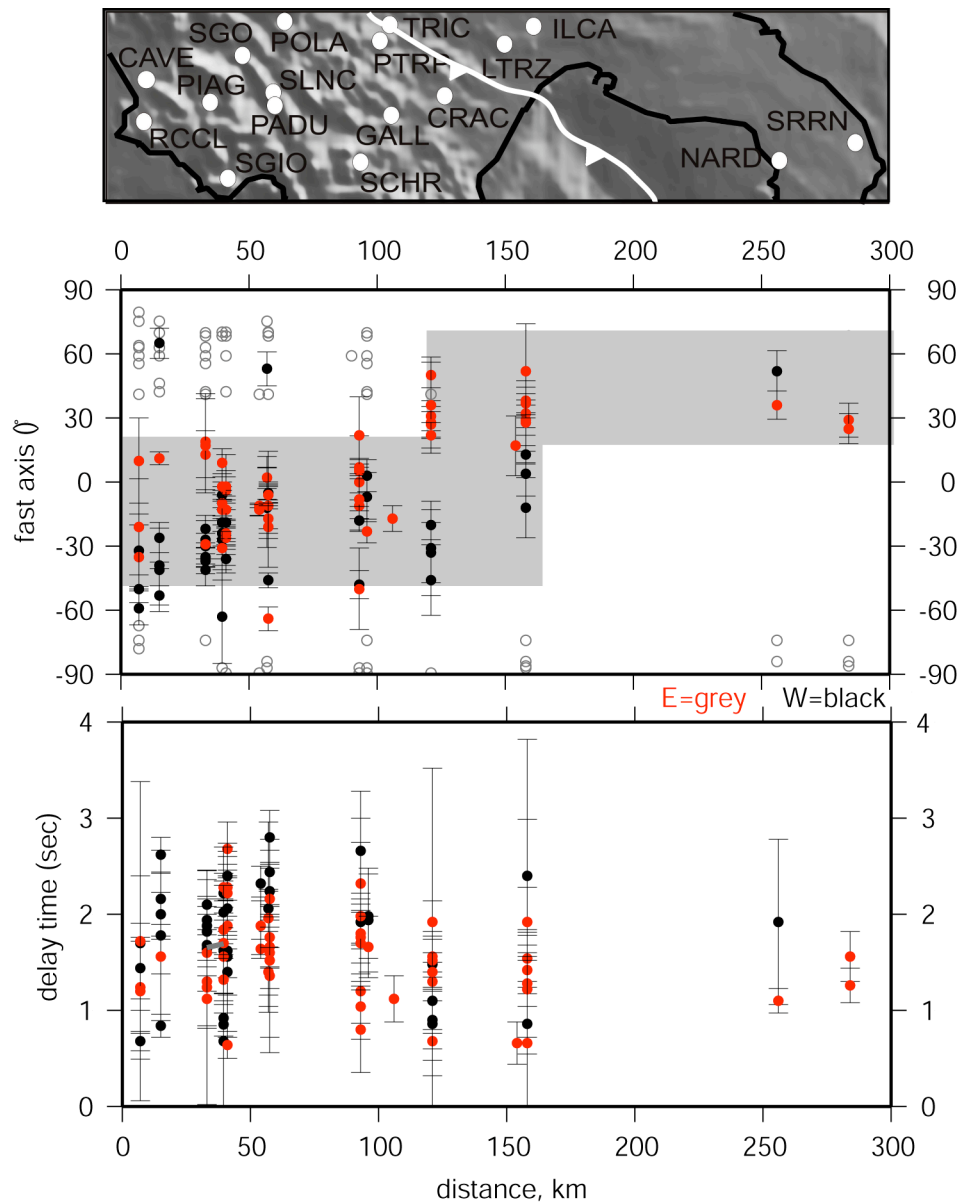
Figure 3.7 Splitting parameters across the Southern Apennines and Apulia Platform along the E–W transect from the Tyrrhenian coast to the Adriatic coast (box AA′ in Figure 3.4). φ and δt (second and third panel) are plotted as a function of the distance of the stations from the Tyrrhenian coast. Black solid circles: events coming from the west (back-azimuths between 0° and −180°); red solid circles: events coming from the east (back-azimuths between 0° and 180°). Open circles: null measurements. The first panel shows the map location of the stations. The white line represents the thrust front. The change in the fast directions between the Southern Apennines and the Apulian Platform domains occurs at 120–150 km distance from the Tyrrhenian coast. The shaded area in the middle panel shows the most frequent fast directions in the two domains. The third panel presents the delay times versus distance.

At stations located at this transition, NW-SE fast directions are found for events coming from west and NE-SW fast directions are found for events coming from east. This may imply the presence of a steep boundary between the two domains.

3.2.3 Lateral variation and depth of seismic anisotropy from Fresnel zones

The variability of splitting parameters at the stations located near the boundary between the Southern Apennines and the Apulia Platform for events coming from opposite back-azimuths allows us to hypothesize the existence of a near vertical boundary between these two anisotropic regions. If this assumption is correct and if I am in presence of two anisotropic domains with horizontal fast axes, it is possible to give some constrains on the depth of the anisotropic region. According to the method described by Alsina and Sneider [1995], I have estimated the upper limit of the depth of the anisotropic region by calculating the Fresnel zones. The size of the Fresnel zone at a given depth is given by [Pearce and Mittleman; 2002]:

$$Rf = \frac{1}{2} \sqrt{Tvh}$$

where Rf is the radius of the zones, T is the SKS dominant period (10 s), v is the wave velocity (4.5 km/s from the IASP91 model) and h is the depth.

Considering two teleseismic events with opposite back-azimuth recorded at the same station and with different splitting results, the anisotropic domain is estimated to be deeper than a certain depth I note as Z_1. Above Z_1 the rays travel through the same medium and the corresponding Fresnel zones overlap. Below this depth the ray paths and Fresnel zones for the two events are distinct, as shown by the difference in splitting parameters observed for the two events. For our analysis I have used three stations (TRIC, ILCA and CRAC) located along the transect at the transition zone between the Southern Apennines and the Apulian Platform (Figure 3.8). At each of those stations, I have analyzed two teleseisms with opposite back-azimuth, obtaining two different values of fast directions. I have calculated the Fresnel zones at 50, 100, 150 and 200 km depth. Our results show that the Fresnel zones partially overlap at a depth of 50 km, indicating that above that depth they will be sampling roughly the same volume. In contrast, for the other depths, the corresponding Fresnel zones are separated, indicating that the rays sample different volumes below 50 km depth. These considerations allow us to suggest that the main source of anisotropy is located below 50 km depth and that the

primary source is therefore not in the crust, at least a the transition zone between the Southern Apennines and the Apulian Platform.
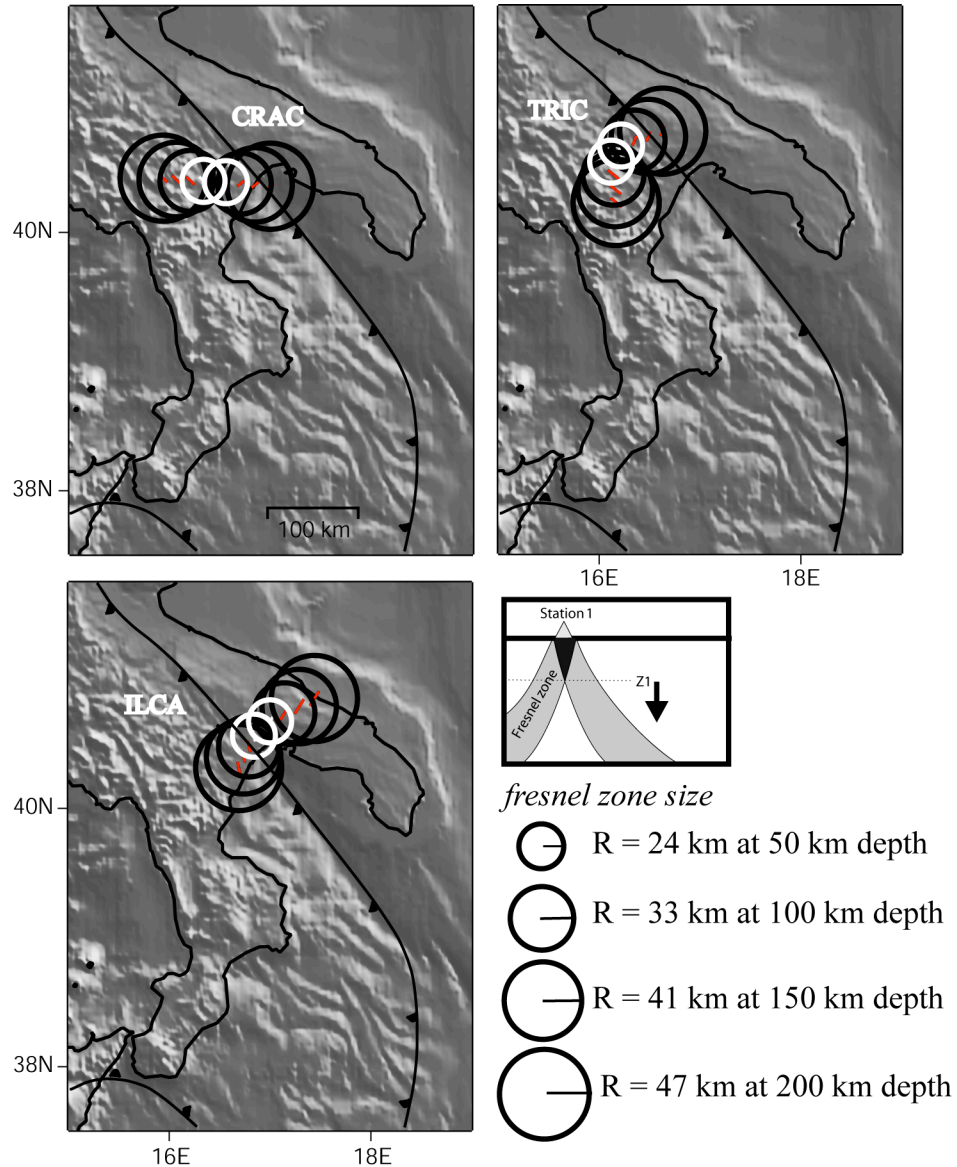
Figure 3.8 Fresnel zones calculated at the stations CRAC, TRIC and ILCA close to the tectonic and geological boundary between the Southern Apennines and the Apulia Platform. For each station I used two teleseisms with opposite back-azimuth and I have calculated the Fresnel zones radius at 50 km (white circles), 100, 150 and 200 km (black circles) depth. The circles particularly overlap at 50 km depth, indicating that below this depth the path of the rays differ. This suggests that the anisotropic domain is below 50 km depth. The trench is drawn as solid black line.

3.3 Discussion

The increased number and the close spacing of seismic stations installed in Southern Italy in the framework of the CAT/SCAN and CESIS (Centro per la Sismologia e l'Ingegneria Sismica) projects enabled us to collect a large number of shear wave splitting measurements that has helped us to characterize the anisotropy distribution and the mantle fabric of Southern Italy.

It is widely accepted that in the upper mantle, the most likely mechanism that generates seismic anisotropy is lattice preferred orientation (LPO) of the anisotropic olivine crystals. Several studies show that subduction zones exhibit a broad range of splitting directions. Many convergent margin zones are characterized by arc-parallel fast directions, as in the Tonga [Fischer and Wiens, 1996] and in the Mariana subduction zones [Fouch and Fischer, 1998; Pozgay et al., 2007]. Trench-sub parallel fast directions are found in New Zealand [Audoine et al., 2000], in the Ryukyu arc [Long and van der Hilst, 2006], in Japan [Long and van der Hilst, 2005] and South America [Polet et al., 2000]. Other subduction zones exhibit both trench-perpendicular and trench-parallel fast directions, as in Lau back-arc [Smith et al., 2001] and Kamchatka [Peyton et al., 2001]. This variable pattern of shear wave polarization direction can be explained considering the large and extremely different factors which affect and complicate the anisotropy, such as the influence of water on olivine deformation [Jung and Karato, 2001], effects of dynamic recrystallization [(Kaminski and Ribe, 2001], strain partitioning between melt-poor and melt-rich regions [Holtzman et al., 2003; Kaminski, 2006], local-scale flow in the mantle wedge induced by the subducting plate motion [Vinnik and Kind, 1993; Gledhill and Gubbins, 1996], and frozen lithospheric anisotropy in the slab (Plomerova et al., 2006). Moreover, the presence of slab edges, their geometry, tears in the slab and discontinuities may further complicate the flow pattern [i.e., Peyton et al., 2001].

The orientation of anisotropy can be altered by the water [Jung and Karato, 2001]. For systems with very little or no hydration, LPO of olivine fast axes are aligned with the direction of flow in the dislocation creep regime [Zhang and Karato, 1995; Tommasi et al., 2000]. Experimental studies suggest that olivine slip systems change under higher stress and hydration states [Jung and Karato, 2001]. Since in subduction zones there are regions where these last conditions likely exist, the development of olivine LPO may be significantly influenced by them [Kaminski et al. 2004], especially in the forearc [Kneller et al., 2005]. In this study, such a volume corresponds to the offshore region in the Tyrrhenian Sea between Calabria and the Aeolian Islands and, likely, is not sampled by the SKS rays analyzed. Our SKS splittings are

the results of anisotropy in the slab and subslab mantle and I interpret them in terms of LPO of olivine due to strain associated with flow in the asthenospheric mantle.

3.3.1. Is anisotropy related to lithospheric fabric or asthenospheric flow?

The pattern of splitting parameters observed in this study seems to be consistent with a primary source of the anisotropy localized into the asthenosphere. Most of the delay time values are larger than 1.5 s. The average value is 1.8 s: if I consider an anisotropy of about 5% [Mainprice et al., 2000], a δt of 1.8 s would correspond to a thickness of the anisotropic layer of ~ 200 km. This implies that the main source of anisotropy cannot be contained in the lithosphere, which is not thicker than 100 km in the area [Panza et al., 2007]. The Fresnel zone analysis seems to exclude the source of shear wave splitting from being located in the upper 50 km, at least at the boundary between Southern Apennines and Apulian Platform. Moreover, the presence of the slab rollback is a reasonable cause of an active asthenospheric flow induced by the motion of the slab and which I interpret as being responsible for most of the observed anisotropy. In Southern Apennines and in Calabrian Arc, the observation of some back-azimuthal dependence of fast directions and delay times allow us to hypothesize the existence of vertical variations in anisotropy and also suggests a possible lithospheric contribution to the anisotropy there.

3.3.2. Possible pattern of asthenospheric flow

If i interpret the anisotropic parameters in terms of asthenospheric flow, the trench-parallel fast directions observed in Southern Apennines and in Calabrian Arc are likely due to the pressure induced by retrograde motions of the slab [Buttles and Olson, 1998] which induces the mantle to move horizontally around it creating a local-scale mantle flow below the subducting plate. The slab acts as a barrier at depth, forcing the mantle to flow parallel to its strike [Russo and Silver, 1994]. Moving from south to north fast axes rotate to follow the arcuate shape of the mountain chains and the curve of the continuous Calabrian slab. Between the Calabrian Arc and the Southern Apennines I see a great continuity in fast directions, but I also observe a lack both of null and non-null measurements in the transition zone between these two different geological domains. Geological models for the evolution of the Calabrian Arc include a left-lateral offset between the Calabrian Arc and Southern Apennines of variable size [Rosenbaum and Lister, 2004; Faccenna et al., 2005], which could result in a complex transition zone characterized by incoherent anisotropic fabric in the mantle [Plomerova et al. 2001]. Mantle flow may also be

complicated by the presence of tears at the edges of the Calabrian slab, as revealed by some tomographic images [Piromallo and Morelli, 2003]. A tear in the slab may allow the mantle to flow through it, creating a return flow from behind the subducting plate to the front of the slab [Matcham et al., 2000]. Some local studies of anisotropy [Civello and Margheriti, 2004] identify a mantle return flow beneath the Sicily Channel through the tear at the SW edge of the Calabrian slab. Baccheschi et al. [2007] did not find such a return flow also in the N-E edge of the same slab, where tomographic models identify another tear. In this study I have added measurements below the southern Apennines, which show fast axes oriented prevalently NNW-SSE. This confirm the idea that any existing tear is not wide enough to allow to the mantle to flow horizontally through it (Figure 3.9), or that the tear is too young to reorganize the olivine structure [Faccenna et al., 2005]. The delay times corresponding to the slab parallel fast directions are very high (several measurements are higher than 2.0 s) suggesting that the mantle is deformed by the retrograde motion of the slab up to a depth of about 300 km, where no tear is shown by tomographic images (Figure 3.9).

3.3.3. Anisotropy in the subduction foreland

Interesting results are observed in the Apulia. The main observation is the absence of fast directions parallel to the strike of the slab. This different pattern of splitting measurements could be related to previous geodynamic events frozen in the Apulian Platform lithosphere and, more generally, in the Adriatic microplate. Fast axes are oriented N-S in the northern sector, which show the same pattern of splitting measurements found by previous studies [Margheriti et al. 2003, Schmid et al., 2004] in the Adriatic microplate along the Italian Coast and along the Dalmatian Coast on the western flank of the Dinarides mountains. In particular, in the easternmost sector of the Northern Apennines not arc-parallel and oblique fast directions were found [Plomerova et al. 2006]. Moving toward the southern sector of the Apulia Platform fast axes rotate and show a prevalently NNE-SSW to ENE-WSW directions; in this sector most of the analyzed waveforms return null measurements. This change in splitting parameters between the northern and southern sector of the Apulia Platform is found around latitude 40°N which could testify some past or current deep discontinuities inside the Adriatic microplate. The orientations of fast directions found in the Apulia Platform are different from to the ones observed in the adjacent Southern Apennines. This change takes place almost at the surface tectonic boundary between those two different geological sectors.
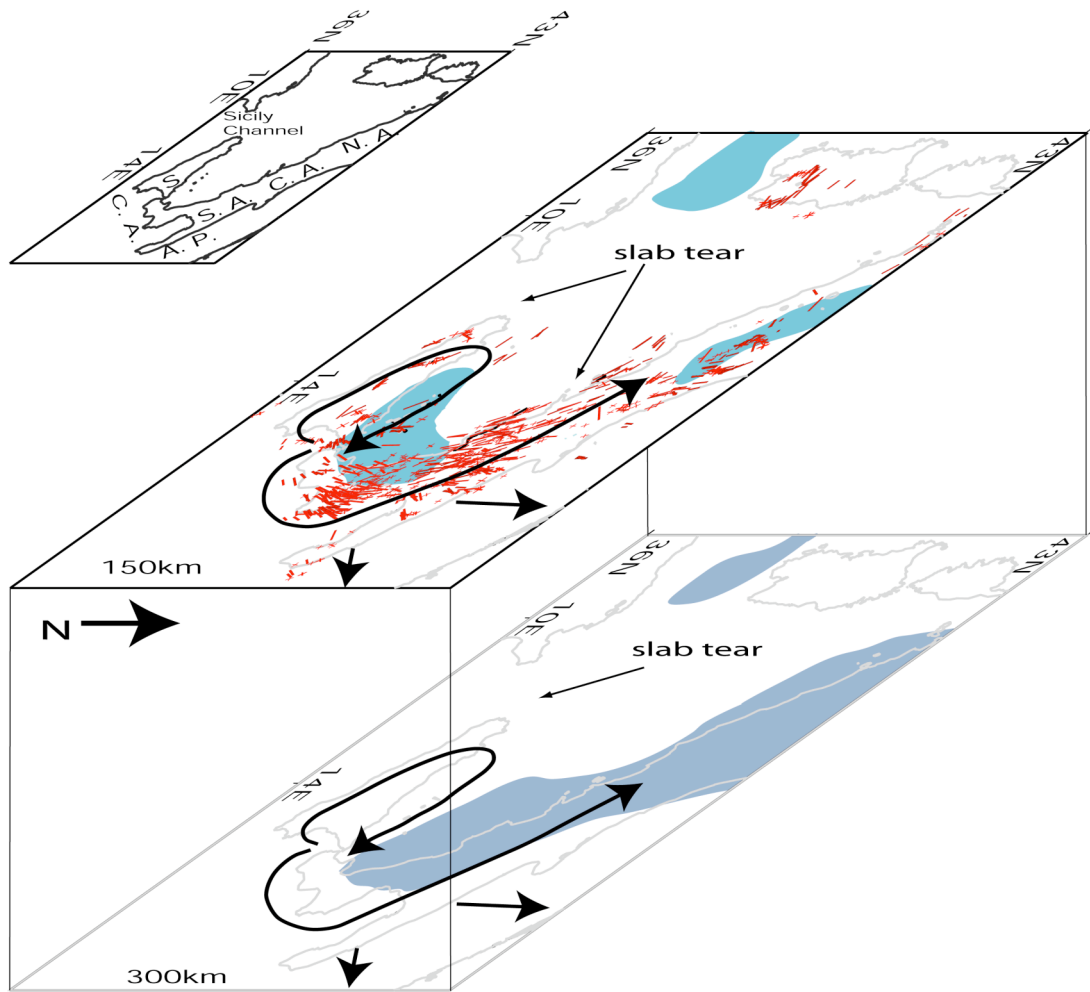
Figure 3.9 Model of possible mantle flow trajectories induced by slab rollback and subduction. The SKS splitting measurements at 150 km depth are shown as black bars. I display the image of the slab (grey blobs) at 150 and 300 km depth, as inferred from the P-waves tomography [Piromallo and Morelli, 2003]. At 150 km depth, two slab tears are evident, one below the Sicily Channel and the other one below the transition zone between the Southern Apennines (S. A.) and Central Apennines (C. A.). At 300 km depth, the tear below the Sicily Channel still exists, while the tear below the Southern Apennines–Central Apennines is absent and the slab forms a continuous body. The large black arrows indicate the mantle flow trajectories around the slab. According to the SKS splitting results, mantle is hypothesized to flow around the slab, describing a ring around the SW edge of the slab through the tear imaged at 150 km and 300 km depth beneath the Sicily Channel. Our results do not identify such a return flow also through the tear at the N–E edge of the slab, where the pattern of SKS fast directions allow us to hypothesize a mantle flow parallel to the strike of the slab. The black arrows in the Apulian Platform (A. P.) indicate the possible frozen-in deformation not controlled by the slab rollback, as deduced by the slightly not trench-parallel pattern of fast axes.

If the flow beneath the Southern Apennines represents the zone of flow induced by the rollback of the slab, then the edge of the zone where the flow is sufficiently strong to have reoriented the mantle fabric is relatively sharp. The almost trench-perpendicular splitting distributions in Apulia could be interpreted as a mantle flow not controlled by the slab presence and geometry and not involved in the retrograde motion of the slab. Together, these considerations suggest a very focused mantle flow below the slab and that the presence and the rollback of the slab horizontally influence directly the mantle deformation only in a limited zone (less than 100 km) close to the subducting plate. In contrast, the observed seismic anisotropy properties in Apulian Platform could be related to frozen-in fossil flow beneath the Adriatic microplate or to local asthenospheric flow deflected by the roots of the Dinarides away from the orogen-parallel direction. Moreover, the slightly lower values of δt and the abundance of nulls in the weakly deformed Apulian foreland would suggest a possible lithospheric contribution in this domain.

3.4 Conclusion

SKS splitting results collected in this study reveal the existence of strong and complex seismic anisotropy beneath the Southern Italy. Numerous and closely spaced stations allowed me to better constrain the anisotropic structure of the mantle. I observe different fast axes orientations in three different tectonic and geological domains, each one is characterized by relatively uniform anisotropic parameters. In the Southern Apennines and in the Calabrian Arc fast axes show predominantly trench-parallel orientation. The clear rotation, from south to north, of fast directions to be parallel to the strike of the slab suggest that the anisotropy is closely controlled by subduction and by the rollback motion of the slab. The combination of those two processes would be responsible for activating mantle flow below and around the slab itself. The scarce number of trench-perpendicular φ at the northernmost stations of the Southern Apennines does not favour the hypothesis of a return flow around the NE edge of the Calabrian slab through a slab gap in the Southern Apennines. I conclude that any slab tear below the Southern Apennines is young and not wide enough to have allowed the reorganization of mantle flow. I observe a large average delay time (1.8 s) especially in Southern Apennines and in Calabrian Arc that seems to be consistent with the primary source of anisotropy localized into the asthenosphere. Moreover, the observations in Southern Apennines and in the Calabrian Arc of some back-azimuthal variations lead us to consider the existence of depth-dependent anisotropy which should be more complicated than a two-layer model. Moving from the Southern Apennines to the adjacent Apulian Platform, our results show a change in the fast direction orientations from

trench-parallel to oblique with respect to the slab strike. This not trench-parallel fast axes distribution reflects the pattern observed in the larger Adriatic microplate, with fast directions ranging from N-S to NNE-SSW to ENE-WSW. Therefore in this microplate the anisotropic fabric appears not to be controlled by subduction geodynamics but could be related to a frozen-in lithospheric fossil flow or to a local asthenospheric flow determined by the interaction between Calabrian slab motion and the Dinarides roots.

CHAPTER FOUR

Anisotropy patterns in the subducting lithosphere and in the mantle wedge from slab earthquakes

After discovering the large scale anisotropic structure of the region, the second purpose of this study has been to investigate the anisotropic fabric of the descending slab and of the mantle wedge above the slab. The aim was to better comprehend how the slab deforms and how interacts with the surrounding mantle. To do this, a useful approach has been the splitting analysis on direct S waves originating within the descending plate. There exist some advantages in using this approach. Indeed, unlike SKS waves, which are sensitive to anisotropy from the core-mantle boundary to the station, local S phases propagate from a seismic source within the slab to the stations and, therefore, sample anisotropy only in the subducting lithosphere, in the mantle wedge above it and in the overriding plate. Furthermore, while the SKS have incidence angle close to the vertical (10°–15°), the incoming local shear waves arrive at the station with incidence angles varying from vertical to horizontal. This wide range of incidence angles can be only partially utilized for anisotropy studies: in fact, only waves with incidence angle smaller than 35° can be analyzed. Anyway, this large range os incidence angles allows the direct S to be more receptive to the lateral variations of the anisotropic structures than SKS.

The Southern Italy Subduction system presents unique station distribution relative to the geometry of the subduction itself: the main massif of Calabria is an uplifted fore-arc centered 100 km trenchward of the volcanic arc (Figure 4.1). Generally, most of the stations monitoring subduction systems are located along the volcanic arc (i. e. Japan). This peculiar setting of outcropping land allows most of the S rays coming from the deep local earthquake to stations in Calabria to travel for almost their entire ray-path inside the slab, giving us a unique opportunity to detect and isolate anisotropy in the slab. Therefore, this study represents the first attempt to distinguish the different sources of the anisotropy in the Southern Italy subduction system.

4.1 Data

I analyzed the shear wave splitting from earthquakes recorded by 78 stations of the INGV national permanent network. I also used the data recorded at 40 temporary digital broadband seismic stations operating from 2003 to 2005 in the study area [CAT/SCAN project: Calabrian-

Apennine-Tyrrhenian/Subduction-Collision-Accretion Network] (Figure 4.1). I used earthquakes located within the slab and recorded during the period 2003-2008. The local S phases propagate from the seismic source within the slab to the station and, therefore, sample anisotropy only in the slab itself, the mantle wedge, the overriding plate and the crust. In addition, the local shear waves arrive at the station with incidence angles varying from 0° to 35°, making the splitting measurements more sensitive to the lateral variations of the anisotropic structures.
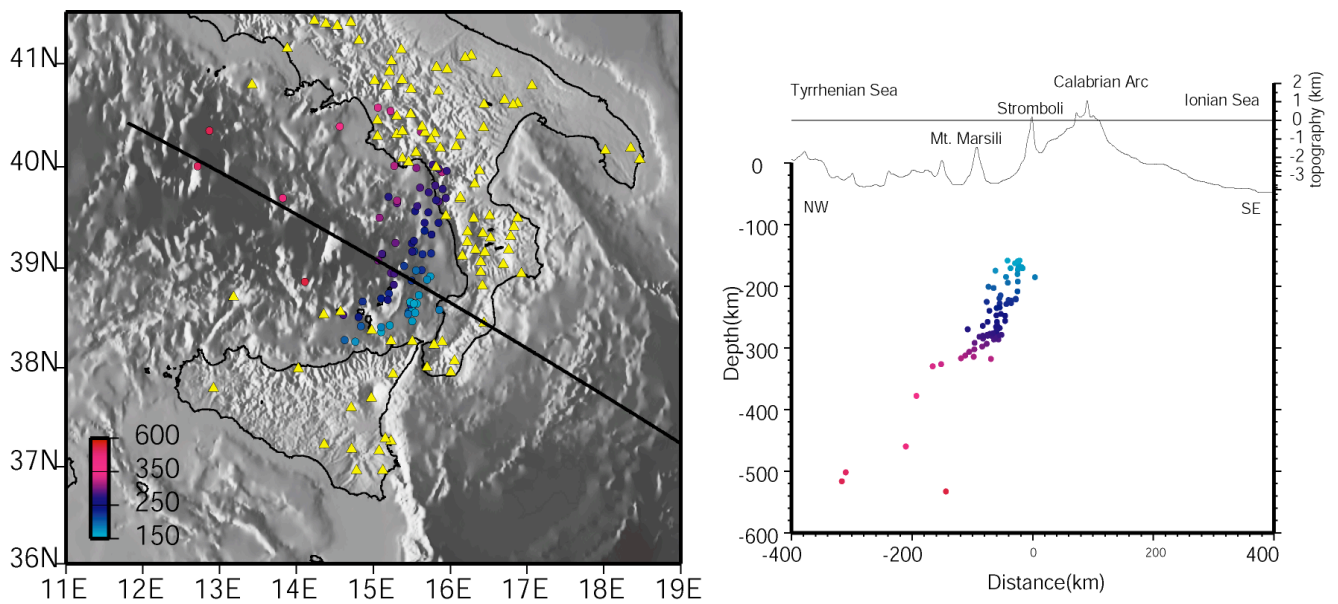
Figure 4.1 (Left) Map of the intermediate and deep earthquakes used in this study (black circles) The events were selected with M ≥ 3.0 and with depth ≥ 150 km. We collected 76 earthquakes. The stations used for the splitting analysis are symbolized with triangles. The line is the trace of the section in b. (Right) Intermediate-deep earthquakes analyzed projected into cross-section oriented NW-SE across the Ionian slab from the Tyrrhenian Sea to Ionian Sea. The hypocenters delineate a plane that well define the geometry of the NW steeply dipping slab down to about 550 km. The vertical section crosses Stromboli as well as Marsili (see also the Figure 1): Stromboli is one of the volcanic island of the Eolian Island. Marsili is a submarine volcano and has been recentrly interpreted as a super-inflated spreading ridge of the surrounding Marsili basin [Nicolosi et al., 2006].

I selected 76 local deep events with hypocentral depth ranging from 150 to 550 km. Most events are located between 200 and 300 km depth (Figure 4.1). In order to ensure the high quality of the splitting measurements, event-station pairs were selected using the following criteria: 1] I searched only for earthquakes located within the shear wave window, analyzing

ray paths with geometrical incidence angle < 45°, which correspond to about 35° of incidence angle. The shear-wave window is defined by a critical angle, ic = arcsin(*Vs/Vp*), where *Vp* and *Vs* are the P-wave and S-wave velocities, respectively. If the incidence angle is greater than ic, then the shear waves interact with any free surface or interface. Keeping the angle less than ic avoids complications on particle motions deriving from S to P converted phases [Booth and Crampin, 1985], free-surface effects [Nuttli, 1961] and phase changes at crustal discontinuities [Liu and Crampin, 1990]. The critical angle defining the shear-wave window is about 35°, but ray curvature due to low-velocity surface layers usually allows the window to be enlarged to angles of geometrical incidence of 45 or 50 degrees; 2] I defined a magnitude threshold M=3.0 and retained only events that showed, at visual inspection, a good signal-to-noise ratio at most stations. In order to improve the signal-to-noise-ratio all the events have been filtered applying a four-pole Butterworth band-pass filter with corner frequencies at 0.5 Hz and 2.0 Hz. 3] I retained only events that showed a clear S-wave arrival phase on the horizontal components. To compute the shear-wave polarization azimuth and delay time, I used the method described by Silver and Chan [1991], assuming that shear waves pass through a medium with homogeneous anisotropy and with an horizontal fast axis. The aim of this method is to linearize the particle motion of the first S-wave arrival on the horizontal plane by minimizing the smaller of the two eigenvalues of the covariance matrix. The method utilizes a grid search over the possible values of φ and δt and gives an error associated to the measurement equivalent to its 95% confidence.

I retained as good the splitting parameters that, when the method is applied to the waveforms to minimize anisotropy, result in a rectilinear polarization of the horizontal particle motion and a good correlation between the fast and slow waves. In Figure 4.2 I show three examples of splitting results measured at the stations SERS, PALZ and AMUR

4.2 Shear wave splitting results

The splitting parameters φ and δt were calculated for each event-station pair. I analyzed a total of 2533 pairs and the final collection consists of 433 well-constrained anisotropy measurements (Figure 4.3; Table 1 in Baccheschi et al, under review, JGR). Stations located on the Eolian volcanic arc (IACL, IFIL, IVPL) are the noisiest: the analysis was performed on 50 event-station pairs, but I retained only 8 good measurements. This could be attributed to the reduced quality of the S wave signal due to the high scattering and attenuation of the S waves in the volcanic region [Salmon et al., 2003: Audoine et al., 2004].
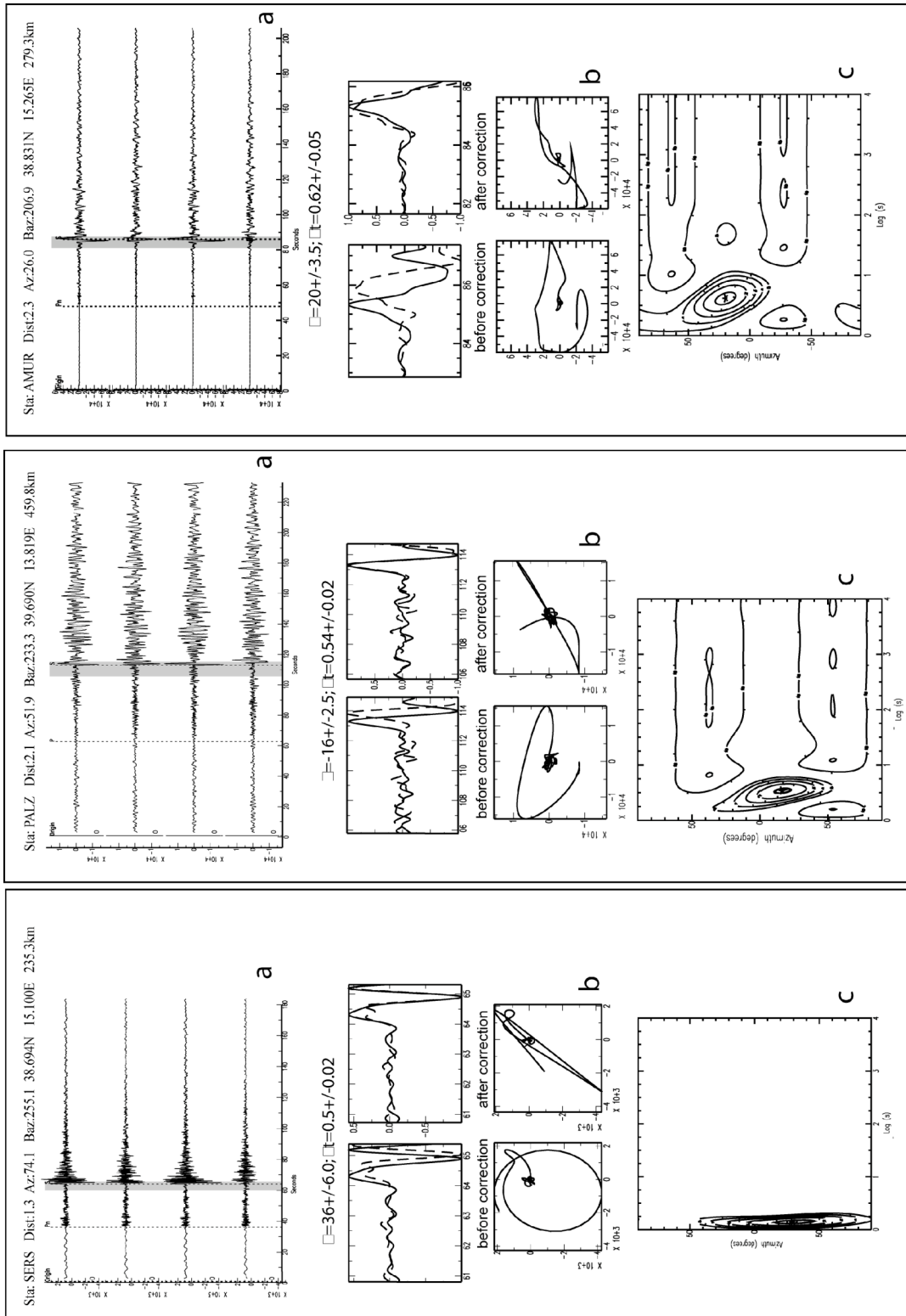
Figure 4.2. Examples of good splitting observations. **a)** The radial and transverse components before (top traces) and after (bottom traces) splitting corrections. **b)** upper panels: waveform rotated into the fast (continuous line) and slow (dashed line) components before (left) and after (right) correction for the anisotropy. Bottom panels: particle motion before (elliptical) and after (linear) correction. **c)** error estimate associated with the φ-δt pairs that best resolve the anisotropy. The star symbol represent the minimum value of the best fitting parameters along with the 95% confidence region (thick contour).

The local S anisotropic results are complex and show high variability in the spatial distributions of fast directions and in the delay time values. The delay time is characterized by values that vary between 0.1 up to 2.2 s. The averaged splitting delay is 0.53 s with a standard deviation of 0.37 s. The values of delay time are not simply and directly related to the event hypocentral depth, even though δt values larger than 1.5 s are only found for events deeper than 200 km (Figure 4.3b). The fast directions span all the possible azimuths with no clear relation to the hypocentral depth (Figure 4.3b). The fast directions are variable but the frequency plot of the entire measurement set shows that most of the measurements are in the NE-SW direction, parallel to the slab strike with a secondary peak roughly perpendicular to this (Figure 4.3a, inset). Single S-wave splitting results are mapped in Figure 4.3, where each measurement is projected to the 100 km depth S ray piercing point. I choose this depth to have measurements distributed in the volume sampled by the rays (all selected events have hypocenters deeper than 150 km) and not concentrated at the stations. In addition, SKS splitting results in previous studies suggested that most of the anisotropy was concentrated between 100 and 200 km depth [Baccheschi et al., 2008 and references therein]. The event-stations pair geometry and the decision to project measurements at depth determines the distribution of the measurements in Figure 4.3a. They very well sample the slab on the western side of Calabria showing variable fast direction and generally small delay times. Moving toward the Tyrrhenian Sea a smaller set of rays sample the mantle wedge above the slab. These also show a large variability of the fast direction but yield larger delay times. In NE Sicily, at the southwestern edge of the slab (as defined by deep seismicity) the measurement coverage is sparse and the delay times in this region are generally on the order of 0.5 s. In the Southern Apennines at the northeastern edge of the slab (as defined by deep seismicity) splitting measurements show larger delay times near the Tyrrhenian coast and a trend of fast directions run parallel to it. The fast axes rotate to become about E-W in the northern part, between 41° and 42° N, near Ventotene. In this region splitting times decrease. They also decrease inland toward the Apennines Chain and southward toward Cilento.

4.2.1 Looking for coherent patterns of splitting results at single stations

In order to check how the fast polarization directions vary with back azimuth and incidence angle we represented the φ and δt results on equal area projection (Figure 4.4). This projection shows the azimuth and incidence angle of the split S waves. We plot the results of this analysis at 16 of 118 total stations, those that recorded more than 8 high-quality splitting measurements.

The equal area projections show that the azimuths at each station span 90-180 degree and the incidence angles are mainly between 15 and 45 degree.
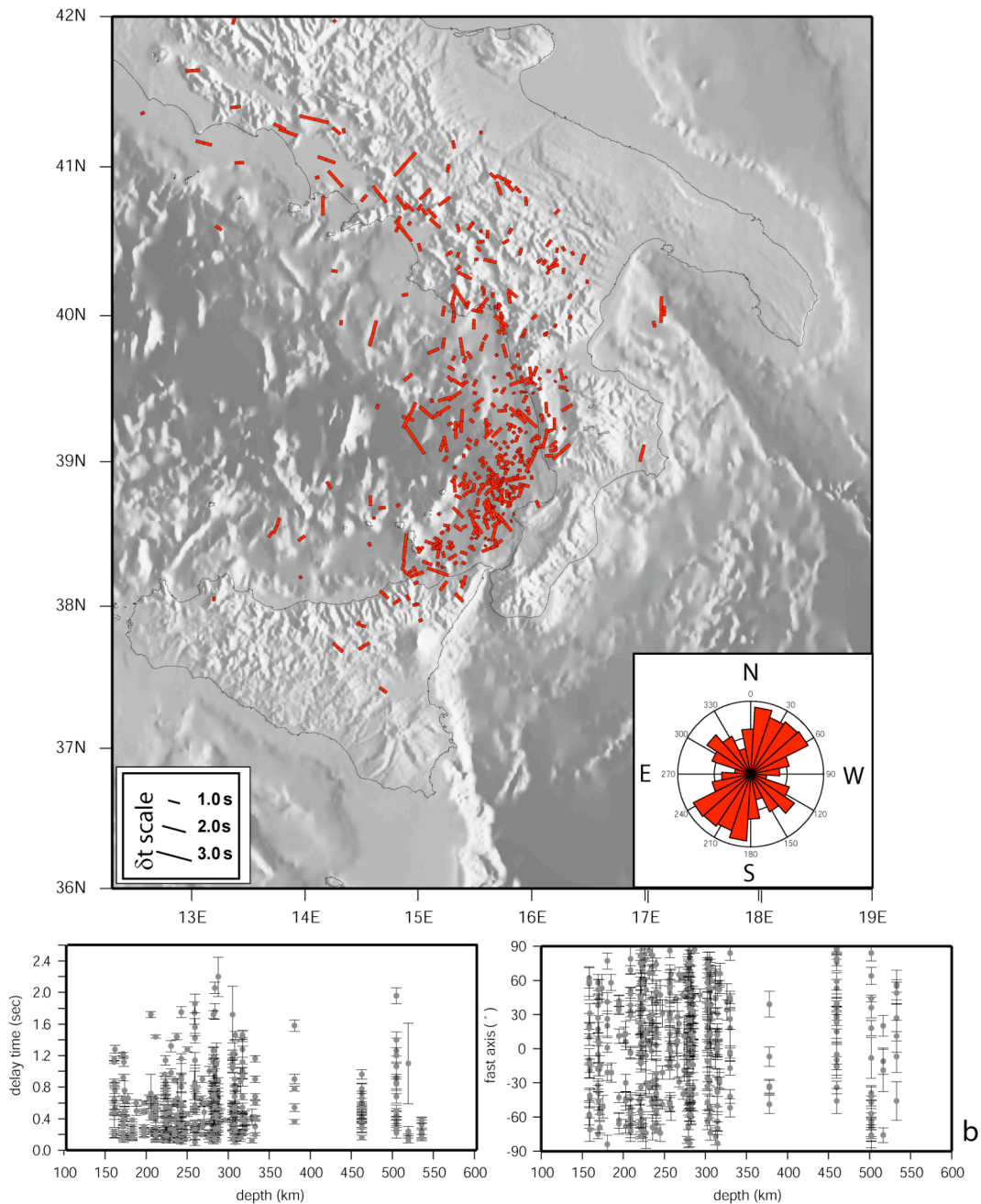
Figure 4.3 a) Distribution of the S fast polarization directions displayed as single measurements for individual station-earthquake pairs. Single measurements are plotted as a bar at the surface projection of the 100 km depth S ray piercing point. The bars are oriented in the φ direction and their length is scaled to the delay time, δt. The results clearly show the high variability of φ and δt. The inset in the lower right corner shows the frequency plot of all of the fast directions: most of the fast direction are about NW-SE, but a secondary peak is observed perpendicular to it in the NE-SW direction. **b)** Delay times and fast directions versus hypocentral depth for all the analyzed events.

The local S waves have generally higher incidence angle than the teleseismic SKS phases analyzed in previous studies (10°-15°).
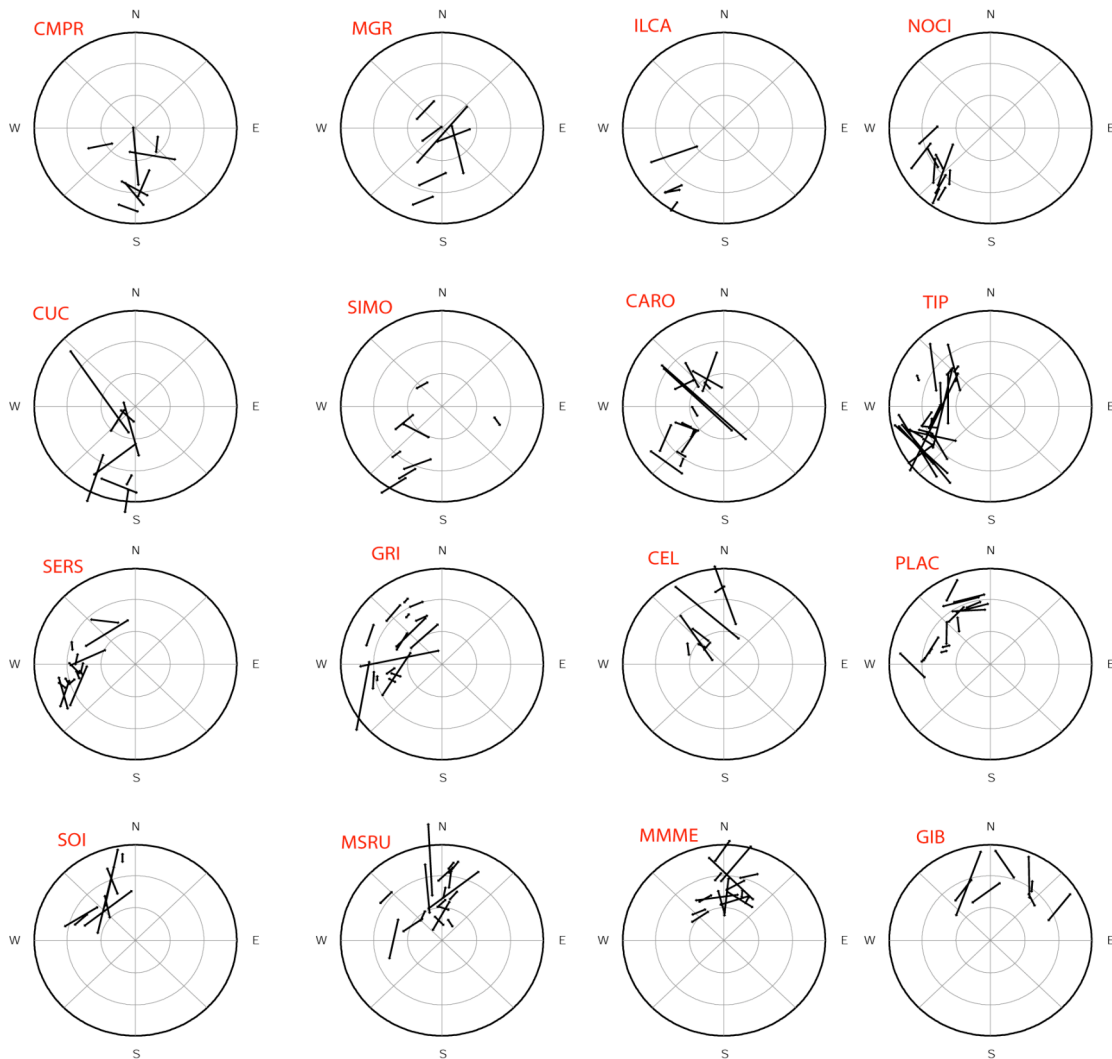
Figure 4.4 Equal area projection for the stations with more than 8 good splitting results, showing the azimuth and incidence angle of the S waves. For each equal area projection, the circles represent the incidence angle from 0° to 45° in 15° increments and all the possible backazimuths.

At most stations, the fast direction trends are not related to changes in incidence angle or back-azimuth. However, at stations with larger azimuth coverage I can distinguish some trends (Figure 4.4). TIP has a preferential fast direction ~ NNW-SSE for events coming from SW and ~ N-S for events coming from W and NW. At station GRI, I found two groups of fast directions: φ are oriented almost NE-SW for events coming from NNW and are oriented N-S for events coming from W. A similar trend is shown by SERS. The station CARO has two large delay values for the two events with smaller incidence angle. The station SOI has NE-SW fast directions for events coming from W an NNW-SSE φ for events from N.

At these 16 stations we have evaluated average fast directions and frequency plots of φ (Figure 4.5; Table 2).
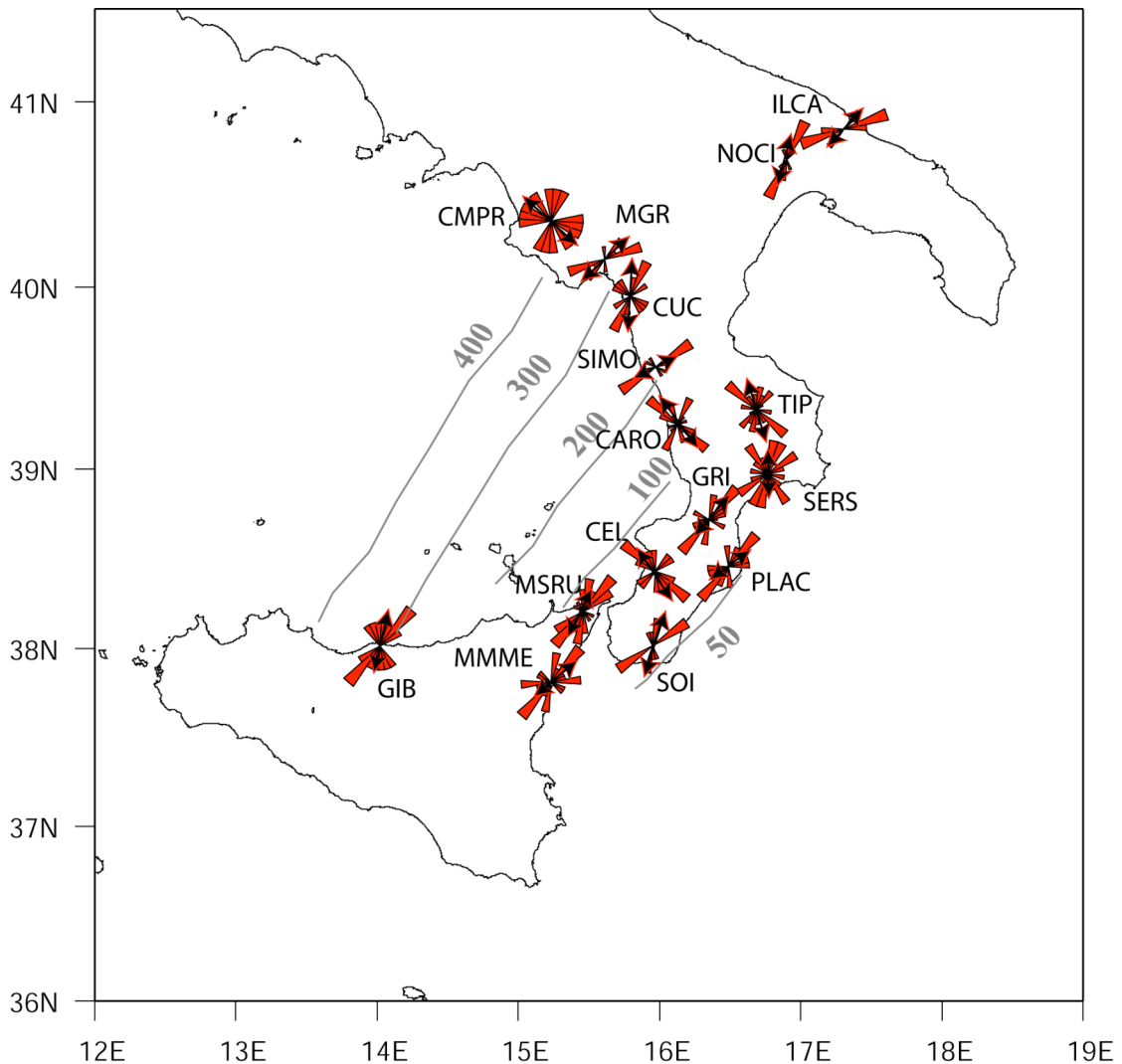
Figure 4.5. Rose diagrams showing the fast direction frequency distribution in 10° intervals. The rose diagrams are only shown for stations with more than 8 good splitting results. The black arrow represent the average values of the splitting parameters. The arrow is parallel to the average fast direction and its length is proportional to the average delay time (see Table 2 for the values).

The frequency plot of fast directions show a large variability of φ but the average fast direction at the stations above the slab is roughly slab parallel (NE-SW at MMME, MRSU, SOI, PLAC, GRI) or slab perpendicular (NW-SE at CEL). Moving northward, other Calabrian stations as SERS, CARO and TIP have an average fast direction of NNW-SSE, while SIMO, CUC and MGR on the Tyrrhenian coast have average fast direction approximately NE-SW, similar to the

two stations in Apulian Platform, NOCI and ILCA. The westernmost station in Sicily, GIB, has an average direction roughly NE-SW. CMPR in Cilento shows a large variability of measurements with an average fast direction parallel to the strike of the southern Apennines. The average values of delay times at these stations are reported in Table 2; average values at each station are close to the average value of the region (0.5 s) and range from the 0.33 s of SERS to the 0.66 s of CUC.

Stations	*Measurements*	$\overline{\phi}$ (°)	$\sigma\overline{\phi}$ (°)	$\overline{\delta t}$ (s)	$\sigma\overline{\delta t}$ (s)
CMPR	8	132	36	0.51	0.2
MGR	8	47	28	0.55	0.29
ILCA	9	43	30	0.38	0.17
NOCI	10	15	22	0.39	0.14
CUC	9	3	33	0.66	0.41
SIMO	8	63	27	0.33	0.12
CARO	16	-37	32	0.55	0.44
TIP	26	-17	33	0.56	0.44
SERS	16	-1	33	0.33	0.22
GRI	17	41	27	0.41	0.34
CEL	8	-34	32	0.53	0.43
PLAC	15	54	29	0.35	0.17
SOI	8	18	27	0.60	0.33
MSRU	18	27	28	0.40	0.30
MME	16	50	33	0.42	0.23
GIB	8	13	27	0.54	0.27

Table 2. Station name, number of measurements, mean and standard deviation of fast direction and delay time evaluated at 16 selected stations which recorded more than 8 high quality splitting measurements.

For these 16 stations I analyzed the depth-dependence of the splitting parameter δt at each station by plotting the δt value versus the hypocentral depth of the analyzed events (Figure 4.6). As for the whole set of measurements, there is no clear increase of δt with the hypocentral depth: at few stations, the ones close to both sides of the slab (MRSU, CMPR, MRG and CUC) an overall increase of δt from 150 to about 300 km depth is noticed, but the deeper events show generally low values of δt.

Other stations, such as SIMO and PLAC, have quite low values for the entire depth range.

The variability shown by the anisotropic parameters at single stations exclude the crust and lithosphere of the overriding plate as major source of the anisotropy. Infact, if the source of

anisotropy were close to the station then the measurements would be quite homogeneous because the shallow volume is sampled by all of the waves recorded at that station.
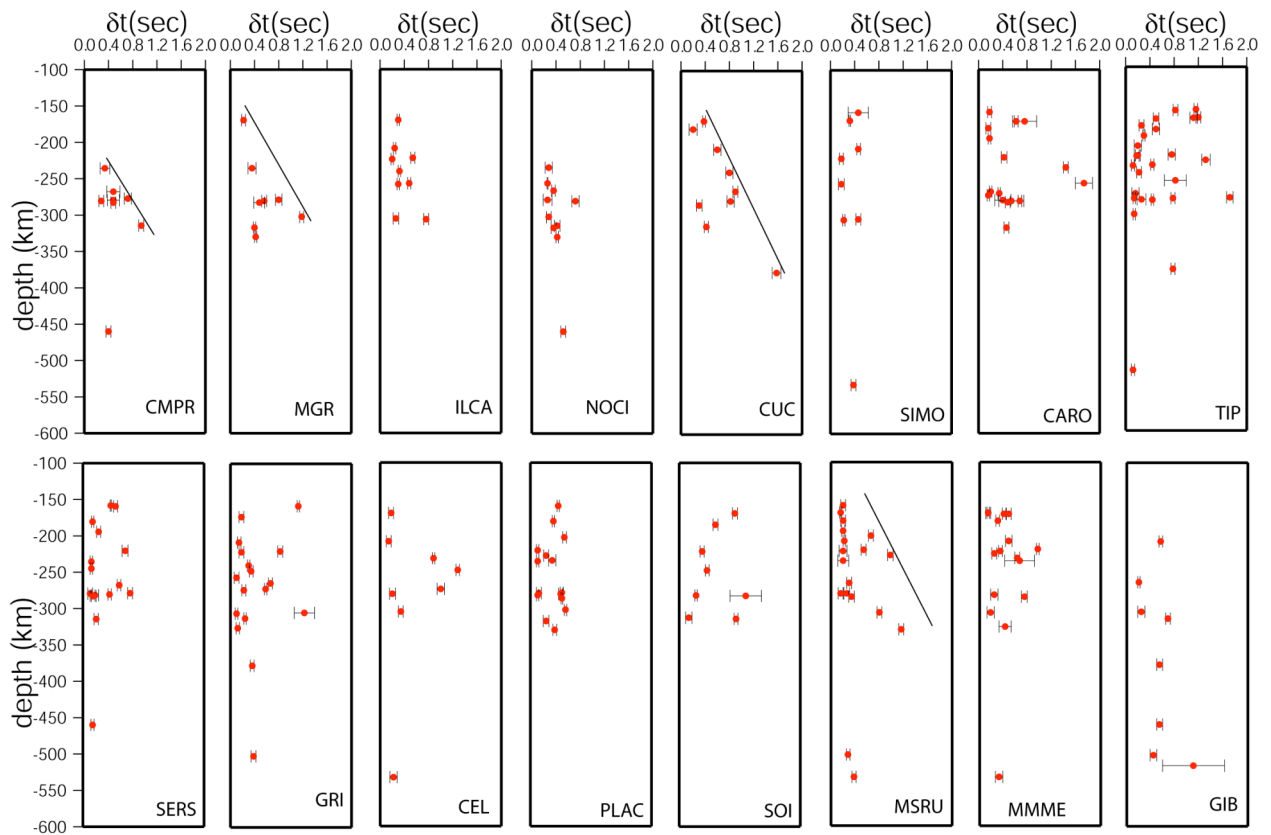
Figure 4.6 Delay times (with their errors) versus the hypocentral depth at the stations that recorded more than 8 high quality measurements. The black line shows an increasing trend of δt with depth at four stations.

4.2.2 Frequency-dependent anisotropy?

If compared with the SKS delay time, which is on average about 1.8 s for the Southern Tyrrhenian subduction zone [Lucente and Margheriti, 2008], the S delay time is very low (on average about 0.5 s). The large discrepancy in delay time between SKS and local S can be the result of the different ray-paths of these different waves: SKS primarily sample the sub-slab mantle while local S generally sample the slab and supraslab wedge. Moreover, teleseismic waves arrives at stations with a steeper angle than the local deep earthquakes. However, the difference between S and SKS splitting times can also be attributed to the different frequency content of the waves: SKS have most of their energy at period between 20 s and 10 s, while the local S I am analyzing are filtered between 2 s and 0.5 s. I check the frequency-dependent

behaviour of anisotropy by reanalyzing the local S with a lower-frequency band-pass filter (0.05 – 0.5 Hz, or a 20-2 s period; hereafter low frequency band). Only the events with a magnitude equal to or greater than 5.0 have sufficient energy in this frequency band for the splitting analysis. In the low-frequency band I obtained 39 well-constrained pairs of φ and δt (Figure 4.7). Many of the results of this analysis are in the areas where we observe higher delay times: central Tyrrhenian Sea and the Tyrrhenian coast toward Naples. Compared to splitting measurements in the high-frequency band for the same set of events (Figure 4.7), the low-frequency dataset reveals a more uniform pattern of fast directions: fast axes show a clear trend NNW-SSE along the Tyrrhenian coast near Naples, and are oriented approximately NE-SW in the Tyrrhenian Sea.
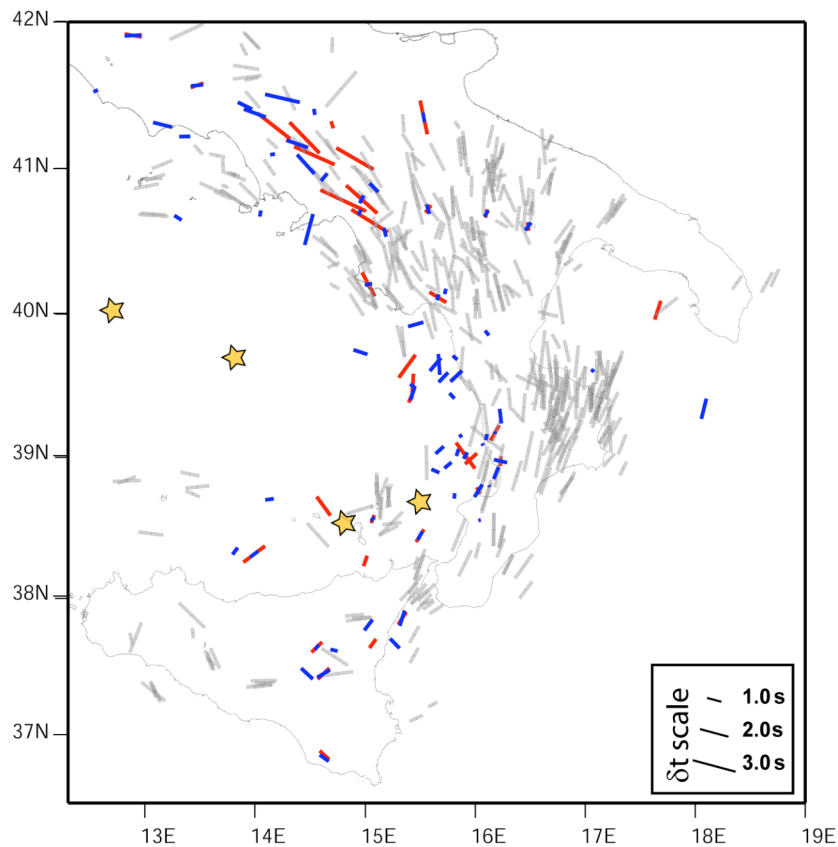
Figure 4.7. Comparison of the S fast polarization directions found in the two different frequency bands (blue bars: high filter 0.5 Hz-2Hz; red bars: low filter 0.05 Hz-0.5 Hz) displayed as single measurements for individual station-earthquake pairs. The earthquakes analyzed have magnitude larger than 5.0 and their epicentres are depicted as stars. Single measurements are plotted as a bar at the surface projection of the 100 km depth S ray piercing point. The bars are oriented in the φ direction and their length is scaled to the delay time, δt. The results of SKS splits from previous studies at their 150 km pierce point [modified from Baccheschi et al., 2008] are the grey bars in the background.

The results on the Tyrrhenian coast near Naples are consistent with the pattern of fast directions and delay times shown by the teleseismic dataset [Figure 4.7; Baccheschi et al., 2007, 2008]. The delay times, observed in the low frequency band with respect to the high-frequency band, are higher on average (1.2 s versus 0.5 s), but actually they are mainly concentrated in the areas where the higher frequency analysis also sees larger δt: along the coasts of Central Apennines and in the Tyrrhenian Sea corresponding to the mantle wedge and the Southern Apennines slab gap [Chiarabba et al., 2005]. The differences in splitting parameters in the two frequency bands for the same event-station pairs are reported in Figure 4.7 (also in Baccheschi et al., under review, JGR). In about 50% of the measurements the parameters are significantly different both in delay time and fast direction values (at the corresponding event-stations pairs average delay times for the lower frequency band is 1.0±0.5s while for the higher frequency band is 0.6±0.2s). The frequency-dependent differences are most pronounced in rays passing through the supra-slab mantle wedge, while they are minimal for rays sampling only the slab. This can be interpreted as an indicator of a frequency-dependent anisotropy that is likely due to the presence of small anisotropic heterogeneities. Such small scale-length anisotropic structures are best detected when the wavelength of the analyzed S is smaller than their dimensions [Marson-Pidgeon and Savage, 1997]. This can explain why the splitting measurements evaluated in the high-frequency band are less uniform and show the heterogeneity that may exist in the mantle wedge and within the slab. These heterogeneities also scatter the energy at higher frequency and thus mask the large-scale anisotropy visible for lower frequency (SKS and low-passed S).

4.3 Discussion

The anisotropic features of subduction systems have been broadly investigated around the world by studies that used shear waves at both teleseismic and local distances. Several variable physical processes affect the anisotropy, such as corner flow in the mantle wedge [Levin et al., 2007], the effects of dynamic recrystallization [Kaminski and Ribe, 2001], strain partitioning between melt-poor and melt-rich regions [Holtzman et al., 2003, Kaminski, 2006] and lower-crustal foundering [Behn et al., 2007]. Deformation in the mantle wedge is controlled by the edges [Kincaid and Griffiths, 2003; Funiciello et al., 2006] and geometry (tears and changes in the dip) of the descending slab [Kneller and van Keken, 2007, 2008; Buttles and Olson, 1998; Hall et al., 2000; Peyton et al., 2001] and by plate boundary geometry [Lowman et al., 2007]. Furthermore, the anisotropy in subduction is affected by style of the convergence [Hall et al.,

2000] and by slab rollback motion [Long et al., 2006; Nakajima and Hasegawa, 2004; Liu et al., 2008].

The S-wave birefringence observations across the Southern Italy subduction system exhibit a complex pattern of fast directions and delay times, so in order to investigate the relations between splitting results and subduction structures I tried to follow the different path of the S-rays inside the different subduction environments. Due to the source-station geometry, the rays from deep sources within the descending plate travel mainly through the thick Mesozoic subducting lithosphere. In a minority of cases S-waves leave the slab to travel in the mantle wedge, in the overriding plate and in the sub-slab region (Figure 4.10). In Figure 4.8 I plot splitting results (at 100 km piercing point) over the average P-wave velocity model between 100 and 200 km depth [*Vp* model from Chiarabba et al., 2008]. The green line designates the smoothed contour bounding the high velocity region. In Figure 4.9b the splitting parameters are averaged over a regular grid. The average values of the delay times are given by the colors and the average ϕ are shown by the white bars. To aid in interpretation, I also considered the SKS splitting results (Figure 4.9) together with the new S results to better characterize anisotropic pattern of the different subduction environments: crust and overriding lithosphere, slab, mantle wedge and the sub-slab mantle.

4.3.1. Anisotropy in the crust and lithosphere of the overriding plate

The shear-wave splitting can be caused by the deformation within the crust [Silver and Chan, 1991; Silver et al, 2002]. Our splitting times range from 0.08 s up to 2.2 s, with an average value of 0.5 s. The higher values are much higher than I would expect from the crustal anisotropy, estimated to be about 0.04-0.2 s [Savage, 1999], and imply a dominantly mantle contribution. Moreover if the crust were the primary locus of anisotropy I would observe a quite homogeneous pattern of splitting parameters at single stations because all the waves recorded by each station sample the crust and lithosphere below it. Therefore, the variability shown by the anisotropic parameters at single stations exclude the crust and lithosphere of the overriding plate as major source of the observed anisotropy.

4. 3.2 Slab anisotropy

The particular geometry of the Tyrrhenian subduction zone relative to the distribution of the land areas and consequently locations of the seismic stations provide an opportunity to collect

unique data. First, Calabria is an uplifted fore-arc that lies well trenchward of the volcanic arc; second, the slab dips at high angle (about 70°) below Calabria; third, the lateral extension of the slab is limited and bounded at its edges by the Southern Apennines and Sicily. Seismic stations are distributed throughout Calabria, the Southern Apennines and in Sicily, while only few ones are in the Eolian volcanic arc. This allows most recorded rays to travel through and along the subducted lithosphere. This is not frequently observed worldwide since in most subduction zones, as in Japan, land corresponds to the volcanic arc and trenchward of this most of the forearc is submerged.

The pattern of S waves splitting in the slab is very complex and shows spatial variability in both φ and δt (Figure 4.8). On the other hand average values testify that most of measurements located corresponding to the slab below Calabria show small values of delay times. In fact, the purple region in Figure 4.9 (δt < 0.5 s) corresponds closely to the Ionian slab fast *Vp* anomaly. Also the spatial averaging of fast axes identifies a region in the Ionian slab with a coherent slab parallel fast direction orientation about NNE-SSW. The northern portion of the high *Vp* anomaly below the Southern Apennines have slightly higher average δt values (about 0.8 s) and a dominant fast orientation about NE-SW while the strike of the mountains in this region is NNW-SSE. However, consideration of the ray paths (Figure 2) suggest that many to the rays to the Southern Apennines slab also passed through the mantle wedge. In addition, this is the region where there is a slab gap from 150-300 km depth [Chiarabba et al., 2008]. Average fast directions parallel to the Southern Apennine mountain are found toward the north along the Tyrrhenian coast near Naples and inland where a steeply dipping slab to 300 km is observed by tomography [Chiarabba et al., 2008]. Our results have some differences compared to the anisotropic parameters founded in previous SKS waves studies [Margheriti et al., 2003; Civello and Margheriti, 2004; Baccheschi et al., 2007, 2008]; SKS delay times in Calabria are on the order of 1.8s and fast directions rotate from NNE-SSW in Calabria to NE-SW in Southern Apennines following the curvature of the mountains and of the high *Vp* anomaly interpreted as slab. The teleseismic nature of SKS did not allow the source of this slab-parallel anisotropy to be conclusively determined. However, I note that the majority of the rays analyzed in Baccheschi et al. [2007, 2008] were from the E-NE and therefore sampled the sub-slab mantle.

The S-wave splitting in this study clearly identify the slab as a weak source of anisotropy. The causes for low inherent slab anisotropy are not readily determined since the detailed structure of the Ionian lithosphere and its faulting style are not well known. The Ionian microplate is

supposed to be a remnant of the Mesozoic neo-Tethys Ocean and thus one of the oldest oceanic crusts in the world [Catalano et al., 2001].
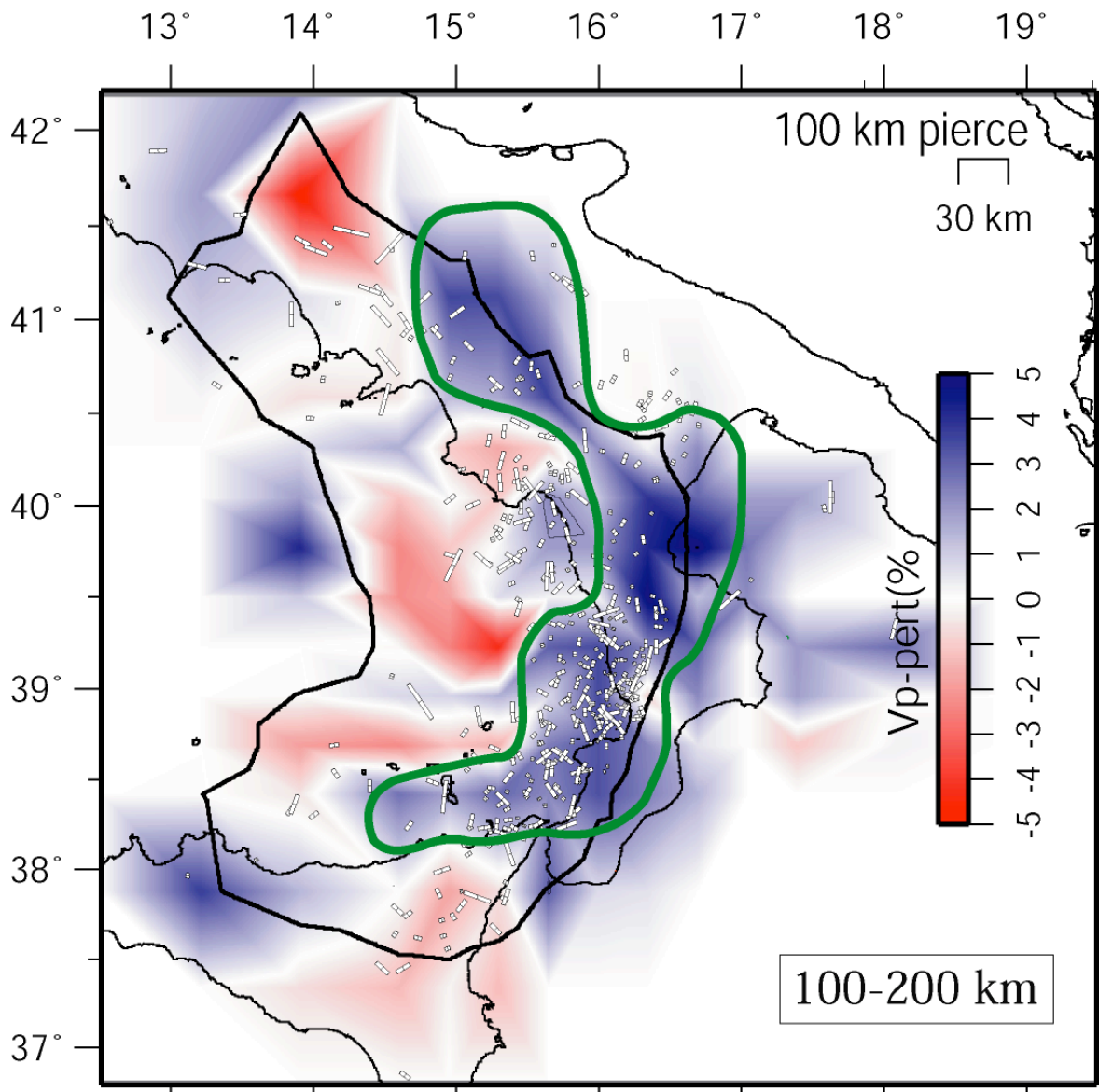
Figure 4.8 Comparison between P-wave velocity anomalies averaged between 100 and 200 km depth [Courtesy of P. De Gori, from Chiarabba et al., 2008] and S splitting measurements projected at 100 km depth (the same as Figure 4.3, white bars) in the Southern Italy subduction system. The green line delineate the smoothed contour bounding the high *Vp* velocity region.
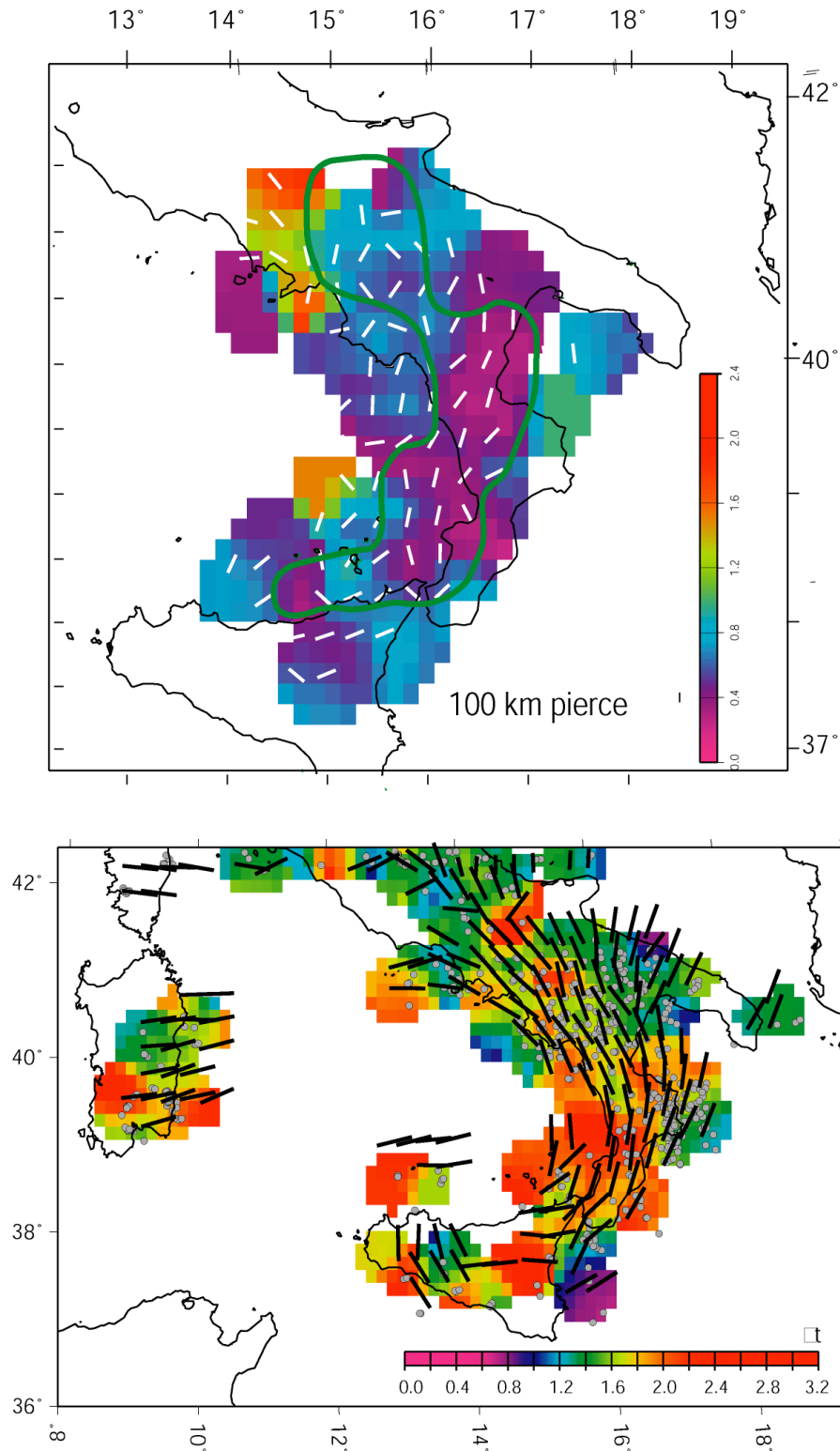
Figure 4.9 Representation of the anisotropic parameters on a regular grid. Average fast directions (S = solid white bars; SKS=solid blackline) are obtained smoothing the raw splitting data beneath sampled grid boxes. Individual splitting time delays were interpolated using a nearest neighbour algorithm which averages, over a 10′ (latitude) × 10′ (longitude) grid, measurements within a 1° radius, if there is at least one value inside each of the three 120° azimuthal sectors. Average delay times are represented by the color scale.

54
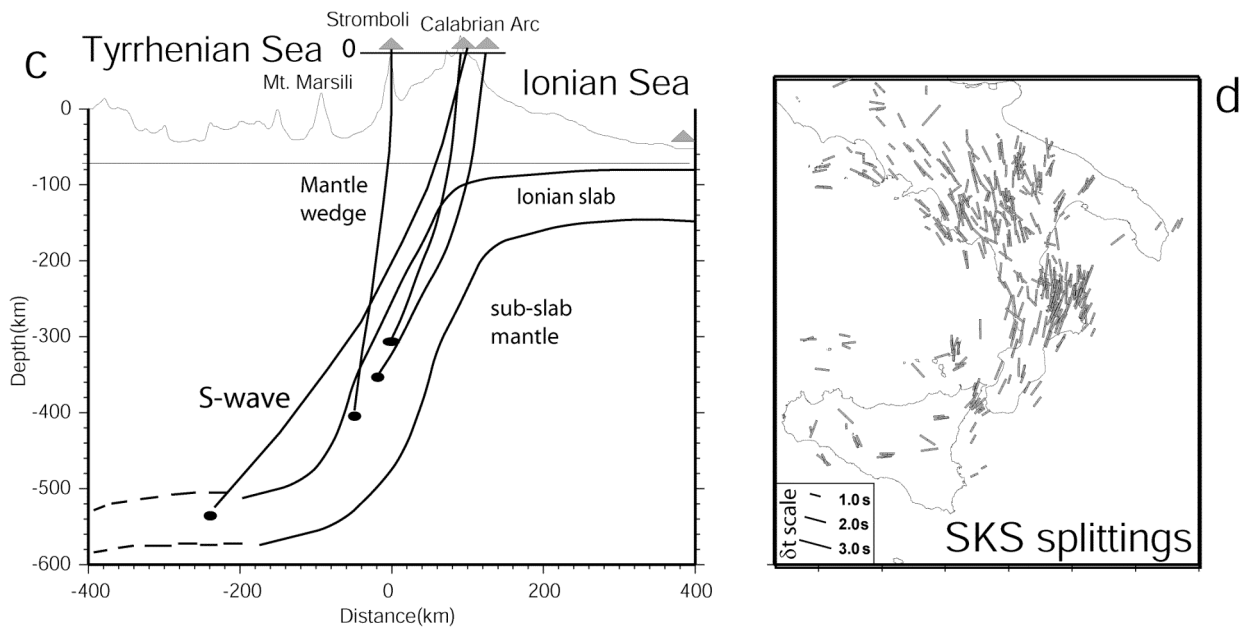
Figure 4.10 Map view of local ray-paths travelling inside the subduction system. Black circles are representative of slab earthquakes. Due to the relative earthquake stations distribution most of the rays travel mainly inside the slab. Compilation of the SKS splitting measurements available for the same area (modified from Baccheschi et al., 2008) used in this study to integrate the S splitting results.

One of the arguments in favor of the oceanic nature of the oceanic Ionian crust is the low heat flow of the Ionian Sea and its deep bathymetry (3000-5000 m depth). Refraction of the Ionian Sea crust south of Calabria shows a typical oceanic crustal structure [de Voogd et al., 1992]. Moreover, the subducted lithosphere beneath the southern Tyrrhenian Sea has clear oceanic seismic characteristics: high Vp, high Qp and low Vp/Vs anomalies [Chiarabba et al., 2008]. The subduction and the long history of this lithosphere may have cancelled the Ionian lithosphere's original anisotropic fabric, whose orientation can only be speculated [e. g. Stampfli et al., 2002].

4.3.3 Mantle wedge anisotropy

The mantle wedge is only partially sampled, in the region below the Eolian Magmatic Arc and along the coast of the Tyrrhenian Sea. Averaged fast directions are variable from slab-parallel to slab-perpendicular. I generally observe higher average values of delay time (up to 2s) connected with the low *Vp* zones in the Tyrrhenian Sea and along the coast near Naples (Figure 4.9). Rays from deep events to the stations near the Tyrrhenian coast must pass through the

wedge. The S split delay times and fast directions in this region are consistent with the SKS teleseismic splitting: fast axes are parallel to the strike of the Apennines.

In low *Vp* regions above the slab I observe also small values of delay times (Figure 4.9) that may be compatible with the existence of localized patches, not seen by the longer SKS waves, of B-type olivine (the presence of water is expected above the slab; Jung et al., 2009; Long, 2009) that have their fast and slow axes swapped: the resultant complex field of anisotropy will show quite complicated waveforms (I see them at the Eolian stations), lower δt and variable fast directions.

In NE Sicily fast axes rotate around the high velocity body following the edge of the slab reproducing at smaller scale and with generally lower δt values the toroidal flow around this slab edge, already seen by the SKS measurements (Figure 4.9).

4.3.4 Anisotropy in the sub-slab region

To discuss about sub slab-anisotropy our results are added to the results obtained in previous studies analyzing SKS waves that found strong seismic anisotropy in the mantle beneath the Southern Italy. The teleseismic nature of SKS did not allow identification the source of anisotropy, which could be the slab and/or the sub-slab mantle. Only a few of our S measurements sample the sub-slab volume. Rays going toward the Apulia region have average fast directions aligned roughly N-S. This orientation is consistent with the SKS fast orientation in the region. The SKS splitting results in the mantle beneath the Southern Italy showed a quite homogeneous pattern of splitting parameters with trench-parallel φ and delay times of the order of 1.8 s [Figure 4.8b, Baccheschi et al., 2008 and references therein].

The fast directions rotate from NNE-SSW in Calabria to NE-SW in Southern Apennines following the curvature of the mountains and of the high *Vp* anomaly interpreted as slab. The authors related this pattern either to slab itself or to the presence of mantle material below the slab strained by the rollback of the retreating Calabrian slab. S-waves splitting exclude the slab as strong source of anisotropy leaving the sub-slab mantle as the sole candidate.

4.3.5 Anisotropy vs analogue and numerical modeling results

In order to search for a reliable pattern of mantle circulation both above and beneath the downgoing lithosphere, different geometries and motions of slabs have been modelled by a number of authors and in some cases compared to the observed anisotropic patterns. Models,

which focus on the geometry and nature of sub-slab mantle flow field, are particularly suitable for comparison with our anisotropic images. Indeed, the Ionian slab is a natural example of a narrow slab characterized by long term rollback motion [Gueguen et al., 1998] and with anisotropic pattern showing slab-parallel fast directions as well as toroidal flow around its southern edge.

One of the first attempts to model 3-D mantle flow induced by a steeply dipping slab with both downdip and rollback motions was performed by Buttles & Olson [1998]. They found variable flow orientation in the mantle wedge, while trench-parallel mantle flow was observed beneath the slab. Recently a similar sub-slab trench-parallel flow field has been found by Honda [2009] through numerical modelling for certain boundary conditions. These models are compatible with the SKS fast directions observed along Calabria and Southern Apennines. In addition, the slab-parallel alignment in Buttles & Olson, [1998] predominates only in a narrow belt very close to the slab suggesting a finite extent of slab-parallel flow. This is consistent with our splitting results: moving from the slab toward the foreland in the Apulia Platform, the fast axes rotate from slab-parallel to NE-SW, quasi slab-perpendicular [Baccheschi et al., 2008].

Several other authors have conducted 3-D numerical [Stegman et al., 2006; Piromallo et al., 2006; Funiciello et al., 2006] and analogue [Schellart, 2004; Schellart et al., 2008; Funiciello et al., 2006] experiments to study the mantle flow around the slab edges. These models did not focus on mantle flow field beneath the slab, but instead sampled and resolved well the mantle flow field around the slab edges and in the mantle wedge above the slab. In these experiments, generally a narrow slab and a retreating trench were considered, which are very applicable to the present day setting of Calabria. The fast hinge retreat due to slab rollback produced a considerable toroidal flow in which mantle material, initially located beneath the downgoing plate, moved from beneath the slab toward the mantle wedge by flowing around the lateral slab edges. The toroidal mantle flow field obtained in these models is quite consistent with both our SKS- and the S-splitting analyses at the SW edge of Ionian slab (from below the Messina Strait to the Sicily Channel, Ustica Island and Eolian Islands). However, these models do not fit well with the pattern of fast axes at the northern edge of the slab. The anisotropy wraps around the mountain belt from Calabria to the Southern Apennines past the northern edge of the Benioff-Wadati zone. This could be explained by considering a slab tear at the northern edge that is too narrow to allow a significant mantle flow through it. Alternatively, the tear could be much younger than the one at the SW edge and, thus, not provide sufficient time for mantle flow to realign the olivine crystals. There is a suggestion of a return flow farther north at 41° N, perhaps corresponding to when the Calabria slab was wider prior to the Pleistocene stopping of

the Southern Apennines [Patacca and Scandone, 2001]. In this perspective I believe that while the flow at the SW edge of the Ionian slab is successfully modelled by narrow retreating slab [Kincaid and Griffiths, 2003, 2004; Schellart, 2004; Schellart et al., 2007; Piromallo et al., 2006], the flow in its central part and NE edge (together with the Southern Apennines subduction) is better represented by models with longer retreating slabs [Buttles & Olson, 1998; Honda 2009; Lowman et al., 2007]. Moreover, it is important to note that the comparison between the modelled streamlines and the observed fast directions is always qualitative; observed fast directions represent the integrated anisotropy of the entire sampled mantle volume, while the horizontal slices in numerical and analogue models show the local flow lines.

4.3.6 Anisotropy in subduction: interpretative models

A simple interpretative model of the anisotropy delay time in subduction zones was proposed by Long and Silver [2008; 2009]: the sub-slab splitting signal is controlled by sub-slab mantle flow induced by trench migration; SKS measures from Southern Italy (named Calabria) are included in their splitting compilation and fit their category of high trench migration-high splitting delay-times.

For mantle wedge anisotropy, Long and Silver [2008] argue that the anisotropy depends on the relative contributions of trench migration (Vt) and plate convergence (Vc). In subduction environment where the rate of plate convergence and trench migration are comparable (Vt/Vc ~ 0.6), small values of δt are found for local S from deep earthquakes. However, where one component dominates, the wedge anisotropy and therefore the local S δt values are higher. In Southern Italy subduction has been primarily driven by the trench rollback. Vt/Vc ~ 1 and should be dominated by 3D flow around the slab. Until the last ~ 1 Ma, they were both higher by a factor of 5 than the Africa-Eurasia convergence velocity [Faccenna et al., 2004]. While the rate of trench migration has drastic slowed over the last ~ 1 Ma, the mantle fabric should still reflect the earlier high rate of retreat. With this perspective, I expect in the Southern Tyrrhenian values of S delay time to be higher than 1 s and trench-parallel. I actually see such high delay times in the central Tyrrhenian area and along the Tyrrhenian coast near Naples areas where the S rays sample the low velocity regions seen by tomography. However, the δt are much lower for the rays that sample the slab. Therefore, I believe that the mechanism invoked by Long and Silver [2009] to explain the strength of anisotropy in the mantle wedge is applicable to the Southern Italy case but that the results from S-wave splitting in subduction system should be

carefully selected, taking care to evaluate average values of delay times only for the rays which sample mantle wedge.

Our results thus favour identifying mantle flow as a primary source of seismic anisotropy: the subducting lithosphere moving relative to the surrounding mantle generates flow. The most important mechanism responsible for the anisotropy in the Southern Italy Subduction zone is the mantle flow field surrounding the slab, induced by the rollback of the lithosphere to its present position, which can be described by the combination of its dip and its curvature.

A different model, not involving the mantle flow field, to explain seismic anisotropy in subduction zones around the world was proposed by Faccenda et al. [2008]. The authors invoke the hydration of pre-existing faults in the subducting oceanic lithosphere as the primary source of slab-parallel shear wave splitting observed worldwide mainly using teleseismic waves.

The complex pattern of fast directions and the small values of δt that I observe for the S rays sampling the slab, does not seem to be compatible with this model. In fact, as the S wavelength for local earthquakes are smaller than for SKS, the S waves should be sensitive to the presence of hydrated fault structures within the slab. Moreover, even if trench-parallel hydrated faults occur in the Ionian lithosphere (starting hypothesis in Faccenda et al., [2008] model), the steep dip of the slab (about 70°) would not produce the vertical layering of dry and hydrated anisotropic material obtained by the author for a 30°dipping slab. Therefore the slab itself would not likely be the source of slab-parallel fast directions and delays seen by SKS in this region, but these splitts are more likely to have been generated by flow in the sub-slab mantle (Figure 4.11).

4.4 Conclusions

The results presented in this study indicate the dominant role played by active mantle flow induced by the slab motion in generating seismic anisotropy in subduction environments.

The S shear wave splitting measurements from local deep events show variable fast directions and delay times. The geometry of the slab, the distributions of the earthquakes and of the stations, particularly on the elevated Calabrian forearc, allowed most of the recorded rays to travel through the mantle wedge and the slab. Only a few rays sampled the sub-slab mantle. Rays sampling the slab have generally low δt values and on average slab-parallel fast directions (NNE-SSW), implying that there is only a weak contribution from the slab to the anisotropy. The lack of contribution from the slab suggests that large published teleseismic SKS splits are due to mantle flow beneath the slab.
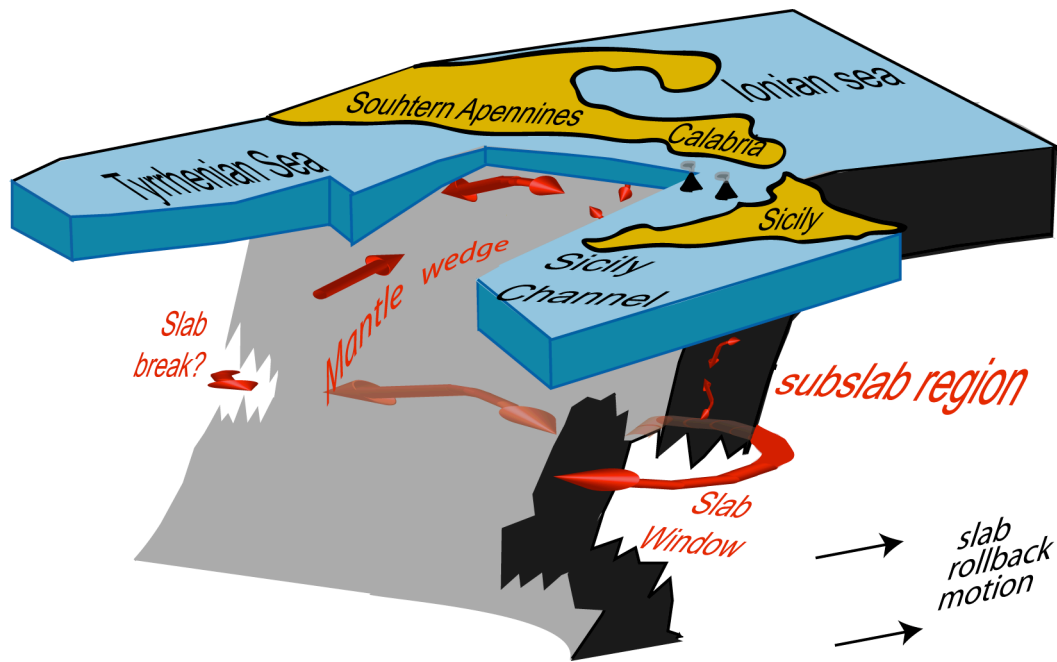
Figure 4.11 Schematic 3D sketch for a possible model of seismic anisotropy in Southern Italy subduction system as controlled by the retrograde motion of the Ionian slab. In the slab and in the mantle wedge the S splits reveal a complex pattern of splitting parameters, with scattered fast axes and smaller values of δt (small red double-arrows) in the slab suggesting a weak contribution from the slab to the anisotropy. In the mantle wedge S splittings show higher delay times (red double arrow beneath Southern Apennines). In the sub-slab region, the rollback motion of the slab induces mantle flow parallel to the strike of the slab. This is mainly revealed by the SKS splits pattern, which shows a predominantly slab-parallel fast axes with higher delay time (large red double-arrows). In addition, both S and SKS indicate that the slab window beneath the Sicily Channel promotes mantle flow around the SW slab edge, creating a toroidal flow from behind to front the slab (wrapped red double-arrow). At the NE edge of the slab this return flow seems to be not well organized.

The rays sampling the supra-slab mantle wedge also have higher delay times (on average higher than 1 s) than the slab, but quite variable fast directions. The S-wave splitting parameters show some frequency-dependent behaviour that is likely due to the presence of small-scale anisotropic heterogeneities. These heterogeneities scatter the energy at high frequency masking the large-scale anisotropy that is observed at low frequency (SKS δt is ~ 1.8 s, low-passed S δt is > 1.0 s). The heterogeneities would also contribute to the directional scatter in the high frequency S-wave splits. The presence of pockets of *b*-axis olivine in the mantle wedge is a possible explanation for the observed pattern.

The patterns of local S-wave and teleseismic SKS-waves fast directions are similar. They both show NW-SE anisotropy in the Southern Apennines near Naples and show a toroidal pattern around the SW edge of the slab in northeastern Sicily. The later is consistent with numerical and analogue models of mantle flow around a slab edge.

The across-subduction variation of delay time values I observe can be explained considering the fabric of the slab as only a weak source of anisotropy in the horizontal plane, relative to the mantle above and below it. I conclude that the main source of seismic anisotropy in subduction zones is the deformation of the mantle above and below the slab induced by the retrograde motion of the slab.

CHAPTER FIVE

Seismic attenuation tomography beneath the retreating subduction system

After investigating the anisotropic structure of the Southern Tyrrhenian Subduction System, in the last chapter I will describe the attenuation properties of the study region.

In recent years, there has been a growing number of laboratory studies that have shown how seismic attenuation is of primary importance to investigate the mechanical and thermal properties of the Earth. This is particularly true for the subduction zones, where seismic attenuation can help in identifying spatial variations in temperature, volatile and water content, and melting occurring in a very limited volume.

The aim of this study has been to estimate in detail the three-dimension attenuation structure of the Southern Tyrrhenian Subduction System. Hence, starting from the general equations for the attenuation described in paragraph 2.3 (Chapter Two), I have determined the 3-D attenuation structures for the slab and for the surrounding regions down to 300 km depth, as well as of the crustal layers. There exist several works on the Q_P attenuation structure for the study area, while the Q_S attenuation model has been determined using primarily the teleseismic events. In this work, I have analyzed several earthquakes located within the descending slab and recorded by several stations available in the area. The collection of numerous high quality waveforms gave me the opportunity to determine for the first time the 3-D Q_S attenuation model using S phases from intra-slab events and, in addition, to improve the previous reconstruction of the 3-D Q_P attenuation model.

The results have allowed to reconstruct the spatial variation of Q in the Southern Tyrrhenian Subduction System.

5.1 Data and method

As illustrated in Chapter Two, the 3-D attenuation structure can be determined starting from the equation 2.09. I therefore need to resolve for the t^* parameter, since it will be then used in the inversion for 3-D Q_P and Q_S attenuation models. A good measure of the t* values depend on a reliable estimate of: i) the travel times, which requires well-defined 3-D Vp and Vs models and

well-localized earthquakes; and ii) signal recorded by seismometers with a aflat response over a wide frequency range interval.

Hence, the first part of this study has been dedicated to the creation of the traveltimes dataset. P and S arrival times are extracted from INGV bulletin, except for the earthquakes recorded by CAT/SCAN temporary network. In this case in fact, I have been carefully handpicked P- and S-arrival times on temporary and permanent stations.

The starting hypocenters have been located using the HypoEllipse code [Lahr, 1989] and a reference 1-D velocity model [Chiarabba et al., 2005]. Then, I have selected only events with rms < 1.0 s, azimuthal gap < 200° and with a minimum of 10 P phases and 4 S phases, obtaining 360 events.

In the last step, the selected earthquakes have been relocated by using a reference 3D velocity model [Chiarabba et al., 2008], resulting in an improved hypocentral localization. The final dataset consists of 314 earthquakes accurately localized, and achieving a final rms < 0.5 s (Figure 5.1).

The final dataset useful for the attenuation study consists of 314 events with magnitude between 2.8 and 4 occurring from 2003 to 2009 at hypocentral depth greater than 30 km. The total number of stations used is 264 and they cover the study area from the Southern Apennines down to the western sectors of Sicily.

Once the accurate travel times have been determined, I am now able to perform the attenuation tomography beneath the study region.

The *Q* attenuation structure has been obtained in two steps: first, I have performed the spectral inversion in order to compute the high frequency decay (this quantity is defined as t*) of the far field displacement spectra; as second step t* are inverted on the basis of a-priori traveltimes to reconstruct the 3-D *Q* unknown structure. They are discussed in the followings.

5.1.1 Spectral inversion

To compute the t* parameter, I have estimated the spectral decay at high frequency using the 314 relocated earthquakes.

As described by Scherbaum, [1990] the far-field displacement spectrum of a body wave is expressed as:

$$\log_{10}(D(f)) = \log_{10}(\Omega_0) + \left[\frac{f_c^\gamma}{f_c^\gamma + f^y} \right] - 0.434\pi f t* \qquad (5.1)$$

D(f) is the observed amplitude on the displacement spectrum at a given frequency *f*; f_c is the corner frequency; Ω_0 is the low frequency level that is a function of the seismic moment; γ is the spectral fall-off.
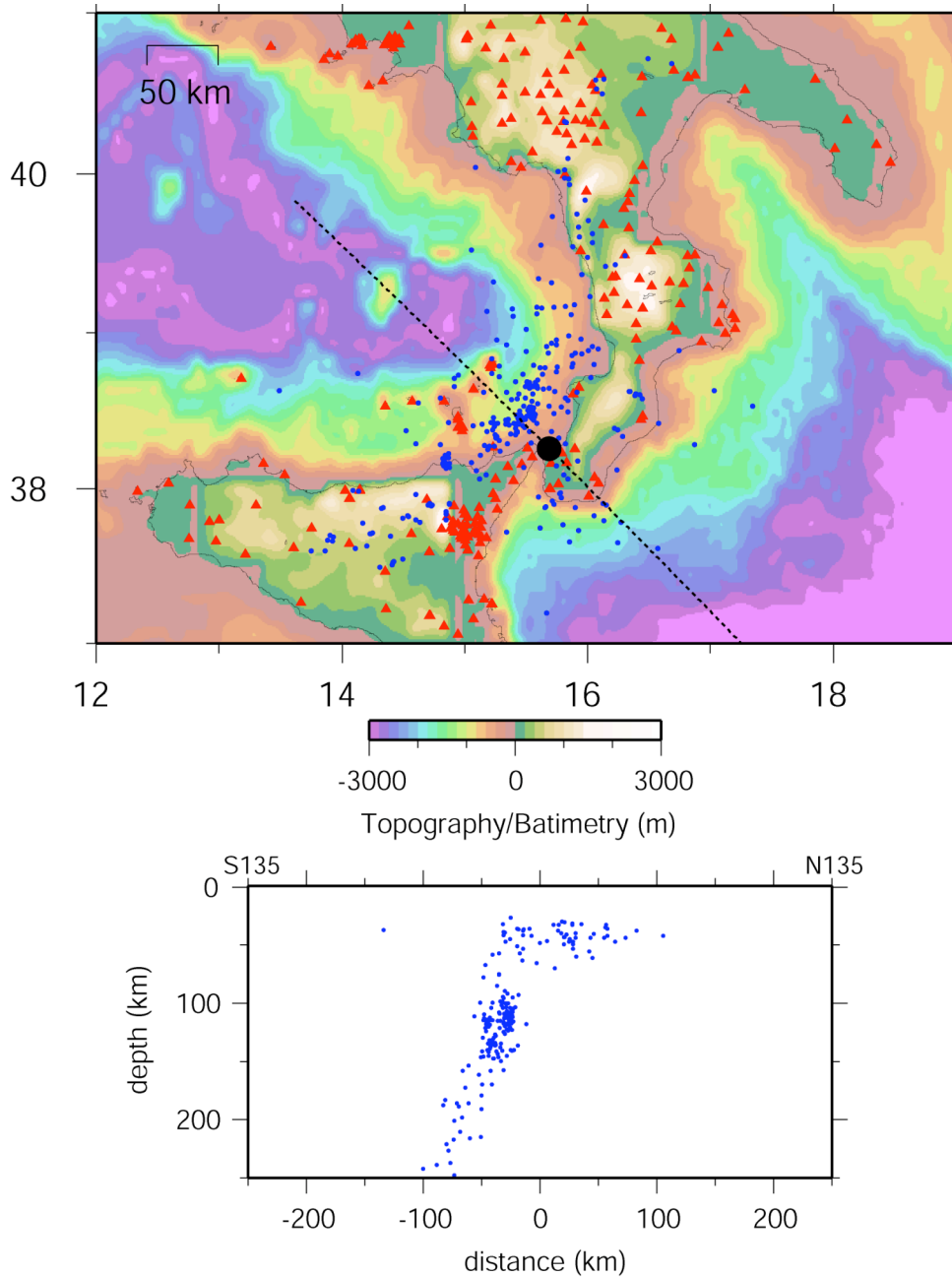
Figure 5.1 Hypocentral distribution of the 314 relocated events which will be then used for attenuation tomography. The vertical section is oriented NW-SE across the Ionian slab and show a clear distribution of the events along a steeply, NW dipping plane. Earthquakes are represented as blue closed circle; red triangles symbolized the station used for tomography.

I have estimated an event corner frequency performing a grid-search [Scherbaum, 1990; Eberhart-Phillips and Chadwick, 2002] over the whole usable frequency range (0.5-25 Hz) using all the spectra of each event, assuming a Q frequency independent and a Brune source model (γ=-2). Once a trial event f_c is assumed, we compute for each spectrum the low frequency level and t* by a linear regression using (5.1). The event RMS quantify the goodness of the computed model. This operation is repeated for each f_c within the considered frequency interval. The function of the rms versus the trial corner frequency allow us to select the real event corner frequency where the curve has an absolute minimum (Figure 5.2). Therefore, for a single event, the best estimate of the f_c will be that value for which the minimum rms between calculated and observed spectrum is attained. The f_c for the for the P waves ranges from 1.39 Hz to 8.9 Hz, while for the S waves it varies between 1-7.7 Hz.
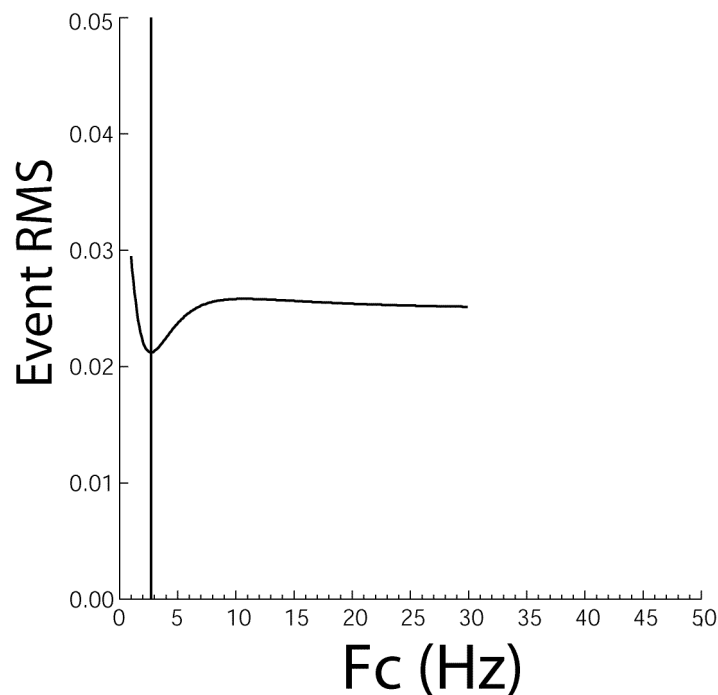
Figure 5.2 Example of the grid search evaluated using all the waveforms of a single event. The grid search is done in the frequency range 1-30 Hz. For the event of the given example, the minimum rms between calculated and observed spectrum is achieved for f_c = 3 Hz.

The displacement spectrum has been calculated by the FFT on a time window of 2.52 s following the P-and S-arrival times, while the noise spectrum was calculated from a segment prior the arrival

time (Figure 5.3). For a spectrum to be fit, the S/N ratio must be above a threshold assumed 1.3 in the frequency band between 1 and 10 Hz.
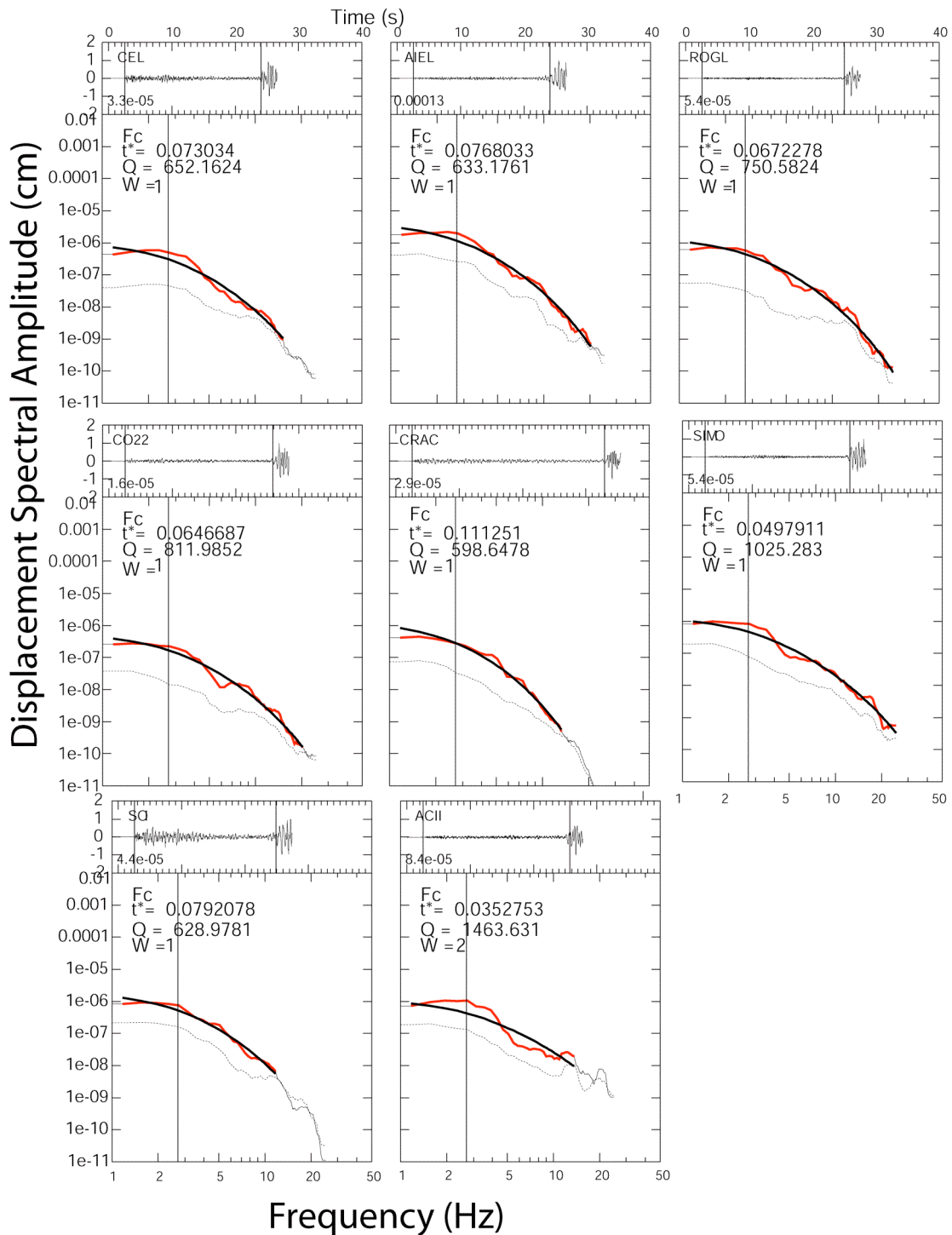
Figure 5.3 Example of fitting t* for one earthquake. The f_c, common for the event, the spectral level and the t* are estimated. Dotted line show the noise spectra; black line show the fit of the data over the frequency range with S/N > 1.3 (red line). For each spectra panel I report the trace window analyzed, the t* value and the t*weight (W) scaled from 0 (smaller rms) to 4 (worst rms), and the f_c.

Additionally, if for frequency > 10 Hz the S/N is greater than 1.3, then the upper frequency limit is extended to the recording limit of 25 Hz and thus also these higher frequencies are considered for the spectral analysis. In order to estimate a reliable value of t*, the minimum number of the spectra for each event has been fixed to 4. If the number of spectra is less than this threshold, then the event has been skipped. All the spectra are processed using *Q* frequency-independent, thus considering *α*=0. This hypothesis is widely adopted to figure out the attenuation structure when local earthquakes are used in the inversion [Scherbaum, 1990; Lees and Lindley, 1994; Rietbrock, 2001; Haberland and Rietbrock, 2001; Eberhart-Phillips and Chadwick, 2002]. To verify the goodness of the frequency-independent assumption I have calculated the displacement spectra for the whole dataset varying each time the *α* values from 0 to 1. This was done both for the P- and S-waves (Figure 5.4). As shown in figure 5.4 the best value for which the global rms between the observed and computed spectra is minimum is for *α* = 0.
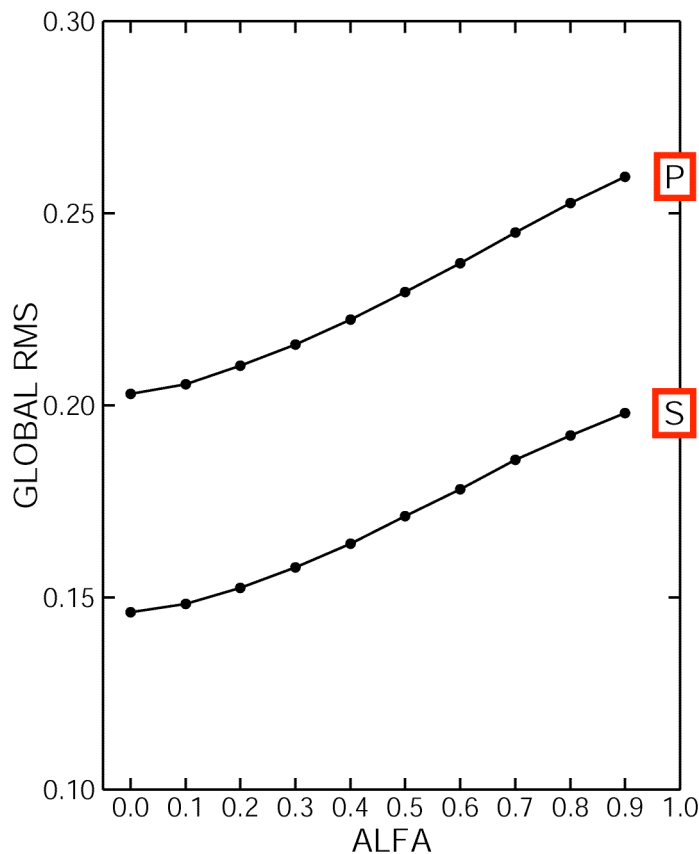
Figure 5.4 The global rms between the observed and computed spectra with respect to the α values ranging between 0.0 to 1.0.

The total number of events that have been used for the spectral analysis is 314, which have allowed to obtain, respectively, 1435 and 1015 P- and S-waves t* observations. In addition, the quality of the final fit is estimated by the rms between the observed and the computed spectrum. Therefore, the rms values are used to assign the weights for the inversion, with values 0, 1, 2, 3, where 0 is referred to an excellent observation, while 4 is assigned to the worst observation, not usable for the $Q_{P,S}$ inversion. Weight of 0 is assigned for rms < 0.1, and weights of 1, 2, 3, and 4 are assigned for rms between 0.1-0.2, 0.2-0.3, 0.3-0.4, and > 0.4, respectively. Therefore, the fitting of the spectra are discarded if RMS is > 0.4 [Eberhart-Phillips and Chadwick, 2002].

5.1.2 Attenuation tomography

After determined the t* values, we are able to resolve for the *Q* attenuation tomography.

In the computing for *Q*, the attenuation effects close to the recording site (the t*$_{station,}$ see equation 2.17 in Chapter Two) are took into account since they can affect the shape and the content of the observed spectra. Moreover, the rays are traced in a ll known 3-D velocity model, then t* depend only on the *Q* values along the path.

The Q_P and Q_s inversion has been parameterized using a grid of 30 km nodes spacing in *x* and *y* and 50 km node spacing in *z* for a total of 465 nodes (Figure 5.5). For each node I have used a reference 3D velocity structure, kept fixed, [Chiarabba et a., 2008] and an initial uniform value of *Q* fixed at 700 for the Q_P inversion, and at 600 for the Q_s inversion. Q_P and Q_S adjustments are computed only for nodes that are crossed by more than 30 rays (257 nodes).

A total of 1435 t* events for Q_P model and 1015 t* from 157 events for Q_S model have been inverted using the damped least squared technique of Thurber [1993] as modified for attenuation by Rietbrock [2001]. Earthquake locations and velocity parameters are kept fixed during the inversion.

In order to calculate the reasonable damping to be used in the inversion I have tested several damping parameter and for each value of damping, one-iteration inversion run has been performed and the corresponding residual variance has been calculated. The inversions were done until a correct balance between the model complexity and residual variance was found and the results are used to construct a trade-off curve where the tested damping parameters are correlated with the respective residual variance. A damping parameter of 0.01 s has been selected and used for both Q_P and Q_S inversion.
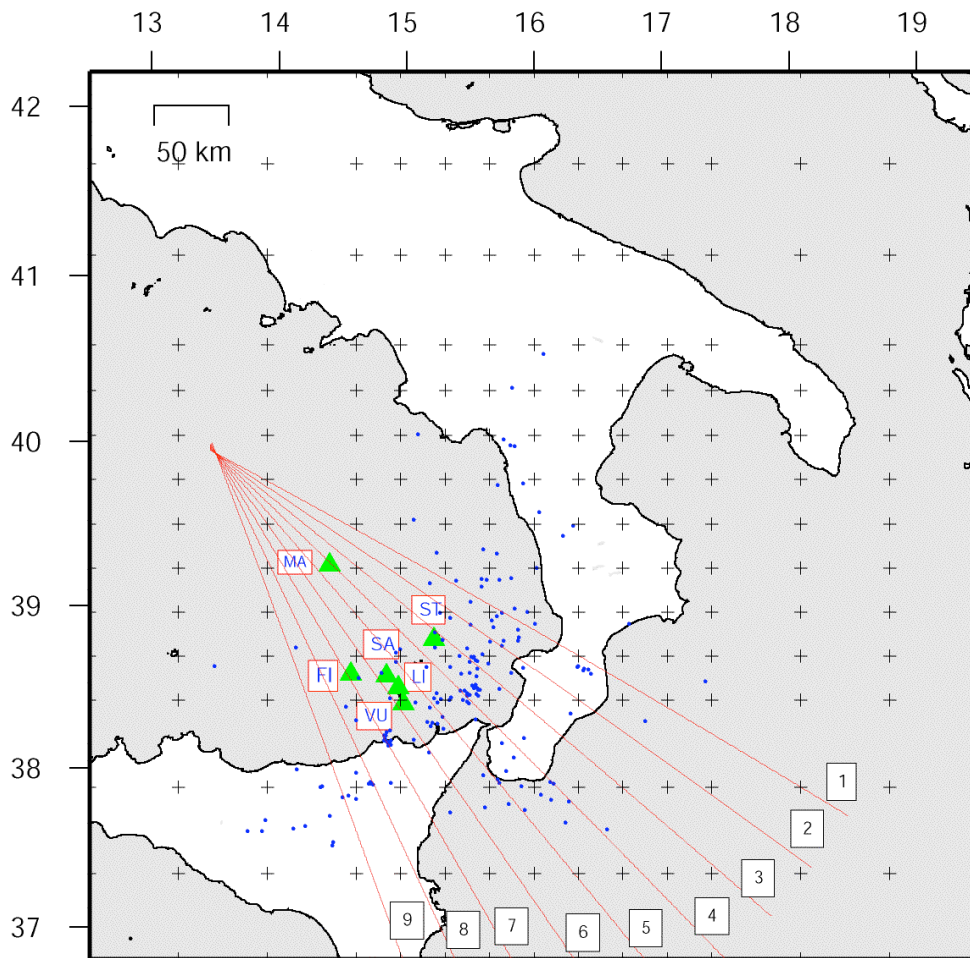
Figure 5.5 Map view of grid nodes (crosses) and earthquakes (blue dots) relocated in the 3D *Vp* model [after Chiarabba et al., 2008] and used for our inversion. The green triangles indicate the main volcanoes of the Tyrrhenian basin and Aeolian Islands complex (MA: Marsili; ST: Stromboli; SA: Salina; FI: Filicudi; LI: Lipari; VU: Vulcano). Red numbered lines are the traces of vertical cross sections in the attenuation models shown in Figs. 5.11, 5.12, 5.13, 5.14, 5.15, 5.16, 5.17, 5.18 and 5.19. Horizontal scale bar is 50 km.

After 4 iterations, the variance improvement is 47% (final rms= 0.020 s) and 39% (final rms =0.023 s) for Q_P and Q_S inversion, respectively.

Formal errors on the final Q parameters, calculated with the covariance matrix, are less than 10 percent of the observed Q_P and Q_S variations.

5.1.3 Synthetic tests

The final 3-D attenuation tomographic models contains errors related to the inexact both of the Q starting and the velocity models, errors in the t* determination and lack of resolution within certain parts of the model. Therefore, the reliability of the attenuation tomographic results has also been performed using synthetic tests (Figure 5.6).
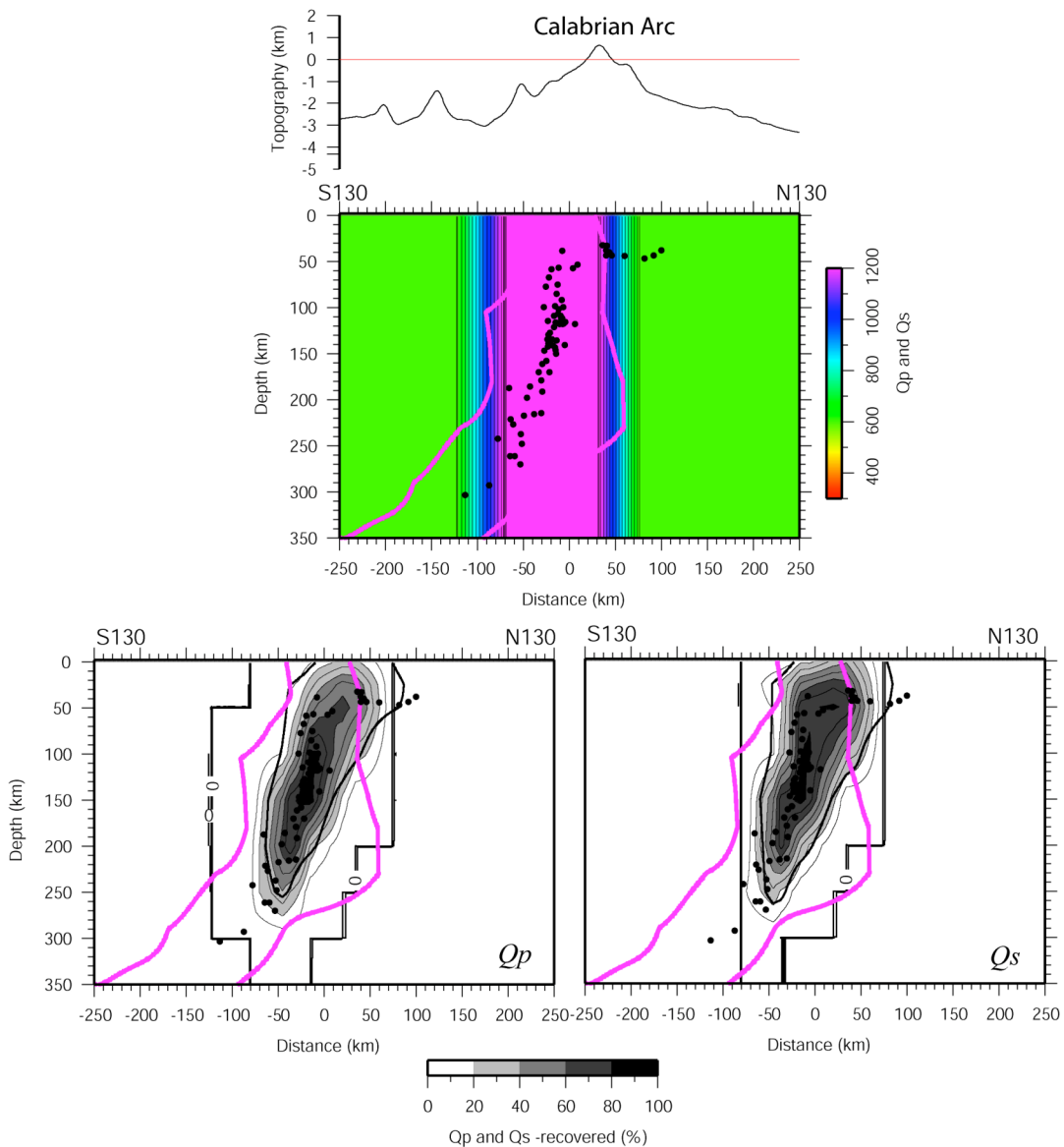
Figure 5.6 Synthetic test inversion result, using the same real inversion procedure and damping as in the actual data inversion. Top figure represent the input model, while the bottom two figures show the recovered models for the Q_P (left) and the Q_S(right). Colored line represents the geometry of the slab as inferred from teleseisms tomography [Giacomuzzi et al., 2011]

I have used the same event-station distribution and the 3-D velocity model of the inversion, and known synthetic $Q_{P/S}$ model. The synthetic model consists of a high-$Q_{P/S}$ anomaly ($Q_{P/S}$ = 1200) located in the region where we have high $Q_{P/S}$ anomalies related to the subducting plate. The synthetic t* data are determined by forward calculation through the synthetic model. Furthermore, a random noise of 10% of the observed t* average value was added to the synthetic t* dataset. Finally, I have inverted the synthetic t* dataset using the parameters of the real case in the same manner I did for the real data; the aforementioned procedure has been done both for the P and the S waves. The tests show that the anomalies are generally recovered. Synthetic anomalies appear well reproduced in their shape and dimension but with respect to the original model the absolute values are less pronounced. The most striking feature is the low attenuation body, which is fairly well reproduced. The region of good recovery corresponds to the area of the slab: a good resolution is achieved with the lower attenuation structure in the inner part of the slab itself. In Figure 5.6 is shown an example of synthetic model for a section crossing normal to the slab.

5.1 Attenuation results

The 3D attenuation models have allowed to reconstruct the main attenuation properties throughout the subducting plate and at the top of the slab. The attenuation anomalies of the mantle wedge are not well-reproduced due to the peculiar geometry of the Southern Tyrrhenian Subduction System with respect to spatial distribution of the seismic stations. Indeed, the source-station geometry relative to the shape and extent of the subducted slab force the rays coming from deep intra-slab earthquakes to travel mainly for almost their entire path inside the slab. Hence, only in a minority of cases the P- and S-waves leave the slab to travel within the mantle wedge. The latter is pretty well reproduced along the northeasternmost and southwesternmost sections. The distribution of Q_P and Q_S attenuation anomalies are presented either as map view at different depth layers (where triangles denote the main volcanic districts in the Tyrrhenian Sea) and as vertical sections across the subducting plate. The distribution of hypocenters along vertical sections and the topography are also reported, together with the outline of the subducted Ionian plate extending from shallow to over 350 km depth (derived by teleseismic tomography, after Giacomuzzi et al., 2011). Therefore, layers and cross-sections are extended from the lower crust down to 350 km depth. In addition, vertical sections are designed in order to follow the curved shape of the slab and being normal to its strike. The top of the

subducted slab is estimated by considering the upper limit of the slab seismicity. In each figure the same color code for the Q_P and the Q_S parameters has been used to facilitate comparison.

5.2.1 Map layers

The Q_P and Q_S models clearly show the most striking features of the study region, with both Q_P and Q_S anomalies revealing a pronounced heterogeneous structure. The highs and lows in Q_P and in Q_S exhibit a strong variability in the upper layers, down to about 50 km depth, while in the deeper layers they show a more organized pattern. Shallow layers (0-25 km depth) are characterized by heterogeneous Q_P and Q_S structures. Low Q_P (400-500) are observed behind the Messina Strait, beneath the northern-central sector of Sicily, and beneath the southern sector of the Calabrian Arc..High Q_P (800-900) are recognized along the northern Ionian Calabrian coast and below the central sectors of Calabrian belt and also in the southeastern coast of Sicily. (Figure 5.7) The Q_S models show considerably different features. Q_S values are extremely low, with a minimum of ~ 300-500 beneath the central-northern sector of Sicily, and form a continuous arcuate anomaly running from Sicily up to the central sector of the Calabrian belt. These high attenuation regions seem to be consistent with thick crustal material, and may be related to the flexured crustal material and to high pore fluid pressures. This is consistent with what observed a few kilometres to the north, beneath the central sector of Calabrian belt, where Piana Agostinetti et al. [2009] from receiver function analysis found a 25 km thick crust overlying the subducted sediments of the oceanic Ionian slab. A volume of high value of Q_S (~1100) is also found beneath southeastern Sicily, reproducing the high Q_P value at the same depth range. The so far described attenuation features are also reproduced at deeper layers. Map layer at 25 km depth in fact shows highs and lows of Q anomalies to be quite similar to the upper layer, broadens their size. High Q_P ~ 1000 are recognized in two regions, one located south of the Messina Strait and the other one beneath the northern Calabrian Arc. These two regions are separated by two area of high attenuation with two Q_P minima centred on northern-central Sicily and southern Calabria. At the same depth, also the Q_S attenuation structure shows the same two high attenuation areas, with Q_S ~ 300-500, Small pockets of high Q_S are also visible beneath the northern Calabrian.

Going down to deeper layers, at 50 km depth both Q_P and Q_S are characterized by very high values (~ 1200) along the Tyrrhenian coast of Calabria and W of the Eolian Islands. The transition between these two highs is marked by a N-S elongated low Q_P (~ 300-400) region, extended from the Eolian Islands to the Mt. Etna. While for the Q_P model this feature is well

reproduced, in the Q_S model it is not well reconstructed and appears barely visible. Indeed, shear wave attenuation shows an area of very high Q_S extended from northern Sicily to the western coast of southern Calabria.

The passage to the deeper layer is marked by a lesser small-scale variability between low and high attenuation zones. Starting from the layer at 100 km depth, the most striking feature is the presence of a well-defined high Q_P and Q_S (up to 1200) anomaly beneath the Tyrrhenian coast of the Calabrian Arc. The high Q_P anomaly is sharply bounded at its NW and SW edges by pockets of high attenuation (Q_P 300-500). Moreover, this feature appears less pronounced in the Q_S model (~500), particularly along the western coast of Calabria. These features strongly suggest the presence of a continuous slab and adjacent asthenospheric material rising beneath the Tyrrhenian Sea. Another striking feature is the migration of the high attenuation anomaly (particularly the low
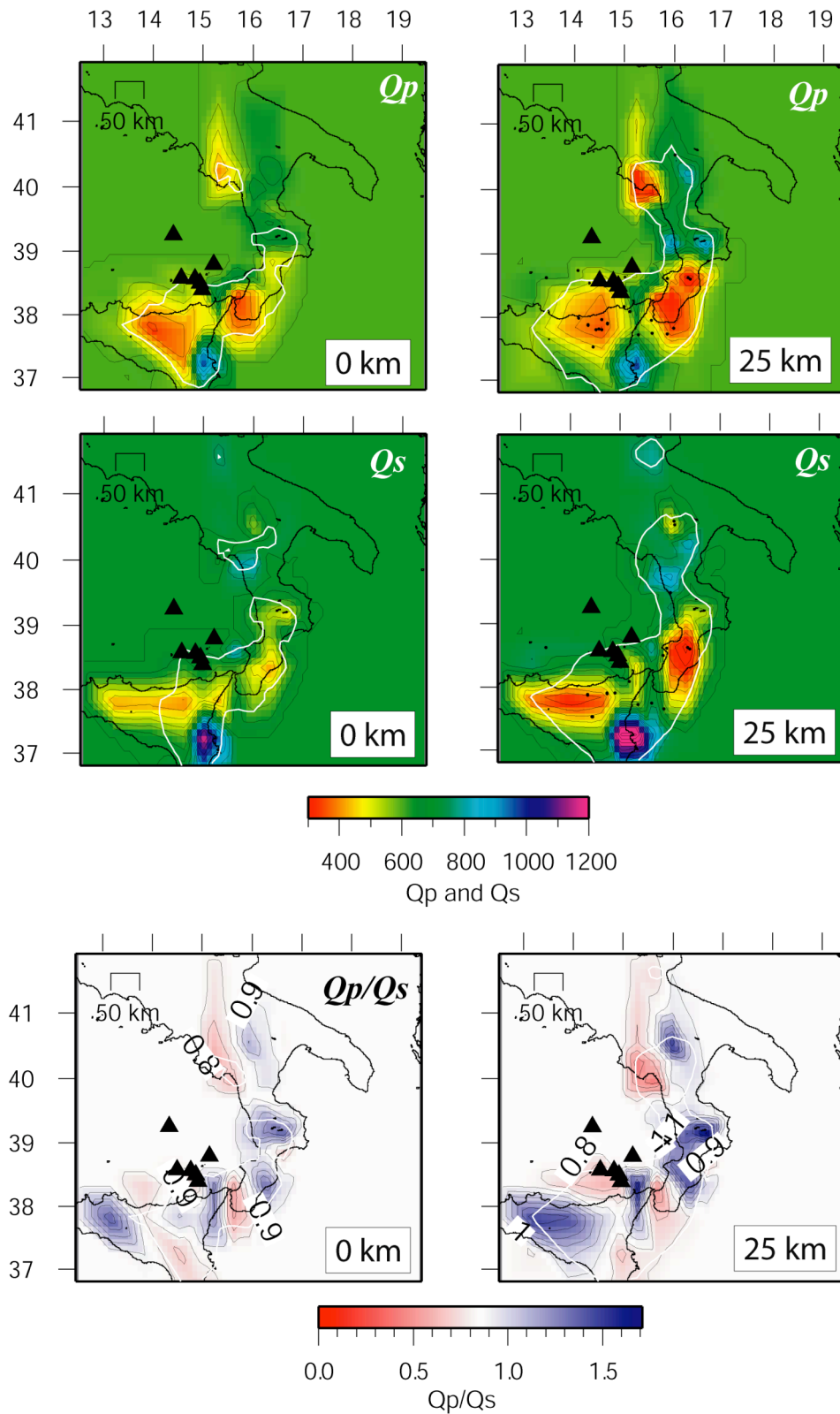
Figure 5.7 Upper panel: map view of Q_P parameter at 0 km depth (left) and 25 depth (right). Middle panel: map view of Q_S parameter at 0 km depth (left) and 25 km depth (right). Lower panel: map view of Q_P/Q_S ratio at 0 km depth (left) and 25 km depth. Black triangles indicate the main volcanoes of the Aeolian Islands complex. White line encloses the slab Black dots are the earthquakes relocated in the 3D Vp model (after Chiarabba et al., 2008) and used for our inversion. Horizontal scale bar is 50 km. See details in the text.
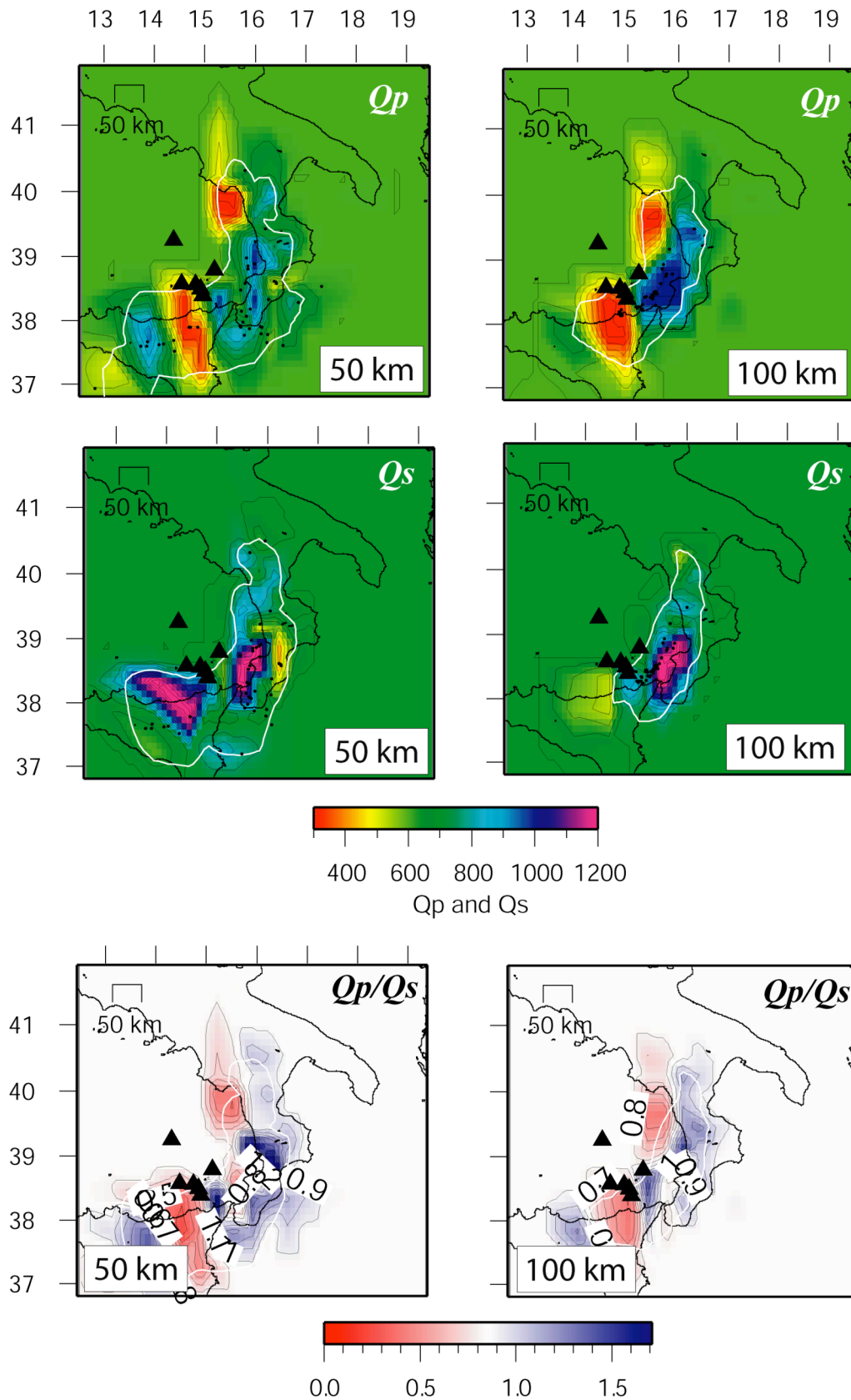
Figure 5.8 Upper panel: map view of Q_P parameter at 50 km depth (left) and 100 depth (right). Middle panel: map view of Q_S parameter at 50 km depth (left) and 100 km depth (right). Lower panel: map view of Q_P/Q_S ratio at 50 km depth (left) and 100 km depth. For other symbols refer to previous Figure 5.7.

75
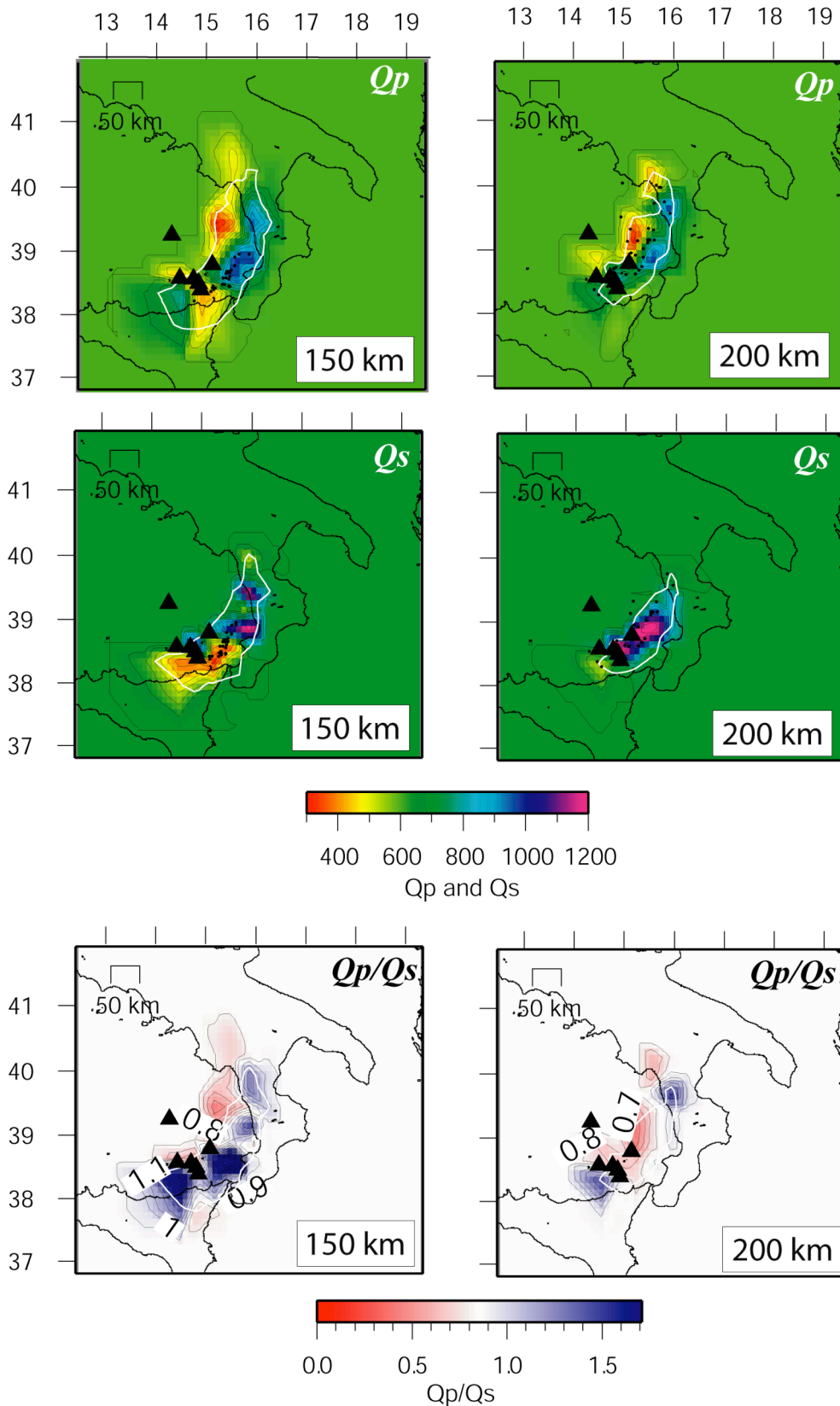
Figure 5.9. Upper panel: map view of Q_P parameter at 150 km depth (left) and 200 depth (right). Middle panel: map view of Q_S parameter at 150 km depth (left) and 200 km depth (right). Lower panel: map view of Q_P/Q_S ratio at 150 km depth (left) and 200 km depth. For other symbols refer to previous Figure 5.7.
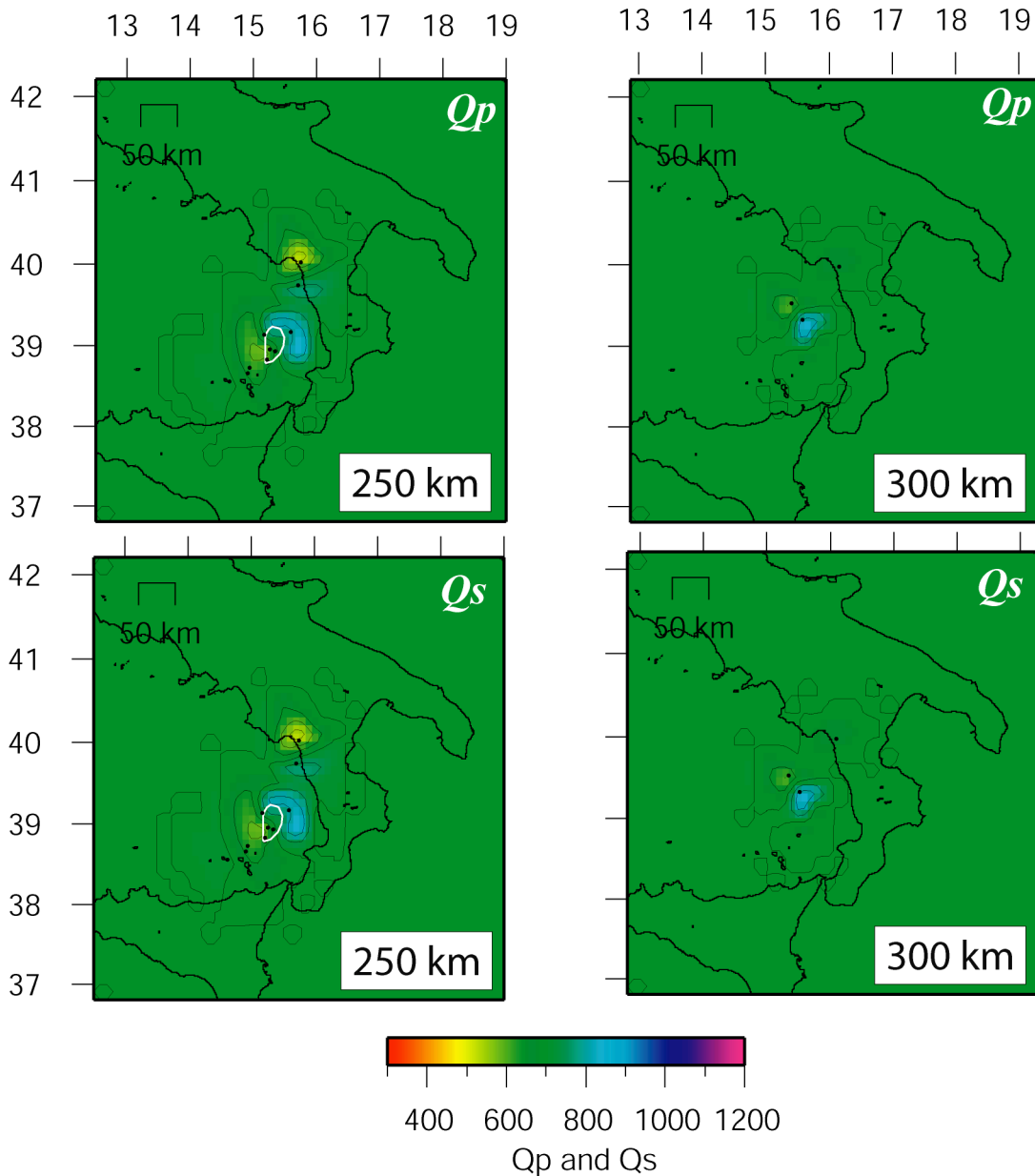
Figure 5.10 Upper panel: map view of Q_P parameter at 250 km depth (left) and 300 depth (right). Lower panel: map view of Q_S parameter at 150 km depth (left) and 300 km depth (right). For other symbols refer to previous Figure 5.7.

Q_P values) from the Calabrian-Sicilian belt toward the Southern Tyrrhenian Sea as the depth increases. Finally, the attenuation structure of the deeper layers, from 200 to 300 km depth, is barely defined. the deepest earthquakes (about 300 km depth) we selected for our inversion do not contribute to resolve the attenuation models below 250 km depth, because of scarce ray coverage and criss-crossing

5.2.2 Cross section

The vertical sections across the Ionian slab clearly show the main feature of the Southern Tyrrhenian Subduction system, explicitly the overall low attenuation of the subducted slab. Moreover, the vertical sections reveal a rather heterogeneous attenuation structure of the slab and of the adjacent regions. Shallower layers, down to 50 km depth, confirm the nature of high attenuation region, with Q_P and Q_S values ~ 300-500. This feature is most clearly showed in the Q_S models rather than Q_P and can be related to fluid content in the crustal layers [Reyeners et al., 2006], as also suggested by Piana Agostinetti et al. [2009] to the north.

Moreover, the most prominent feature of the vertical attenuation images is the continuous low attenuation region that we identify as the Ionian slab. The very high Q_P and Q_S (900-1200) features are well recognized where there is the most resolution and can be distinguished in the sections between the central sector of the Calabrian Arc (section 1) and east of Messina Strait (section 5). The low attenuated volume is imaged as a narrow body dipping toward NW at ~ 75°-80°.

The core of the slab at a first glance is characterized by a very low attenuation, with maximum values of Q_P and Q_S ~ 1200 and it extends primarily between 50 and 160 km depth. Moderate to high values of Q_P and Q_S persist also at greater depth, down to 350 km. This suggests that the slab has likely high Q_P also at greater depth and this is consistent with the very old aged [Catalano et al., 2001] Ionian slab being relatively cold. The same feature is also well recognized by recovery tests. Indeed, the synthetic test (Figure 5.6) reveals a uniformly low attenuated region extending continuously down to 250 km depth, with maximum Q_P and Q_S ~ 1200 in the core of the slab, between 80 and 200 km depth. Comparing the synthetic data with the actual results, the maximum Q_P and Q_S values are near the actual values.

The sections from N130° to N 150° (section 3 and 7) show a worthy to note attenuation structure. The *Qp* and *Qs* are different: starting from section 5 for Q_P, and section 3 for Q_S, an important attenuation is imaged in a wide region (Q_P and Q_S, ~ 300-500). This volume of high attenuation is located in the middle of the slab (compare the position of anomalies with respect to the slab outline), at depth between 130 and 180 km. Moving southwest towards Sicily throughout the Messina Strait the well-defined low Q_S attenuation region is almost centred at ~ 150 km depth. On the other hand, the Q_P anomaly broadens moving to the south (vertical sections 6 to 9; Figure 5.16 to 5.19) and seems to involve a shallower volume (around ~75-100 km depth) where the slab most probably disappears.

The unusual features of high shear wave attenuation are located where there is a cluster of intermediate and deep earthquakes, which can be related to the considerable dehydrations and metamorphic reactions occurring in the slab favouring and subsequently release a conspicuous amount of fluids. Conversely, the Q_P low anomalies, particularly in correspondence of the Messina Strait, show a reduction of intra-slab seismicity.

The shallowest regions, above 50 km depth, generally show higher attenuation, with Q_P and Q_S ~ 300-500.

5.2.3 Q_P/Q_S ratio

The Q_P/Q_S models show moderate variations, appearing fairly heterogeneous in the whole area with values ranging between 0.0 and > 1.7 (Figure from 5.7 to 5.19). Q_P/Q_S ratio reproduces the high variable features imaged by the Q_P and Q_S models. In the shallowest layers, from surface down to 25 km depth, the Q_P/Q_S ratio shows a continuous belt with values > 1.5 and, going down to deeper layers, the Q_P/Q_S ratio seems to reproduce both the Q_P and Q_S structures. Q_P/Q_S > 1.5 are identified in the southeastern sector of the Tyrrhenian Sea, in front of the Calabrian coasts, and beneath Sicily east of Mt. Etna Volcano. This > 1.5 volume seems to shift toward NW in the deeper layers, accordingly to the NW dip of the slab, but at 200 km depth it is replaced by very low Q_P/Q_S ~ 0.5-1.0.

Vertical sections (Figure 5.11 to 5.19)show the presence of high Q_P/Q_S between 130-180 km depth, bounded, above and below, by regions characterized by generally low Q_P/Q_S. In particular, Q_P/Q_S > 1.5 well corresponds to minima in the Q_S distribution, where also intermediate to deep earthquakes cluster (sections 3 to 5, Figure 5.13 and 5.15), This suggest a relationships between intra-slab seismicity and strong attenuation of shear waves. Furthermore, vertical sections 6 to 9 show that the shallow (~ 75-100 km depth) low Q_P area is also highlighted by Q_P/Q_S < 0.5-0.7, denoting a much stronger P-wave rather than S-wave attenuation in this region, where presumably the slab disappears.

5.3 Discussion

The 3D attenuation models shows a rather heterogeneous Q_P and Q_S structure beneath the Southern Tyrrhenian Subduction System. Looking at the vertical cross sections between northeast Sicily and Southern Calabria (Figure from 5.11 to 5.19), the Q_P and Q_S structure of the Ionian slab shows some interesting complexities. Quite low values of Q_P (< 600 from sections 1 to 9) and Qs (< 500 from sections 1 to 4 and 7 to 9) characterize the uppermost slab
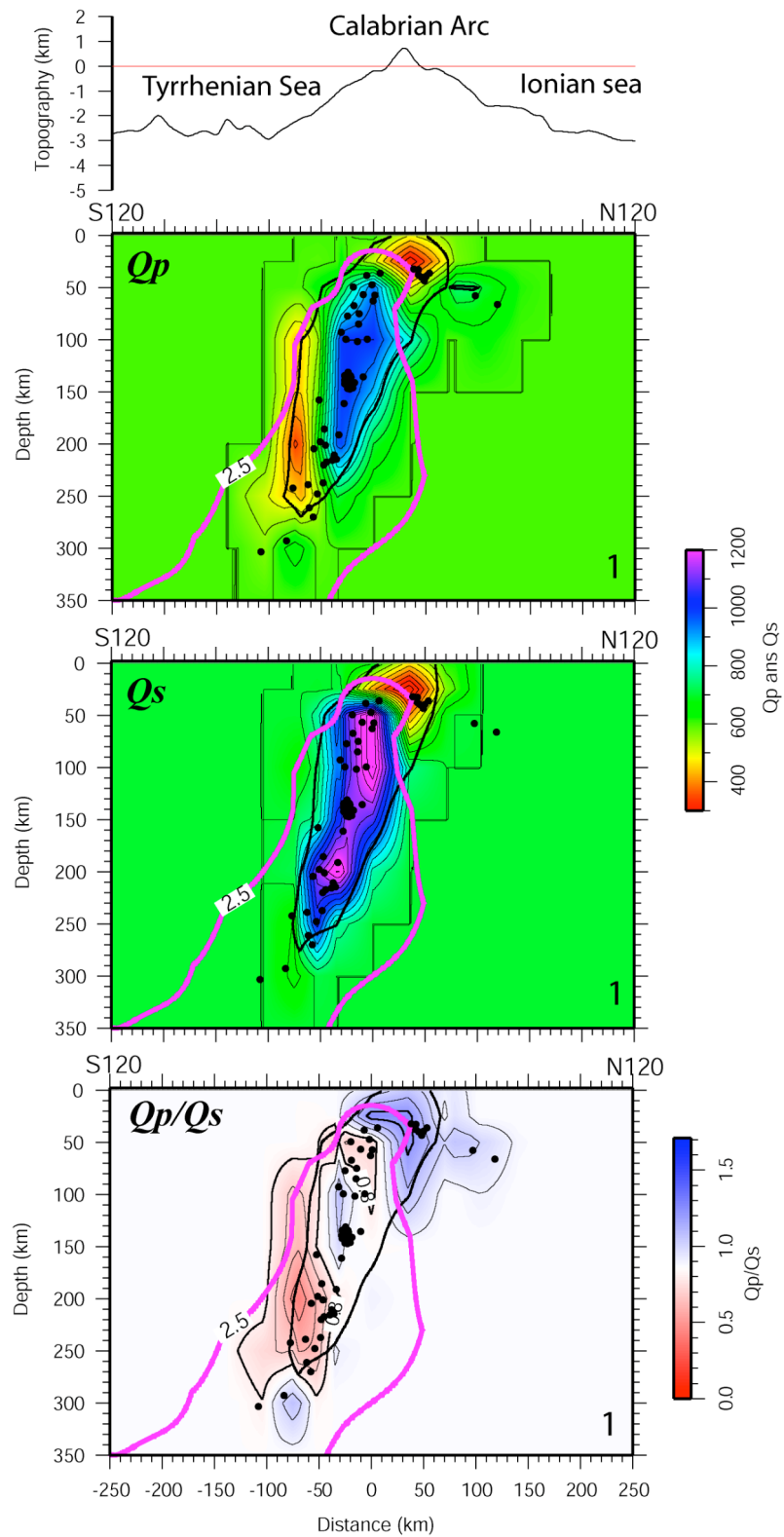
Figure 5.11 Vertical cross section 1 (see location in Fig. 5.5). From top to bottom: topographic profile along the section; Q_P model; Q_S model; Q_P/Q_S model. Black dots are the earthquakes relocated in the 3D Vp model [after Chiarabba et al., 2008] and used for our inversion (see Figs. 5.7, 5.8, 5.9). The violet line encloses the slab as inferred from teleseismic tomography [Giacomuzzi et al., 2010]. Note that the orientation of each section is given by azimuth from the N (right corner) and from the south (left corner) respectively.
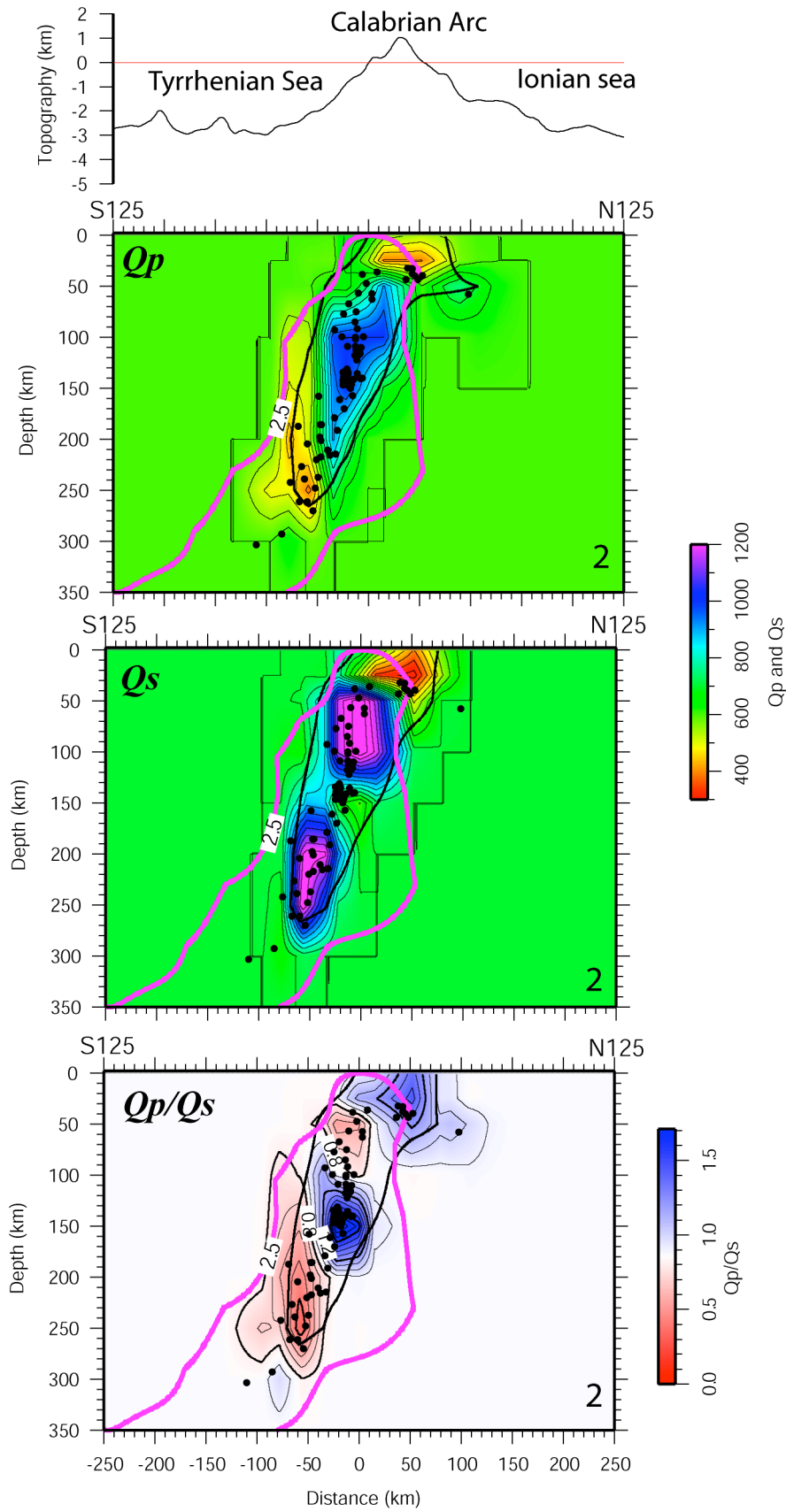
Figure 5.12 Vertical cross section 2 (see location in Fig. 5.5). From top to bottom: topographic profile along the section; Q_P model; Q_S model; Q_P/Q_S model. For other symbols refer to Figure 5.11.
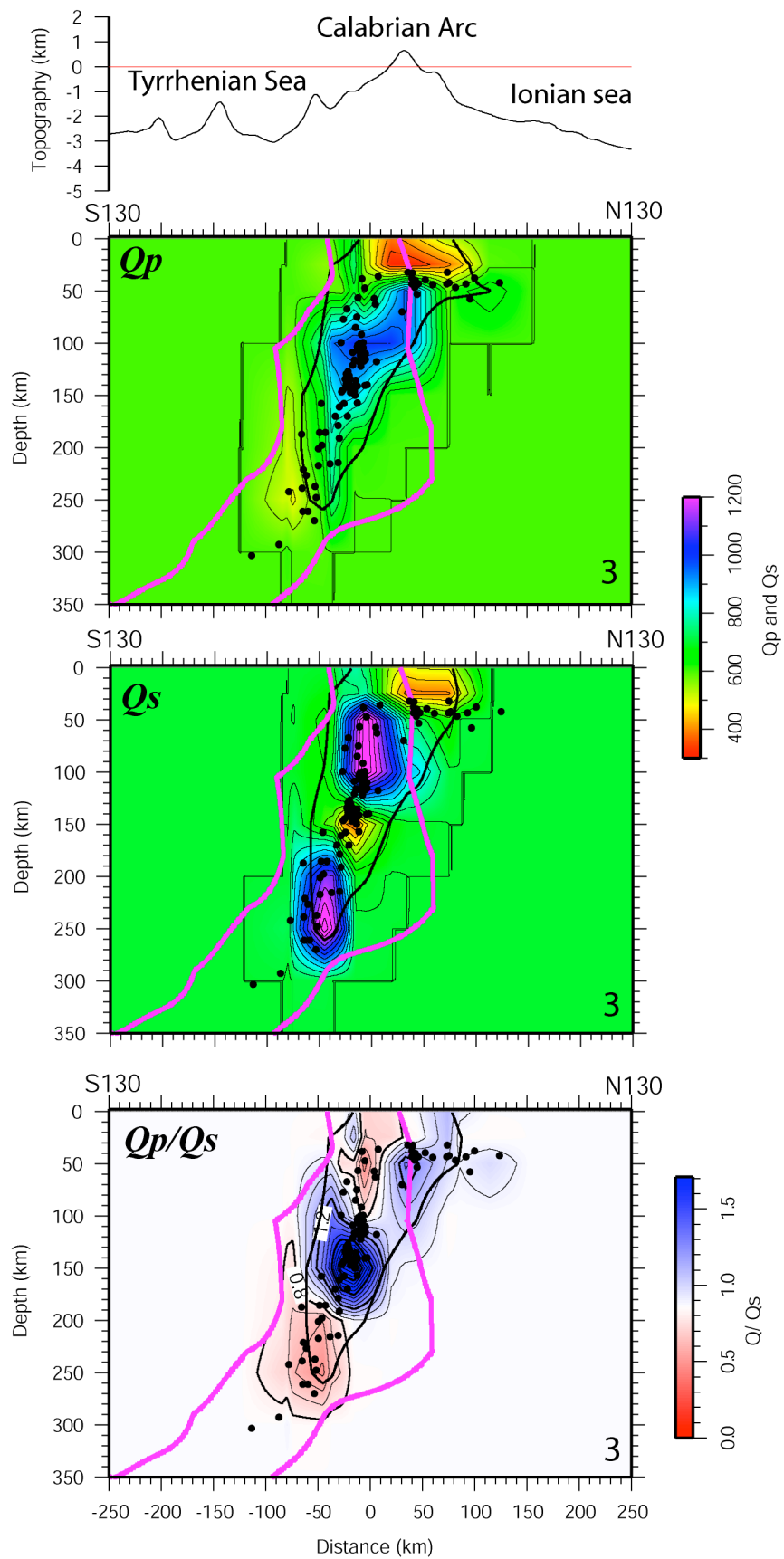
Figure 5.13 Vertical cross section 3 (see location in Fig. 5.5). From top to bottom: topographic profile along the section; Q_P model; Q_S model; Q_P/Q_S model. For other symbols refer to Figure 5.11.
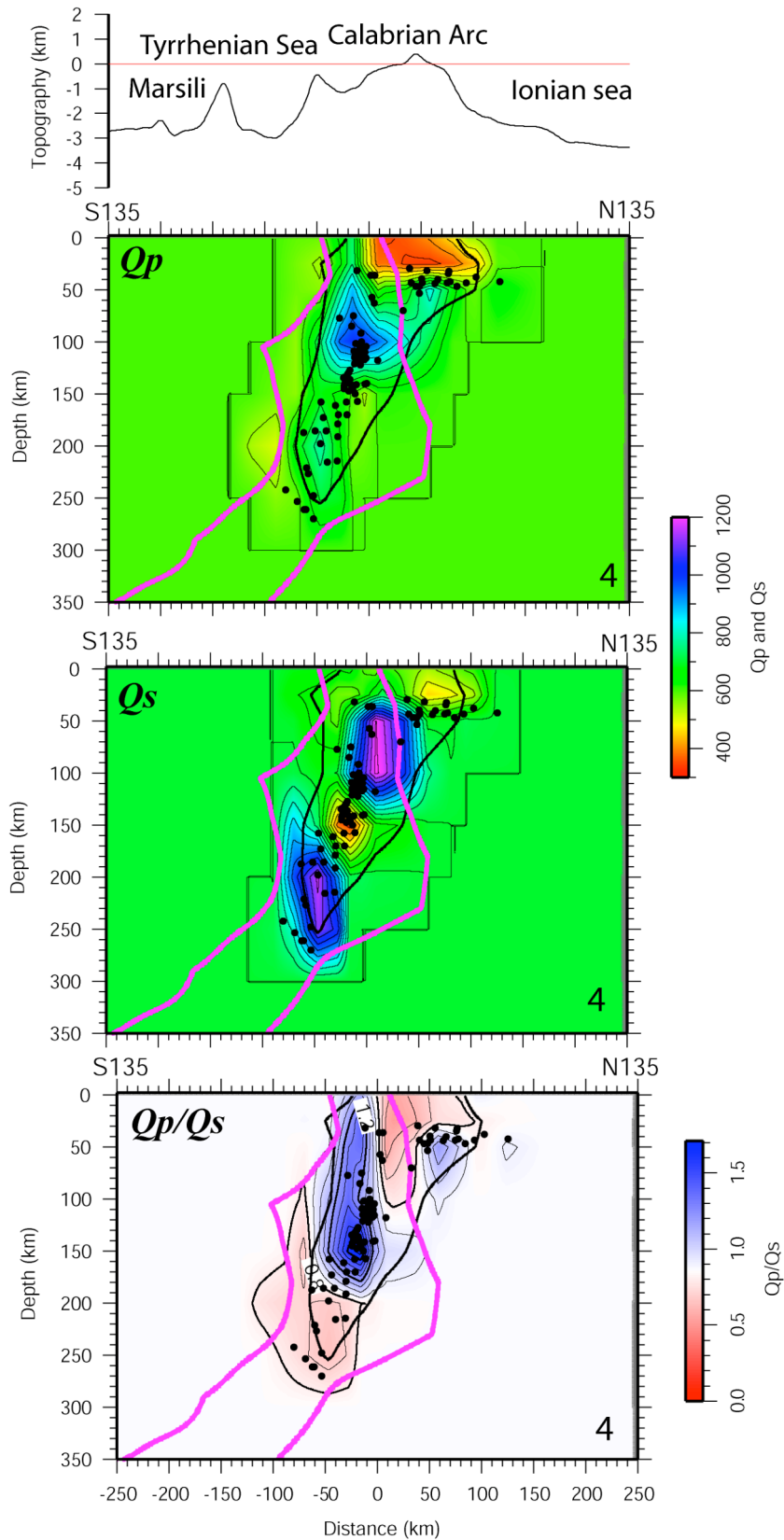
Figure 5.14 Vertical cross section 4 (see location in Fig. 5.5). From top to bottom: topographic profile along the section; Q_P model; Q_S model; Q_P/Q_S model. For other symbols refer to Figure 5.11.
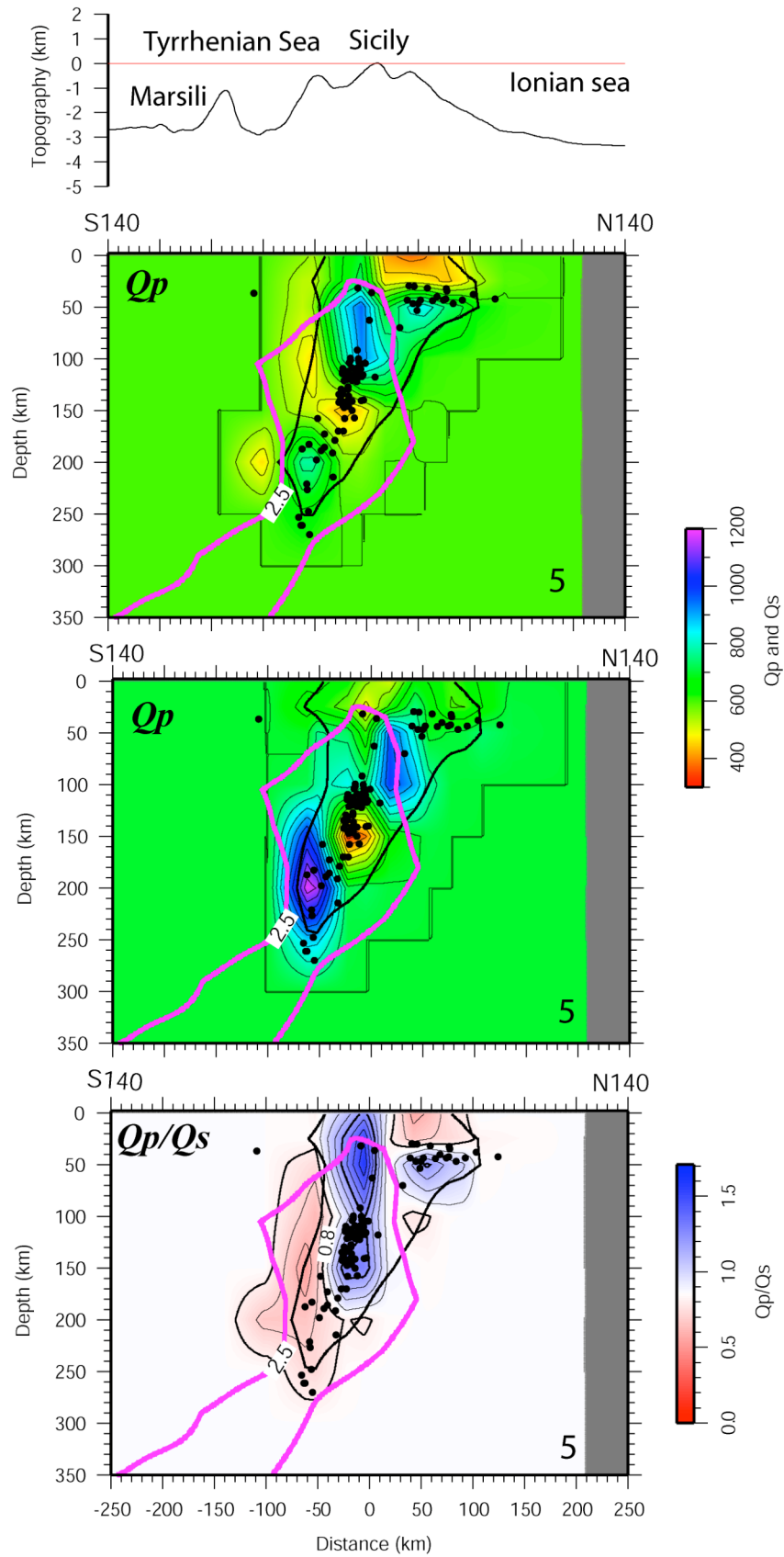
Figure 5.15 Vertical cross section 5 (see location in Fig. 5.5). From top to bottom: topographic profile along the section; Q_P model; Q_S model; Q_P/Q_S model. For other symbols refer to Figure 5.11.
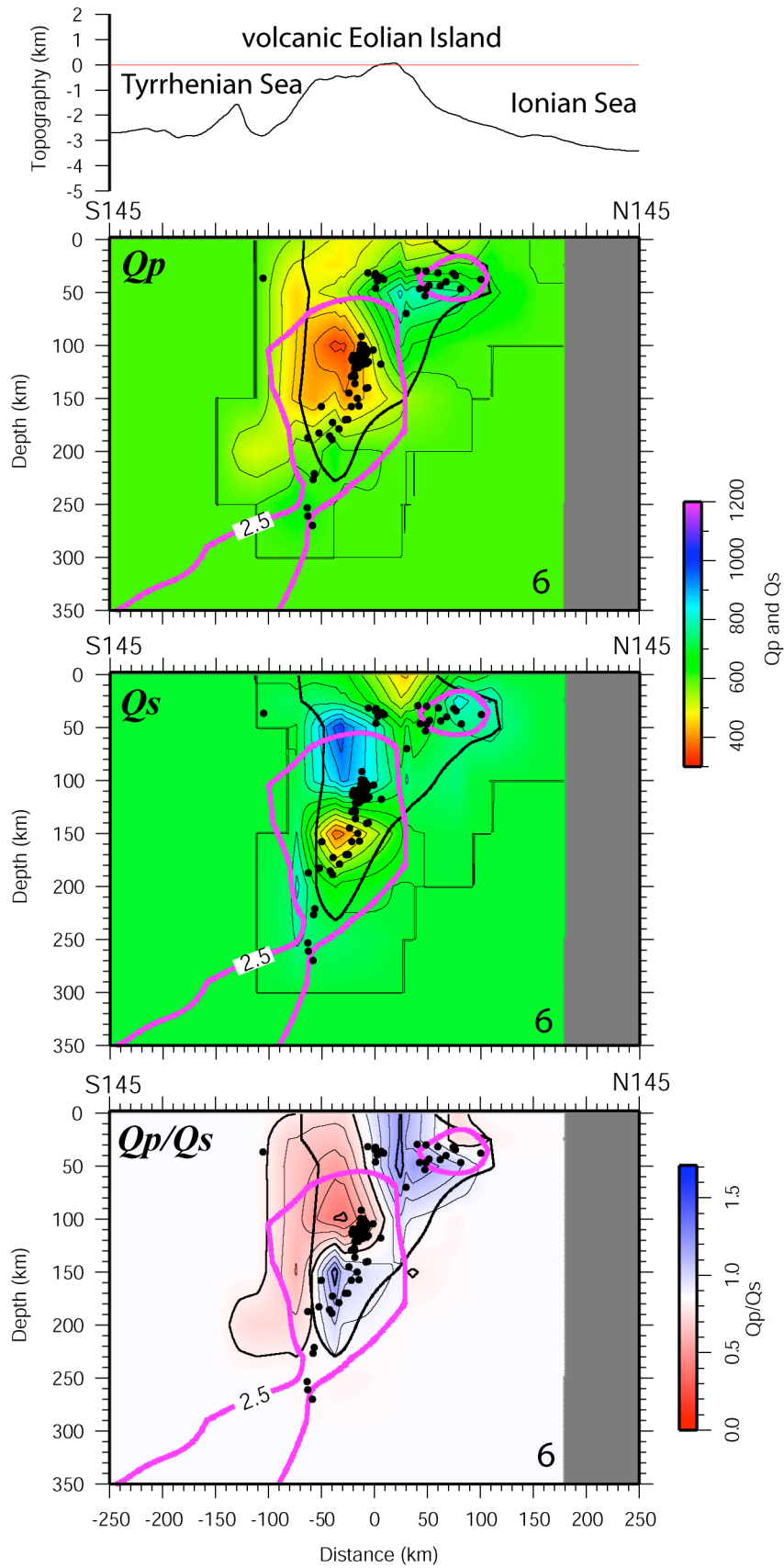
Figure 5.16 Vertical cross section 6 (see location in Fig. 5.5). From top to bottom: topographic profile along the section; Q_P model; Q_S model; Q_P/Q_S model. For other symbols refer to Figure 5.11
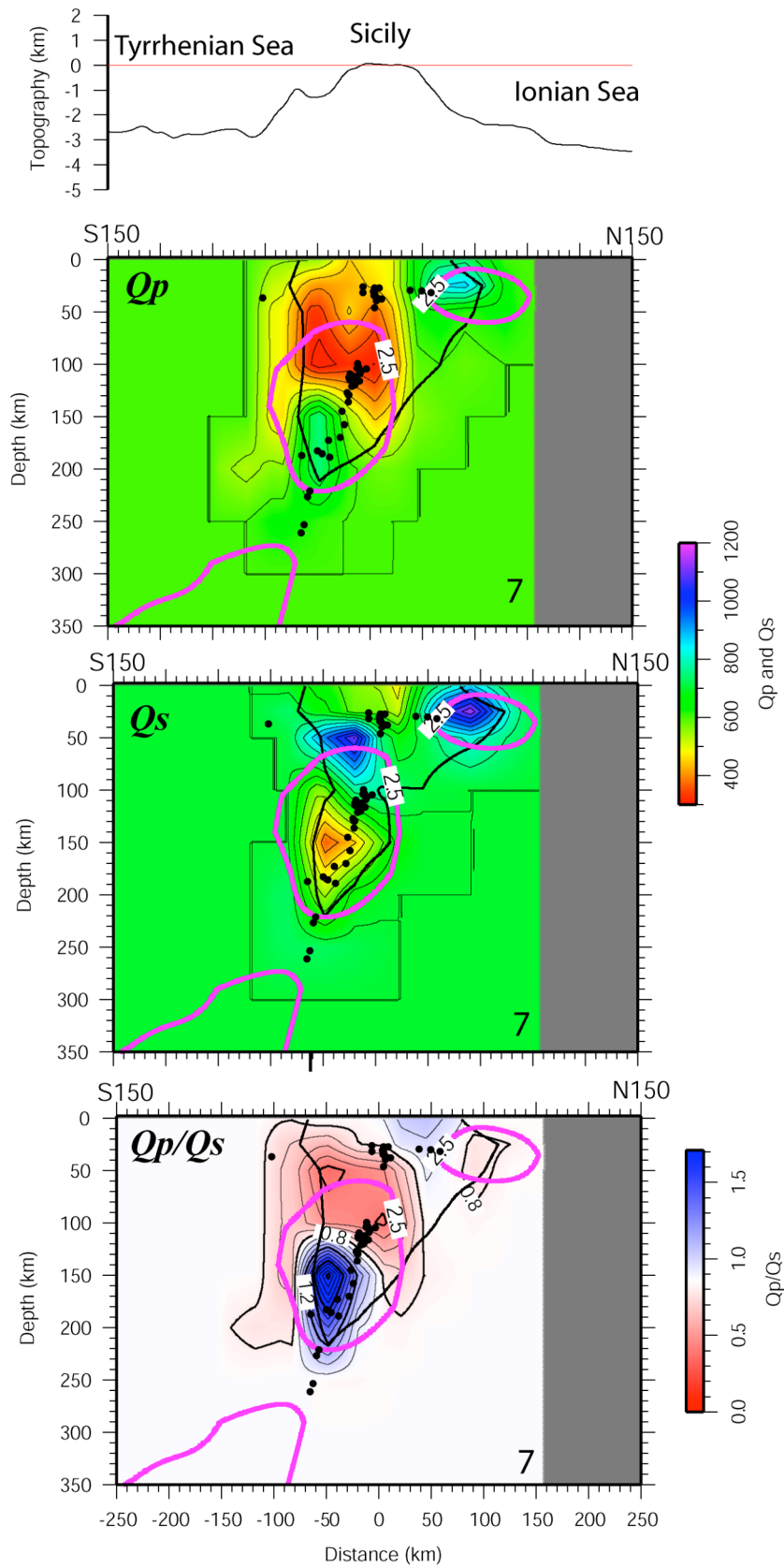
Figure 5.17 Vertical cross section 7 (see location in Fig. 5.5). From top to bottom: topographic profile along the section; Q_P model; Q_S model; Q_P/Q_S model. For other symbols refer to Figure 5.11.
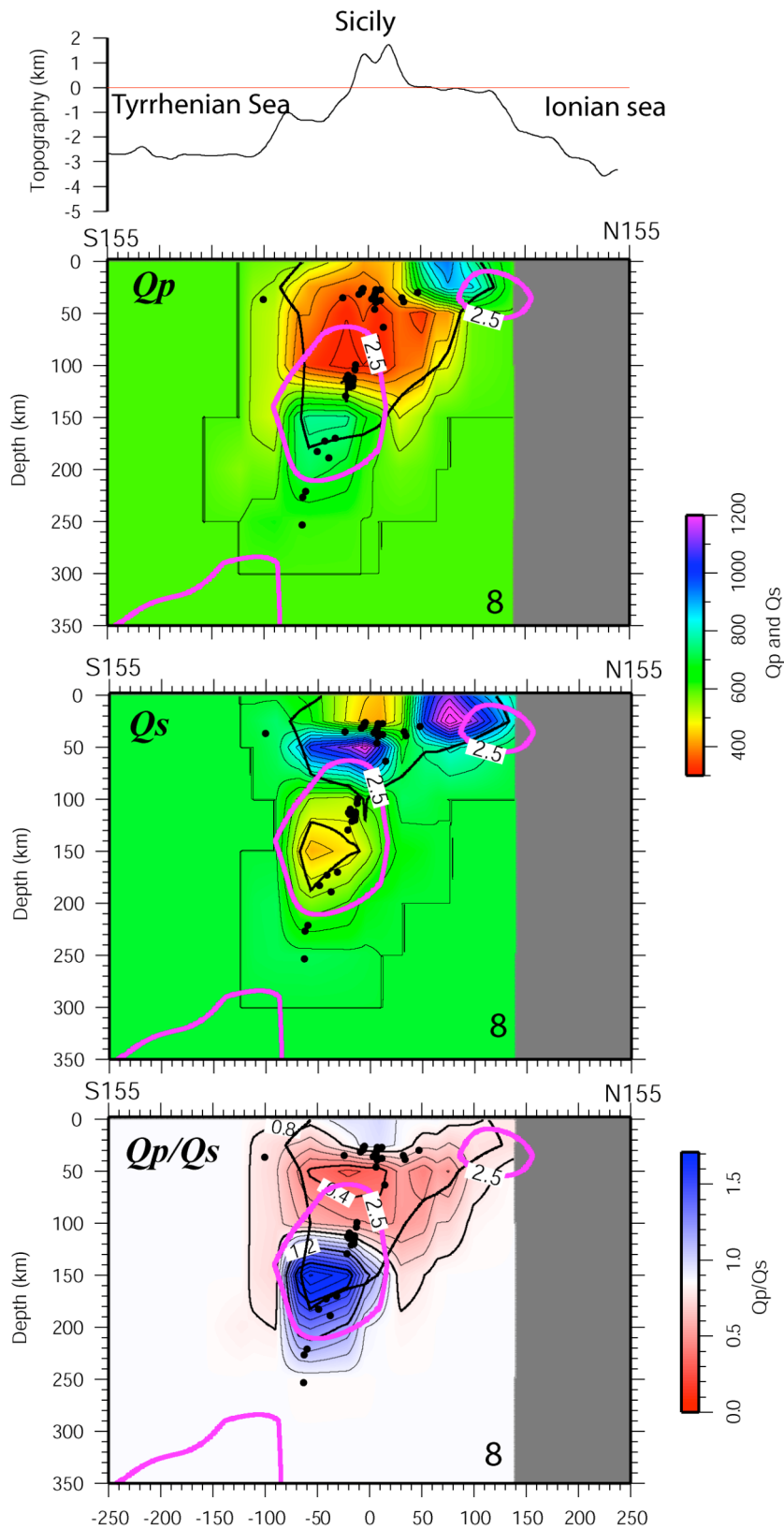
Figure 5.18 Vertical cross section 8 (see location in Fig. 5.5). From top to bottom: topographic profile along the section; Q_P model; Q_S model; Q_P/Q_S model. For other symbols refer to Figure 5.11.
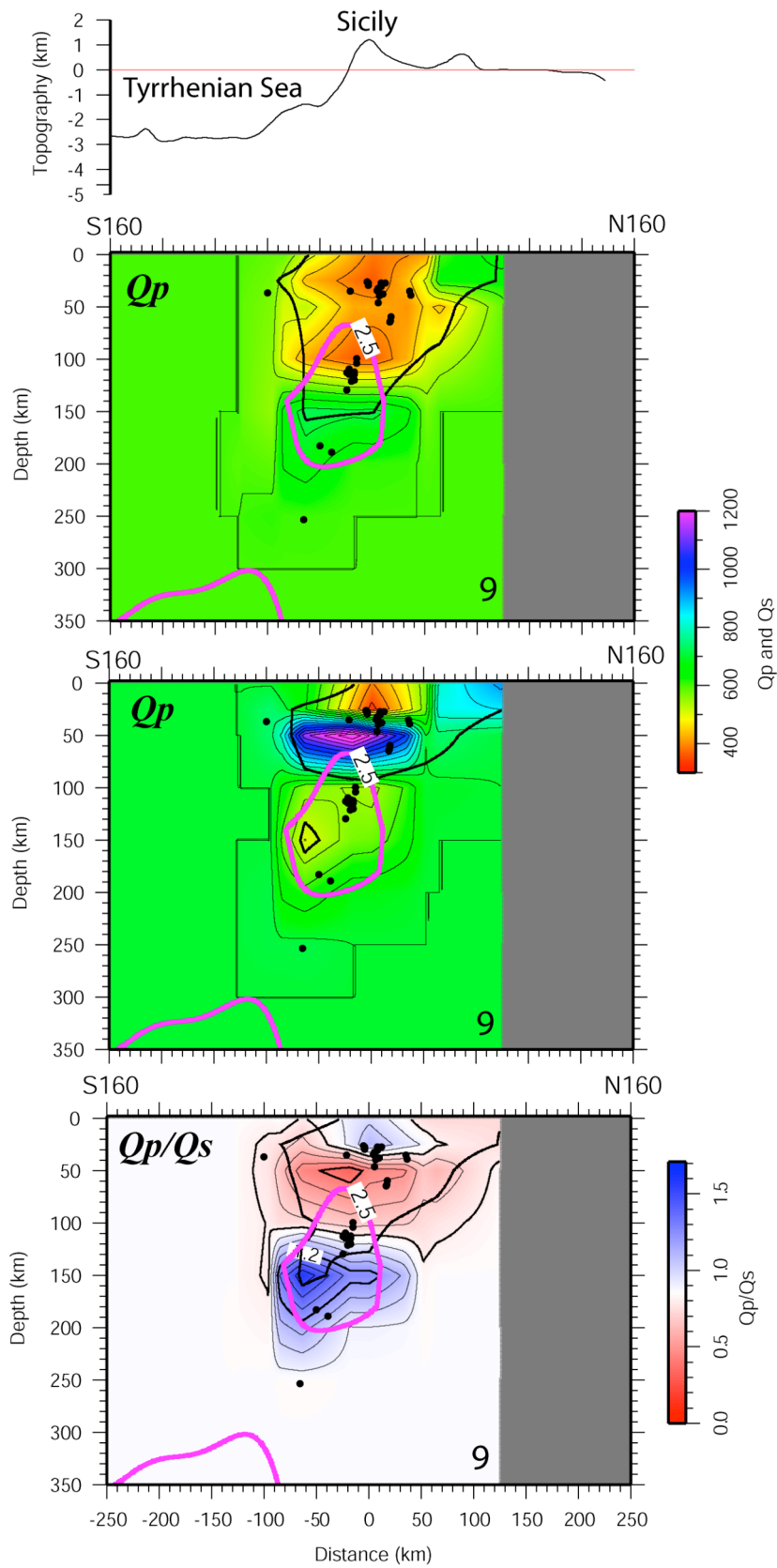
Figure 5.19 Vertical cross section 9 (see location in Fig. 5.5). From top to bottom: topographic profile along the section; Q_P model; Q_S model; Q_P/Q_S model. For other symbols refer to Figure 5.11.

region down to ~ 50 km depth, while most of the remaining slab has Q_P and Q_S values well > 1000, thus denoting the expected low attenuation of a cold, old-aged subducting oceanic body. Important Q_P low anomalies are also found along sections 1 to 2 (depth range: 100-250 km) and sections 6 to 9 down to ~ 150 km depth.

At first glance, the attenuation geometry of the Southern Tyrrhenian Subduction system seems to resemble that of other subduction zones which have volcanic arc, as Mariana [Pozgay et al., 2009],Japan [Tsumura et al., 2000], New Zealand [Eberhart-Phillips et al., 2008], Costa Rica and Nicaragua [Rychert et al., 2008] with low attenuation in the subducting slab and high attenuation in the mantle wedge and in the crust. Nonetheless the results obtained in this study reveal some unusual and unexpected characteristics that have not been observed in the attenuation structure of other subduction zones. This is particularly true for the descending slab that shows different attenuation behaviour when looked by the P or by S- waves. Seismic studies of subduction zones in the majority of cases describe slabs as roughly homogeneous descending bodies featuring very low anelastic attenuation, whereas the mantle wedge above them is always characterized by high attenuation patterns, and this couplet is illustrated by many examples worldwide: the Tonga-Fiji [Roth et al., 1999]; Japan [Tsumura et al., 2000; Peacock, 2001]; the central Andes [Haberland and Rietbrock, 2001; Schurr et al., 2003]; Alaska [Stachnick et al., 2004]; New Zealand [Eberhart-Philips et al., 2008]; Costa Rica and Nicaragua [Richert et al., 2008]; central Mexico [Chen and Clayton, 2009].

In the mantle, seismic attenuation is a function of temperature, grain size, water content, major element chemistry and melt fraction [Faul and Jackson, 2005; Karato, 2006], with temperature and water content having more influence than the other factors on seismic velocity and anelastic energy loss [Shito et al., 2006]. Oceanic slabs indeed typically preserve their cold thermal structure with respect to the warmer surrounding mantle down to great depth, because their descent into the mantle is much faster than rocks heat conduction [Peacock, 2000]. Anyway, both the petrological and thermal structures of slabs may be much more complicated, and their metamorphic evolution is hard to predict, because it depends largely on the age and nature of the down-going plate, convergence rate, thermal field of the upper plate, hydrothermal cooling, inherited faults and fractures, geochemical properties and thickness of oceanic sediments, rate of shear heating at the slab-upper plate interface, the strength and geometry of flow in the mantle wedge and many others [Peacock, 1996].

In the Southern Tyrrhenian Subduction System shallower layers are characterized by high attenuation volumes, which in some cases seem to be better resolved by the Q_P rather than by Q_S anomalies. This high attenuation region is confined in the first 25 km depth and seems to be

correlated to the presence of subducted sediments that will be transported into the mantle [Rüpke et al., 2004]. Thick zones of subducting sediments with high porosity and high fluid pressure have been inferred from seismic velocity, for example, in northeastern Island [Eberhart-Phillips and Reyners, 1999]. The low Q_P and Q_S observed, along with low V_P/V_S (< 1.75) [Chiarabba et al., 2008] seem to be consistent whit the presence of subducting sediments; the reactions involving dehydration of fluid-rich sediments and of the crust, along with serpentinized mantle, represent a source of conspicuous amount of water for this region [Chen and Clayton, 2009; Rüpke et al., 2004]. This feature is also observed looking at the Q_P/Q_S vertical sections, in which the shallower layers are characterized by variable values and pockets of Q_P/Q_S ratio < 1.0. Karato [2006] has shown that an increase in water content leads to a decrease in Q_P and only a modest change in V_P, therefore, low Q_P/Q_S observed in this study, suggests water-saturated conditions which can cause the attenuation of the S waves to be higher than or equal to the attenuation of the P waves [Hauksson and Shearer, 2006].

As in many other subduction zones all over the world, the Ionian slab is imaged as an almost continuous body showing high values of both Q_P and Q_S. Anyway its internal attenuation structure is much more complicated than expected from previous studies (e.g.: Monna and Dahm, 2009).

The most striking feature of our attenuation models anyway is represented by a broad region of low Q_P and low Q_S values (< 500) extending between ∼ 75-200 km depth, which is well documented between cross sections 1 to 9 (Figure from 5.11 to 5.19). The strong attenuation region has different appearance if I look at Q_P and Q_S structure, furthermore it has no clear counterpart in the available 3-D V_P model [Chiarabba et al, 2008], which shows a continuous slab with V_P > 8 km/s. This attenuation region for P- waves is quite shallower than S- waves. The former is in fact localized between ∼ 75-100 km depth and corresponds to Q_P/Q_S < 0.5, while the latter stands at ∼ 130-180 km depth between an upper and a deeper low-attenuated slab portions, corresponding to Q_P/Q_S generally > 1.5. Ratios Q_P/Q_S ∼ 2 indicate that bulk attenuation (that is, the attenuation of the bulk modulus k) is negligible, and thus shear waves must be attenuated more than P waves, while values < 1 need bulk attenuation, and may be explained with partial melt or scattering (e.g.: Pozgay et al., 2009). The indirect presence of an attenuated region in this area of the southern Tyrrhenian, between Sicily and Calabria, has already been assumed by Mele et al. [1997]), due to the attenuation of S waves travelling to the north inside the slab. Recently, a P-wave attenuation model from inversion of teleseismic data [Monna and Dahm, 2009] also reveals the presence of low Q_P regions between ∼ 80-160 km depth close to the Sicily and Calabria northern coasts. Anyway, while the aforementioned

works deal with the properties of the mantle wedge and its possible relations with the Aeolian volcanism, the results of this study show for the first time a clear attenuation signature within the Ionian slab at considerable depth.

The causes of this peculiar low Q_P and Q_S region are not clear, anyway some remarks can be done. In our analysis of displacement spectra, we found an almost frequency independent behavior of attenuation, which, together with the Q_P/Q_S ratio > 2, may account for an important role played by fluids or melts [Faul et al., 2004; Shito et al., 2004].

The strongly P-wave attenuated slab volume between ~ 75-100 km depth and the concomitant S-wave attenuated volume the ~ 120-200 km depth range may be due to the presence of partial melting and fluid release due to metamorphic-dehydration reactions. Dehydration of the subducting lithosphere occurs first at 60 -75 km depth, when the basaltic crust is eclogitized and, second, deeper around 105 km, when in the layer below the crust the high-pressure serpentine phase, known in subduction systems as antigorite [Peacock, 2001; Bostock et al., 2002], becomes unstable [Arcay et al., 2005].

The eclogite metamorphic facies can be found at pressures > 1 GPa (that is below ~ 40 km depth) and for a wide range of temperatures (> 500 °C). In order to melt eclogite under wet conditions in the 100-160 km depth range, there is the need of high temperatures, greater than 700°C [Peacock, 2000]. Therefore, it is possible to suppose that the eclogitization is accomplished by dehydration, with consequent water loss and sudden increase in pore pressure within the above rock volume. Dehydration phase changes within both crust and mantle of subducted slabs are now generally established as the main mechanism for slab embrittlement and earthquake faulting at intermediate depths (down to 300 km depth), whereas the high pressure and temperature conditions would promote plastic flow rather than faulting [Kirby et al., 1996; Peacock, 2001; Dobson et al., 2002; Guillot et al., 2001].

It is very important at this point to underline the pretty clear concentration of seismicity within the high attenuation volume of the Ionian slab in the 120-200 km depth interval (see vertical sections of Q_S from 4 to 9). Thus, we undeniably have the contemporaneous evidence of i) high P-wave and S-wave anelastic attenuation due to the diffuse presence of water and ii) the dehydration-induced seismicity. Beneath the Calabrian Arc indeed the observed cluster of intra-slab seismicity occurs between ~ 130 and 180 km depth, in a region of high S-wave attenuation; this is in agreement with the results found by Schurr et al., [2003] in the central Andean subduction zone. The authors related the seismicity occurred at 90-250 km depth to the fluid release by dehydration reactions, which are responsible of the high attenuation observed in the slab.

A reasonable cause of low Q_P and Q_S values, together with the high Q_P/Q_S ratio in this highly seismic portion of the slab seems therefore in accordance with metamorphic reactions involving noticeable slab volumes, namely the dehydration of antigorite in the mantle lithosphere to form dense anhydrous phases such as forsterite and enstatite, and of the formation of eclogite. The metamorphism and dehydration reactions release a conspicuous amount of water which can lower the Q_S. The slab metamorphic reactions combined with the dehydration of the subducting oceanic crust produce a noticeable amount of water and fluid which migrate toward shallower depths and permeating the mantle wedge, favoring the partial melting of the latter. The depth of dehydration reactions ranges between 130-250 km, if the subducting lithosphere is old aged [Poli and Schmidt, 1995; Abers, 2000]: the Ionian plate has indeed an old aged oceanic crust, hence the locus of such a dehydration reaction could reasonable be located where the low Q_S volume is imaged. The low Q_S values lie where most of the intermediate-deep earthquakes occur, confirming the strict relationship between seismicity and high attenuation [Kirby et al., 1996; Schurr et al., 2003; Hacker et al., 2003; Eberhart-Phillips and Chadwick, 2002; Shelly et al., 2006]. Beneath the Calabrian Belt this occurs in a segment of the descending plate where slab dehydration is reasonably marked by metamorphic reactions involving the eclogite and serpentinite, with consequent release of fluids and lowering Q_S values to < 500. Therefore, the strong attenuation structure observed within the slab between 130-180 km may be related to the ongoing dehydration processes affecting the oceanic Ionian slab with consequently release of enormous amount of water.

The signature of fluid migration from the slab towards the very shallow mantle wedge can be clearly imaged along vertical sections 1, 2 and 5 (Figures 5.11 5.12 and 5.15), where Q_P values < 400 are found from the shallowest layers down to150 km depth and form roughly vertically elongated anomalies. The mantle wedge shows high attenuation behaviour, with $Q_P \sim 400-500$ which seems to be related to melting.

These low Q_P anomalies are partly rooted in the slab and are sometimes associated with a low concentration of seismicity. The reasons for this are unclear. One possible explanation could be the partial melting due to the large fluids release by the deeper portion of the slab itself, or an anomalous increase in temperature responsible for bulk attenuation. The last condition may be also the case of the low Q_P anomalies found at $\sim$ 75-150 km depth in the southernmost part of the Tyrrhenian subduction system (sections 7,8,9; Figures 5.17 5.18 and 5.19), which probably cross a warm mantle wedge where the Mt. Etna magmas are generated.

5.4 Conclusion

In this work I have presented new seismic attenuation models across the Southern Tyrrhenian Subduction zone down to 350 km, along with the high-quality 3D relocation of the intermediate and deep earthquakes. With the aim to gain insights into the physical properties of the mantle wedge and of the slab, the Q_S attenuation structure has also been presented.

Q_P and Q_S 3-D models clearly depict the slab as a generally low attenuated region down to 350 km depth, while the adjacent mantle wedge exhibits a strong attenuation. These two different and strikingly different features may be easily explained in terms of a cold oceanic, rigid plate descending into a warmer, ductile mantle, whose attenuation is even more enhanced by the long-term and continuous release of fluids from the slab itself. Our results anyway depict a much more complex setting, in which the seismic attenuation structure has a marked variability, both vertically and horizontally. As regards the Ionian slab, our analyses point out for the first time an unexpected heterogeneity of the attenuation within the slab. This is highlighted by both the P-waves and S-waves attenuation structures. Q_P values image a wide zone of attenuation located in the southernmost part of the slab, between 75-100 km depth. This slab portion shows a low concentration of intra-slab seismicity, and its location with respect to the important volcanic district of Mt. Etna may lead, as a reasonable explanation, to a warm mantle subject to partial melting. This strongly attenuated region is most probably overlain by a thick and warm mantle wedge, and the low seismicity may account for a more ductile behaviour. Q_S values conversely depict another and deeper region of strong S-wave attenuation and high Q_P/Q_S ratio, located between ~ 80 and 130 km depth. This portion of the slab is also characterized by a clear concentration of seismicity. Current petrological models of metamorphic evolution of oceanic slabs agree in underlining the key role played by dehydration of antigorite (the serpentine polymorph stable at high pressures) in releasing great amounts of water from the slab to the above mantle wedge. Dehydration of serpentine follows at depth the eclogitization of the oceanic crust, and it could be responsible for intermediate to deep slab seismicity (down to 300 km depth). Therefore, a possible explanation for this anomalous low Q_S region and its seismicity the conspicuous presence of water due to ongoing dehydration of slab serpentinite. The ascent of fluids from this ~ 80-130 km depth region seems to be outlined by Q_P anomalies in the adjacent mantle wedge, where vertically elongated regions of low Q_P most probably track the fluid trajectories and depict zones of partial melting. The latter correspond at the surface to the Aeolian volcanic complex in the Tyrrhenian basin, which is a typical example of magmatic

arc related to subduction. Possible pockets of local melting in some portions of the eclogitic slab should be also taken into account.

Finally, as regards the shallowest portion of the subduction system, the Q_P and Q_S anomalies are in agreement with the presence of water expelled by sediments of the Ionian plate subducted under the 25 km thick crust of the Calabrian thrust belt.

Conclusive remarks

The aim of this thesis has been to investigate the past and present-day deformational processes occurred in the Southern Tyrrhenian Subduction zone. I took into account two different geophysical characteristics, the seismic anisotropy and the attenuation. These patterns of these two parameters have allowed to highlights some of the new features concerning the subduction process of the Ionian plate.

The thesis is subdivided into two parts. The first part is focused on the study of the deformation occurred in the upper mantle and in the Ionian descending plate, gain insights about the relationship between the mantle flow and the subduction geometry. To do this, I have used one of the most powerful tools to investigate the deep deformations, that is the shear wave splitting analysis. In the upper mantle, seismic anisotropy is a consequence of the lattice preferred orientation (LPO) of olivine minerals; they are highly anisotropic and when undergo deformation tend to align its fast axes parallel to the mantle flow. I have analyzed several teleseisms recorded from 2003 to 2006 and I have used the method of Silver and Chan to obtain the splitting parameters: the azimuth of the fast polarized shear wave (φ) and delay time (δt). I interpret the pattern of fast directions as related to the rollback of the fragmented subduction system in the mantle of this region. The trench-parallel φ observed in Calabrian Arc and in Southern Apennines has its main source in the asthenospheric flow below the slab likely due to the pressure induced by the retrograde motion of the slab itself. The pattern of φ in the Apulian Platform does not appear to be the direct result of the rollback motion of the slab, whose influence is limited to about 100 km from the slab. The anisotropy in the Apulian Platform may be related to an asthenospheric flow deflected by the complicated structure of the Adriatic microplate or may also be explained as frozen-in lithospheric anisotropy. In addition, seismic anisotropic pattern of the study region has been investigated analyzing several deep earthquakes located within the descending slab. This helped me in gaining information about the deformation status of the descending plate. The local deep earthquakes allow me to analyze ray-paths primarily sampling the slab and the wedge above it giving the unique opportunity to isolate the contribution to the anisotropy from the mantle flow and the slab itself. Mainland Calabria is a forearc high, enabling me to sample rays that propagate up the slab. S-wave splitting parameters show a complex pattern of anisotropy with variable fast directions. I found consistency between averaged S fast directions and the SKS splitting measurements, including a pattern of toroidal mantle flow at the SW edge of the slab. The S-wave splitting parameters

show frequency-dependent behaviour that I attribute to the presence of small-scale anisotropic heterogeneities. Comparison of S splitting measurements to P-wave velocity anomaly at 100-200 km depth shows that where the rays primarily sample the slab the delay times are small. In contrast, where S rays sample the mantle wedge, the delay times are quite high. This δt pattern depicts the slab as a weakly anisotropic region and suggests that the main source of anisotropy in the subduction zone is the surrounding asthenosphere.

The second part of this thesis is focused on the study of attenuation properties of the slab and of the surrounding upper mantle. The attenuation properties have allowed investigating the mechanical and physical properties of the slab and of the upper mantle, provide constrain on the fluid-content and phase changes occurred. Hence, I have create high-resolution Q_P and Q_S models obtained by the inversion of high quality P- and S-waves t* from several local slab earthquakes., I have analyzed several local deep earthquakes. Tomographic inversion shows high-attenuation regions corresponding to the crustal layers with low values of Qs (values down to 200) but high values of Qp. The subducting slab is identified as a body of low attenuation, but heterogeneous in the Qs and Qp structure (Qs values up to 1100; Qp values up to 1200), surrounded by high-attenuation regions beneath the Aeolian magmatic arc. The observed low Qp and Qs anomalies could likely due to the fluids released from dehydrating minerals associated to the slab metamorphism. The observed low Qs anomalies regions between the slab and the Aeolian volcanic arc could be indicative of melting processes in the mantle and also of the large-scale serpentinization.

Chapter Three of this PhD Thesis has been published as: Baccheschi, P., L. Margheriti, and M. S. Steckler (2008), SKS splitting in Southern Italy: anisotropy variations in a fragmented subduction zone, Tectonophysics, 462, 49-67.

Chaphter Four of this PhD Thesis is under review as: P. Baccheschi, L. Margheriti, M. S. Steckler, E. Boschi Anisotropy patterns in the subducting lithosphere and in the mantle wedge. A case study: the Southern Italy subduction system, J. Geophys. Res.

References

Abers, G. A., 2000, Hydrated subducted crust at 100-250 km depth, Earth Planet. Sci Lett., 176, 323-330.

Aizawa, Y., A. Barnhoorn, U. H. Faul, J. D. Fitz Gerald, I. Jackson, and I. Kova´cs, 2008, Seismic properties of Anita Bay dunite: An exploratory study of the influence of water, J. Petrol., 49, 841 855, doi:10.1093/petrology/egn007.

Alsina, D., and R. Snieder, 1995, Small-scale sublithospheric continental mantle deformation: constraints from SKS splitting observations, Geophys. J. Int., 123, 431–448.ù

Alvarez, W., T. Cocozza, F. C. Wezel, 1974, Fragmentation of the Alpine orogenic belt by microplate dispersal, Nature, 248, 309–314.

Anderson, H., and J. Jackson, 1987, Active tectonics of the Adriatic Region, Geophys. J. R. Astronom. Soc., 91, 937–983.

Anderson, J.G., and S.E. Hough, 1969, A model for the shape of the Fourier amplitude spectrum of acceleration at high frequencies, Bull. Seismol. Soc. Am., 74, 1969-1993.

Anderson, M.L., G. Zandt, E. Triep, M. Fouch, and S. Beck, 2004, Anisotropy and mantle flow in the Chile–Argentina subduction zone from shear wave splitting analysis, Geophys. Res. Lett. 31, L23608. doi:10.1029/2004GL020906.

Arcay, D., E. Tric, and M.-P Doin, 2005, Numerical simulations of subduction zones Effects of slab dehydration on the mantle wedge dynamics, Physics. Earth Planet. Int., 149, 133-153.

Atkinson, G. M., 1995, Attenuation and source parameters of earthquakes in the Cascadia region, Bull. Seismol. Soc. Am., 85, 1327– 1342.

Aubouin, J., R. Blanchet, J.-P. Cadet, P. Celet, J. Charvet, J. Chorowicz, M. Cousin, and J.-P. Rampnoux, 1972, Essai sur la géologie des Dinarides, Bull. Soc. Géol. Fr., 12, 1060–1095.

Audoine, E., K.M. Savage, and K. Gledhill, 2000, Seismic anisotropy from local earthquakes in the transition region from a subduction to a strike-slip plate boundary, New Zealand, J. Geophys. Res, 105, 8013–8033.

Audoine, E., and M.K. Savage, 2004, Anisotropic structure under a back arc spreading region, the Taupo Volcanic Zone, New Zealand, J. Geophys. Res., 109 (B11305), doi:10.1029/2003JB002932.

Baccheschi, P., L. Margheriti, and M. S. Steckler, 2007, Seismic anisotropy reveals focused mantle flow around the Calabrian slab (Southern Italy), Geophys. Res. Lett., 34, doi: 10.1029/2006GL028899.

Baccheschi, P., L. Margheriti, and M. S. Steckler, 2008, SKS splitting in Southern Italy: anisotropy variations in a fragmented subduction zone, Tectonophysics, 462, 49-67.

Battaglia, M., M. H. Murray, E. Serpelloni, and R. Bürgmann, 2004, The Adriatic region: an independent microplates within the Africa–Eurasia collision zone, Geophys. Res. Lett., 31, L09605, doi:10.1029/2004GL019723.

Beccaluva, L., P. Brotzu, G. Macciotta, L. Morbidelli, G. Serri, and G. Traversa, 1989, Cenozoic tectono-magmatic evolution and inferred mantle sources in the Sardo-Tyrrhenian area, in The Lithosphere in Italy: Advances in Earth Science Research, edited by A. Boriani et al., pp. 229-248, Accad. Naz. Dei Lincei, Rome.

Beghein, C., and J. Trampert, 2003, Robust normal mode constraints in inner-core anisotropy from model space search, Science, 299, 552–555.

Beghein, C., and J. Trampert, 2004, Probability density functions for radial anisotropy: implications for the upper 1200 km of the mantle, Earth Planet Sci Lett., 217, 151–162.

Behn, M.D., G. Hirth, and P. B. Kelemen, 2007, Trench-parallel anisotropy produced by foundering of arc lower crust, Science, 317, 108-111, doi: 10.1126/science.1141269.

Ben Ismail, W., D. Mainprice, 1998, An olivine fabric database: an overview of upper mantle fabrics and seismic anisotropy, Tectonophysics, 296, 145-157.

Berryman, J.G, P.A. Berge, and B.P. Bonner, 2002, Estimating rock porosity and fluid saturation using only seismic velocities, Geophysics, 67,2, 391-404, doi:10.1190/1.1468599.

Billi, A., G. Barberi, C. Faccenna, G. Neri, F. Pepe, and A. Sulli, 2006, Tectonics and seismicity of the Tindari Fault System, southern Italy: Crustal deformations at the transition between ongoing contractional and extensional domains located above the edge of a subducting slab, Tectonics, 25, TC2006, doi:10.1029/2004TC001763.

Billi, A., D. Presti, B. Orecchio, C. Faccenna, and G. Neri, 2010, Incipient extension along the active convergent margin of Nubia in Sicily, Italy: Cefalù‐Etna seismic zone, Tectonics, 29, TC4026, doi:10.1029/2009TC002559.

Booth, D.C., and S. Crampin, 1985, Shear wave polarizations on a curved wavefront at an isotropic free surface, Geophys. J. R. Astron. Soc., 83, 61-73.

Bostock, M.G., R.D. Hyndmann, S. Rondenay, and S.M. Peacock, 2002, An inverted continental Moho and serpentinization of the forearc mantle, Nature, 417, 536-538.

Bowman, J.R., and M. Ando, 1987, Shear-wave splitting in the upper-mantle wedge above the Tonga subduction zone, Geophys. J. Roy. Astr. Soc., 88, 25–41.

Brune, J.N., 1970, Tectonic stress and the spectra of seismic shear waves from earthquakes. Bull. Seismol. Soc. Am., 60, 4997–5009.

Buttles, J., and P. Olson, 1998, A laboratory model of subduction zone anisotropy, Earth Planet. Sci. Lett., 164, 245–262.

Carminati, E., M. J. R. Wortel, W. Spakman, and R. Sabadini, 1998, The role of slab detachment processes in the opening of the western-central Mediterranean basins: some geological and geophysical evidence, Earth Planet. Sci. Lett., 160, 651-665.

Carminati, E., M. J. R. Wortel, P. Th. Meijer, and R. Saladini, 1998, The two-stage opening of the western –central Mediterranean basins: a forward modeling test to a new evolutionary model, Earth Planet. Sci. Lett., 160, 667-679.

Catalano, R., C. Doglioni, and S. Merlini, 2001, On the Mesozoic Ionian Basin, Geophys. J. Int., 144, 49-64.

Chen T., and R.W. Clayton, 2009, Seismic attenuation structure in central Mexico: Image of a focused high-attenuation zone in the mantle wedge, J. Geophys. Res., 114, B07304, doi:10.1029/2008JB005964

Chiarabba, C., L. Jovane, and R. Di Stefano, 2005, A new view of Italian seismicity using 20 years

of instrumental recordings, Tectonophysics, 395, 251–268.

Chiarabba, C., P. De Gori, and F. Speranza, 2008, The southern Tyrrhenian subduction zone. Deep geometry, magmatism and Plio-Pleistoceen evolution, Earth Planet. Sci. Lett., 268, 408-423.

Christensen, N . I., 1984, The magnitude, symmetry and origin of upper mantle anisotropy based on fabric analyses of ultramafic tectonites, Geophys. J. R. Astron. Soc.,7 6, 89-111.

Cimini, G.B., 1999, P-wave deep velocity structure of the Southern Tyrrhenian Subduction Zone from nonlinear teleseismic traveltime tomography, Geophys. Res. Lett., 26 (24), 3709–3712.

Civello, S., and L. Margheriti, 2004, Toroidal mantle flow around the Calabrian slab (Italy) from SKS splitting, Geophys. Res. Lett., 31, L10601, doi:10.1029/2004GL019607.

Cordier, P., T. Ungár, L. Zsoldos, and G. Tichy, 2004, Dislocation creep in MgSiO3 perovskite at conditions of the Earth's uppermost lower mantle, Nature, 428, 837–840.

Crampin, S, 1994, The fracture criticality of crustal rocks, Geophys. J. Int., 118, 428-438.

D'Agostino, N., and G. Selvaggi, 2004, Crustal motion along the Eurasia-Nubia plate boundary in the Calabrian Arc and Sicily and active extension in the Messina Straits from GPS measurements, J. Geophys. Res., 109, B11402, doi: 10.1029/2004JB002998.

de Voogd, B., C Truffert,, N. Chamot-Rooke, P. Huchon, S. Lallemant, and X. Le Pichon, 1992, Two-ship deep seismic soundings in the basins of the Eastern Mediterranean Sea (Pasiphae cruise), Geophys. J. Int., 109, 536–552, doi: 10.1111/j.1365-246X.1992.tb00116.x.

Dewey, J. F., M. L. Helman, E. Turco, D. H. W. Hutton, and S. D. Knott, 1989, Kinematics of the western Mediterranean, in Alpine Tectonics, edited by M. P. Coward, D. Dietrich, and R. G. Park, Geol. Soc. Spec. Publ., 45, 265–283.

Doglioni, C., F. Mongelli, and P. Pieri, 1994, The Puglia uplift (SE Italy) — an anomaly in the foreland of the Apenninic subduction due to buckling of a thick continental lithosphere, Tectonics, 13 (5), 1309–1321.

Doglioni, C., S. Merlini, and G. Cantarella, 1999, Foredeep geometries at the front of the Apennines in the Ionian sea (central Mediterranean), Earth Planet. Sci. Lett., 168, 243–254, doi:10.1016/ S0012-821X(99)00059-X.

Dobson, D.P., 2002, Simulation of subduction zone seismicity by dehydration of serpentine, Science, 298, 1407, 1409.

Eberhart-Phillips, D., and M. Reyners, 1999, Plate interface properties in the northeast Hikurangi subduction zone, New Zealand, from converted seismic waves, Geophys. Res. Lett., 26, 2565-2568.

Eberhart-Phillips, D., and M. Chadwick, 2002, Three-dimensional attenuation model of the shallow Hikurangi subduction zone in the Raukumara Peninsula, New Zealand, J. Geophys. Res., 107(B2), 2033, doi:10.1029/2000JB000046.

Eberhart-Phillips, D., M. Reyners, M. Chadwick, and G. Stuart, 2008, Three-dimensional attenuation structure of the Hikurangi aubduction zone in the central North Island, New Zealand, Geophys, J. Int., 174, 418-434.

Estey, L., and B. Douglas, 1986, Upper mantle anisotropy: A preliminary model, J. Geophys. Res., 91, 11393-1140

Giardini, D., and M. Velonà, 1991, Deep seismicity of the Tyrrhenian Sea, Terra Nova, 3, 57–64.

Faccenda, M., L. Burlini, V. G. Taras, and D. Mainprice, 2008, Fault-induced seismic anisotropy by hydration in subducting oceanic plates, Nature, 455, 23, doi:10.1038.

Faccenna, C., T. W. Becker, F. P. Lucente, L. Jolivet, and F. Rossetti, 2001, History of subduction and back-arc extension in the Central Mediterranean, Geophys. J. Int., 145, 809-820.

Faccenna, C., C. Piromallo, A. Crespo-Blanc, L. Jolivet, and F. Rossetti , 2004, Lateral slab deformation and the origin of the western mediterranean arcs, Tectonics, 23, TC1012, doi: 10.1029/2002TC001488.

Faccenna, C., L., Civetta, M. D'Antonio, F. Funicello, L. Margheriti, and C. Piromallo, 2005, Constraints on mantle circulation around the deforming Calabrian slab, Geophys. Res. Lett., 32, doi:10.1029/2004GL021874.

Faul, U. H., J. D. Fitz Gerald, and I. Jackson, 2004, Shear wave attenuation and dispersion in melt-bearing olivine polycrystals: 2. Microstructural interpretation and seismological implications, J. Geophys. Res., 109, B06202, doi:10.1029/2003JB002407.

Faul, U. H., and I. Jackson, 2005, The seismological signature of temperature and grain size variations in the upper mantle, Earth Planet. Sci. Lett., 234, 119 –134, doi:10.1016/j.epsl.2005.02.008.

Fischer, K.M., and D.A. Wiens, 1996, The depth distribution of mantle anisotropy beneath the Tonga subduction zone, Earth Planet. Sci. Lett., 142, 253–260.

Fouch, M.J., and K.M. Fischer, 1996, Mantle anisotropy beneath northwest Pacific subduction zones, J. Geophys. Res., 101 (B7), 15987–16002.

Fouch, M.J., and K.M Fischer, 1998, Shear-wave anisotropy in the Mariana subduction zones, Geophys. Res. Lett., 25, 1221–1224.

Frepoli, A., G. Selvaggi, C. Chiarabba, and A. Amato, 1996, State of stress in the Southern Tyrrhenian subduction zones from fault-plane solutions. Geophys. J. Int., 125, 879-891.

Funiciello, F., M. Moroni, C. Piromallo, C. Faccenna, A. Cenedese, and H. A. Bui, 2006, Mapping mantle flow during retreating subduction: laboratory models analyzed by feature tracking, J. Geophys. Res., 111(B03402), doi: 10.1029/2005JB003792.

Giacomuzzi, G., C. Chiarabba, and P. De Gori, 2011, Linking the Alps to Apennines subduction systems: new constraints revealed by high-resolution teleseismic tomography, Eart Plent. Sci. Lett., 301, 531-543.

Gledhill, K., and D. Gubbins, 1996, SKS splitting and the seismic anisotropy of the mantle beneath the Hikurangi Subduction Zone, New Zealand, Phys. Earth Planet. Inter., 95, 227– 236.

Goes, S., D. Giardini, S. Jenny, C. Hollenstein, H. G. Kahle, and A. Geiger, 2004, A recent tectonic reorganization in the south‐central Mediterranean, Earth Planet. Sci. Lett., 226, 335–345.

Gueguen, E., C. Doglioni, and M. Fernandez, 1998, On the post-25 Ma geodynamic evolution of the western Mediterranean, Tectonophysics, 298, 259-269.

Guillaume, B., F. Funiciello, C. Faccenna, J. Martinod, and V. Olivetti, 2010, Spreading pulses of the Tyrrhenian Sea during the narrowing of the Calabrian slab, Geology, 38, 819–822, doi:10.1130/G31038.1.

Guillot, S., K.H. Hattori, J. de Sigoyer, T. Nägler, A.-L. Auzende, 2001, Evidence of hydration of the mantle wedge and its role in the exumation of eclogites, Earth Planet. Sci. Lett., 193, 115-127.

Haberland, C., and A. Rietbrock, 2001, Attenuation tomography in the western central Andes: A detailed insight into the structure of a magmatic arc, J. Geophys. Res., 106, 11,151–11,167.

Hacker, B. R., S. M. Peacock, G. A. Abers, and S. D. Holloway, 2003, Subduction factory 2. Are intermediate-depth earthquakes in subducting slabs linked to metamorphic dehydration reactions?, J. Geophys. Res., 108,B1, 2030, doi:10.1029/2001JB001129.

Hall, C., K. M. Fischer, E. M. Parmentier, and D. K. Blackman, 2000, The influence of plate motions on three-dimensional back arc mantle flow and shear wave splitting, J. Geophys. Res., 105(B12), 28009-28033.

Hauksson, E., and P. Shearer, 2006, Attenuation models (Qp and Qs) in three-dimensions of the southern California crust: Inferred fluid saturation at seismogenic depths, J. Geophys. Res., 111, doi:10.1029/2005JB003947.

Hoernle, K., D. L. Abt, K. M. Fischer, H. Nichols, F. Hauff, G. A. Abers, P. van der Bogaard P, K. Heydolph, G. Alvarado, M. Protti, and W. Strauch, 2008, Geochemical and geophysical evidence for arc-parallel flow in the mantle wedge beneath Costa Rica and Nicaragua, Nature, 451, 1094–1098.

Hollenstein, Ch., H-G. Kahle, A. Geiger, S. Jenny, S. Goes, and D. Giardini, 2003, New GPS constraints on the Africa-Eurasia plate boundary zone in southern Italy, Geophys. Res. Lett., 30(18). doi: 10.1029/GL017554.

Holtzman, B.K, D. L. Kohlstedt, M. E. Zimmerman, F. Heidelbach, T. Hiraga, and J. Hustoft, 2003, Melt segregation and strain partitioning: implications for seismic anisotropy and mantle flow, Science, 301, 1227–1230.

Honda, S., 2009, Numerical simulations of mantle flow around slab edges, Earth Planet. Sci. Lett., 277, 112-122.

Jackson, I., M.S. Paterson, and J.D. Fitz Gerald, 1992, Seismic wave dispersion and attenuation in Aheim dunite: an experimental study, Geophys. J. Int., 108, 517–34.

Jackson, I., J. D. FitzGerald, U. H. Faul, and B. H. Tan , 2002, Grain-size-sensitive seismic wave attenuation in polycrystalline olivine, J. Geophys. Res., 107(B12), 2360, doi:10.1029/2001JB001225.

Jolivet, L., and C. Faccenna, 2000, Mediterranean extension in the Africa-Eurasia collision, Tectonics, 19, 6, 1095-1106.

Jolivet, L., R. Augier, C. Faccenna, F. Negro, G. Rimmele, P. Agard, C. Robin, F. Rossetti, and A. Crespo-Blanc, 2008, Subduction, convergence and the mode of backarc extension in the Mediterranean region, Bulletin de la Società Geologique de France, 179(6), 525-550, doi: 10.2113/gssgfbull.179.6.525.

Jung, H., and S. Karato, 2001, Water-induced fabric transitions in olivine, Science, 293, 1460–1463.

Jung, H., W. Mo, and H. W. Green, 2009, Upper mantle seismic anisotropy resulting from pressure-induced slip transition in olivine, Nature Geosci., 2, 73–77.

Kaminski, E., and N. M. Ribe, 2001, A kinematic model for recrystallization and texture development in olivine polycrystals, Earth Planet. Sci. Lett., 189, 253–267.

Kaminski, E., N. M. Ribe, and J. Y. Browaeys, 2004, D-Rex, a program for calculation of seismic anisotropy due to crystal lattice preferred orientation in the convective upper mantle, Geophys. J. Int., 158, 744–752.

Kaminski, E., 2006, Interpretation of seismic anisotropy in terms of mantle flow when melt is present, Geophys. Res. Lett., 33, L02304, doi:10.1029/2005GL024454.

Karato, S., and P. Wu, 1993, Rheology of the upper mantle: a synthesis, Science, 260, 771–778.

Karato, S., 1998, Some remarks on the origin of seismic anisotropy in the D" layer, Earth Planets Space, 50, 1019–1028.

Karato, S., 2006, Remote sensing of hydrogen in Earth's mantle, Rev. Mineral. Geochem., 62, 343– 375, doi:10.2138/rmg.2006.62.15.

Karato, S., H. Jung, I. Katayama, and P. Skemer, 2008, Geodynamic significance of seismic anisotropy of the upper mantle: new insights from laboratory studies, Annu. Rev. Earth Planet. Sci., 36, 59–95.

Karato, S., 2008, Deformation of Earth materials: an introduction to the rheology of the solid Earth. Cambridge University Press, Cambridge.

Karato, S., and H. A. Spetzler, 1990, Defect microdynamics in minerals and solid-state mechanisms of seismic wave attenuation and velocity dispersion in the mantle, Rev. Geophys., 28, 399– 421.

Katayama, I., H. Jung, and S. Karato, 2004, New type of olivine fabric at modest water content and low stress, Geology, 32, 1045–1048.

Kendall, J.M., and P. G. Silver, 1998, Investigating causes of D" anisotropy. In: Gurnis, M., et al.

(Ed.), The Core-Mantle Boundary Region. American Geophysical Union, pp. 97–118.

Kincaid, C., and R. W. Griffiths, 2003, Laboratory models of the thermal evolution of the mantle during rollback subduction, Nature, 425, 58-62.

Kincaid, C., and R. W. Griffiths, 2004, Variability in flow and temperature within mantle subduction zones, Geochem. Geophys. Geosyst., 5, Q06002, doi: 10.1029/2003GC000666.

Kirby, S. H., E.R. Engdahl, and R. Denlinger, 1996b, Intraslab earthquakes and arc volcanism: dual physical expressions of crustal and uppermost mantle metamorphism in Subducting Slabs, Peacock [2000] - Subduction Factory TEI Page 9 in Bebout, G.E., et al., eds., Subduction: Top to Bottom: American Geophysical Union Geophysical Monograph 96, p. 195-214, 1996b.

Klimentos, T.,1995, Attenuation of P- and S-waves as a method of distinguishing gas and condensate from oil and water, Geophysics, 60, 447–458.

Kneller, E. A., P. E. van Keken, S. Karato, and J. Park, 2005, B-type olivine fabric in the mantle wedge: insights from high-resolution non-Newtonian subduction zone models, Earth Planet. Sci. Lett., 237, 781–797.

Kneller, E. A., and P. E. van Keken, 2007, Trench-parallel flow and seismic anisotropy in the Mariana and Andean subduction systems, Nature, 450, 1222-1225, doi: 10.1038/nature06429.

Kneller, E. A., and P. E. van Keken, 2008, Effect of three-dimensional slab geometry on deformation in the mantle wedge: implications for shear wave anisotropy, Geochem. Geophys. Geosyst., 9, Q01003, doi: 10.1029/2007GC001677.

Kneller, E. A., M. D. Long, and P. E. van Keken, 2008, Olivine fabric transitions and shear-wave anisotropy in the Ryukyu subduction system, Earth Planet. Sci. Lett., 268, 268–282.

Lahr, J.C., 1989, HYPOELLIPSE/version 2.00: a computer program for determining local earthquakes hypocentral parameters, magnitude and first motion pattern, U.S. Geol. Surv Open-File Rep., 89–116, 92.

Lay, T., Q. Williams, E. J. Garnero, L. Kellogg, and M. E. Wysession, 1998, Seismic wave anisotropy in the D00 region and its implications. In: Gurnis M et al (eds) The core-mantle boundary region. American Geophysical Union, Washington, DC, pp 299–318.

Lees, J. M., and G. T. Lindley, 1994, Three-dimensional attenuation tomography at Loma-Prieta: Inversion of t* for Q, J. Geophys. Res., 99, 6843– 6863.

Levin, V., D. Okaya, and J. Park, 2007, Shear wave birefringence in wedge-shaped anisotropic regions, Geophys. J. Int., 168, 275-286.

Levin, V., D. Okaya, and J. Park, 2006, Shear wave birefringence in wedge-shaped anisotropic regions, Geophys. J. Int., 168, 275–286.

Lickorish, W.H., M. Grasso, R. W. H. Butler, A. Argnani, R. Maniscalco, 1999, Structural styles and regional tectonic setting of the "Gela Nappe" and frontal part of the Maghrebian thrust belt in Sicily, Tectonics, 18, 655–668.

Liu, E., and S. Crampin, 1990, Effect of the internal shear wave window: comparison with anisotropy induced splitting, J. Geophys. Res., 95, 11275-11281.

Liu, K.H., S. S. Gao, Y. Gao, and J. Wu, 2008, Shear wave splitting and mantle flow asoociated with the deflected Pacific slab beneath northeast Asia, J. Geophys. Res., 113(B01305), doi: 10.1029/2007JB005178.

Long, M.D., and R.D. van der Hilst, 2005, Upper mantle anisotropy beneath Japan from shear wave splitting, Physics Earth Planet. Inter, 151, 206–222.

Long, M. D., and R. D.van der Hilst, 2006, Shear wave splitting from local events beneath the Ryukyu arc: trench-parallel anisotropy in the mantle wedge, Physics Earth Planet. Inter., 155, 300-312.

Long, M. D., B. H. Hager, M. V. de Hoop, and R. D. van der Hilst, 2007b, Two-dimensional modeling of subduction zone anisotropy and application to southwestern Japan, Geophys. J. Int., 170, 839–856.

Long, M. D., and P. G. Silver, 2009, Mantle flow in subduction systems: The subslab flow field and implications for mantle dynamics, J. Geophys. Res., 114(B10312), doi:10.1029/2008JB006200.

Long, M. D., 2009, Geophysics: Going with the mantle flow, Nature Geoscience, 2(1),10-11, http://dx.doi.org/10.1038/ngeo398.

Long, M. D., and T. Becker, 2010, Mantle dynamics and seismic anisotropy, Earth Planet. Sci. Lett., 297, 341-354.

Lowman, J. P., L. T. Pinero-Feliciangeli, J.-M. Kendall, and M. H. Shahnas, M.H., 2007, Influence of convergent plate boundaries on upper mantle flow and implications for seismic anisotropy, Geochem. Geophys. Geosyst., 8, Q08007, doi: 10.1029/2007GC001627.

Lucente, F.P., C. Chiarabba, G.B. Cimini, and D. Giardini, 1999, Tomographic constraints on the geodynamic evolution of the Italian region, J. Geophys. Res., 104 (B9), 20,307–20,327.

Lucente, F. P., L. Margheriti, C. Piromallo, and G. Barruol (2006), Seismic anisotropy reveals the long route of the slab through the western-central Mediterranean mantle, Earth Planet. Sci. Lett., 241, 517-529.

Lucente, F. P., and L. Margheriti, 2008, Subduction Roll-back, Slab Break-off and Induced Strain in the Uppermost Mantle beneath Italy, Geology, 36(5), 375-378, doi: 10.1130/G24529A.1.

Mainprice, D., and A. Nicolas, 1989, Development of shape and lattice preferred orientations: application to the seismic anisotropy of the lower crust, J. Struct. Geol. 11, 175–189.

Mainprice, D., G. Barruol, and W. Ben Ismail, 2000, The seismic anisotropy of the Earth's mantle: From single crystal to polycrystal. In: Karato, S.I. (Ed.), Earth's Deep Interior: Mineral Physics and Tomography From the Atomic to the Global Scale. Geodyn. Ser. AGU, Washington, D.C., pp. 237–264.

Mainprice, D., A. Tommasi, H. Couvy, P. Cordier, and D.J. Frost, 2005, Pressure sensitivity of olivine slip systems: implications for the interpretation of seismic anisotropy of the Earth's upper mantle, Nature, 433, 731–733.

Mainprice, D., 2007, Seismic anisotropy of the deep Earth from a mineral and rock physics perspective. In: Schubert, G. (Ed), Treatise on Geophysics v. 2, 437-492.

Mainprice, D., A. Tommasi, P. Cordier, P. Carrez, and D. Ferre, 2008, Predicted glide systems and crystal preferred orientation of polycrystalline silicate Mg-perovskite at mantle pressures: implications for the seismic anisotropy of the lower mantle, Earth Planet Sci. Lett., 271, 135–144.

Malinverno, A., and W. Ryan, 1986, Extension in the Tyrrhenian Sea and shortening in the Apennines as result of arc migration driven by sinking of the lithosphere, Tectonics, 5(2), 227–245, doi:10.1029/TC005i002p00227.

Margheriti, L., F. P. Lucente, and S. Pondrelli, 2003, SKS splitting measurements in the Apenninic-Tyrrhenian domain (Italy) and their relation with lithospheric subduction and mantle convention, J. Geophys. Res., 108(B4), doi: 10.1029/2002JB001793.

Marson-Pidgeon, K., and M. K. Savage, 1997, Frequency-dependent anisotropy in Wellington, New-Zealand, Geophys. Res. Lett., 24,24, 3297-3300.

Matcham, I., M. K. Savage, and K.R. Gledhill, 2000, Distribution of seismic anisotropy in the subduction zone beneath the Wellington region, New Zealand, Geophys. J. Int., 140, 1–10.

Mattei, M., V. Petrocelli, D. Lacava, and M. Schiattarella, 2004, Geodynamic implications of Pleistocene ultrarapid vertical axis rotations in the Southern Apennines, Italy, Geology, 32, 789 792, doi:10.1130/G20552.1.

Maupin, V., and J. Park, 2007, Theory and observations—wave propagation in anisotropic media. In: Schubert G. (ed) Treatise on geophysics vol 1. Elsevier, Amsterdam, pp 289–321.

Mavko, G. M., 1980, Velocity and attenuation in partially molten rocks, J. Geophys. Res., 85, 5173– 5189.

Menardi Noguera, A., and G. Rea, 2000, Deep structure of the Campanian–Lucanian Arc (Southern Apennine, Italy), Tectonophysics, 324, 239–265.

Mizutani, H., and H. Kanamori, 1988, Variation of elastic wave velocity and attenuation property near the melting temperature, J. Phys. Earth, 12, 43–49.

Monna, S., and T. Dahm, 2009, Three-dimensional P wave attenuation and velocità upper mantle tomography of the southern Apennines-Calabrian Arc subduction zone, J. Geophys. Res., 114(B06304), doi:10.1029/2008JB005677.

Montuori, C., G. B. Cimini, and P. Favali,, 2007, Teleseismic tomography of the southern Tyrrhenian subduction zone: new results from seafloor and land recordings, J. Geophys. Res. 112(B03311), doi:10.1029/2005JB004114.

Nakajima, J., and A. Hasegawa, 2004, Shear-wave polarization anisotropy and subduction-induced flow in the mantle wedge of northern Japan, Earth Planet. Sci. Lett., 225, 365–377.

Neri, G., B. Orecchio, C. Totaro, G. Falcone, and D. Presti, 2009, Subduction beneath southern Italy is close to ending: Results from seismic tomography, Seismol. Res. Lett., 80, 63–70.

Nicolas, A., and N. I. Christensen, 1987, Formation of anisotropy in upper mantle peridotites - a review. In: Fuchs K., and C. Froideveaux (eds) Composition, structure and dynamics of the lithosphere-asthenosphere system, American Geophysical Union, Washington, DC, pp 111–123.

Nicolosi, I., Speranza, F., Chiappini, M., 2006, Ultrafast oceanic spreading of the Marsili Basin, southern Tyrrhenian Sea: Evidence from magnetic anomaly analysis, Geology, 34(9), 717-720.

Nuttli, O.W., 1961, The effect of the Earth's surface on the S wave particle motion, Bull. Seism. Soc. Am., 51, 237-271.

O'Connell, R. J., and B. Budiansky, 1977, Viscoelastic properties of fluidsaturated cracked solids, J. Geophys. Res., 82, 5719–5735.

Panza, G.F.,A. Peccerillo, A. Aoudia, and B. Farina, 2007, Geophysical and petrological modeling of the structure and composition of the crust and upper mantle in complex geodynamic settings: the Tyrrhenian Sea and surroundings, Earth-Sci. Rev., 80 (1–2), 1–46.

Patacca, E., and P. Scandone, 1989, Post-Tortonian mountain building in the Apennines. The role of the passive sinking of a relic lithospheric slab, in: Boriani, A., et al. (Ed.), The Lithosphere in Italy. Atti Conv. Lincei, vol. 80, pp. 157–176.

Patacca, E., R. Sartori, and P. Scandone, 1990, Tyrrhenian basin and Apenninic arcs. Kinematic relations since late Tortonian times, Mem. Soc. Geol. It., 45, 425–451.

Patacca, E., P. Scandone, and M. Tozzi, 2000, Il profilo CROP04, Protecta, 10–12, 49–52.

Patacca, E., and P. Scandone, 2001, Late thrust propagation and sedimentary response in the thrust-belt-foredeep system of the Southern Apennines (Pliocene-Pleistocene), in Anatomy of an Orogen: the Apennines and the adjacent Mediterranean Basins, edited by G. B. Vai and I. P. Martini, pp. 401-440, Kluwer Academic Publishers, Dordrecht, The Netherlands.

Peacock, S. M., 1996, Thermal and petrologic structure of subduction zones, in Bebout, G.E., et al., eds., Subduction: Top to Bottom: American Geophysical Union Geophysical Monograph 96, p. 119-133, 1996.

Peacock, S.M., 2000, Thermal structure and metamorphic evolution of subduction slabs, in MARGINS Theoretical and Experimental Insitute: Inside the Subduction factory, by M. Hirschmann, T. Plank, and Brian Taylor.

Peacock, S.M., 2001, Are the lower planes of double seismic zones caused by serpentine dehydration in subducting oceanic mantle? Geology, 29,4, 299-302

Pearce, J., and D. Mittleman, 2002, Defining the Fresnel zone for broadband radiation, Phys. Rev., E 66 (5), 056602.

Peyton, V., V. Levin, J. Park, M.T. Brandon, J. Lees, E. Gordeev, and A. Ozerov, 2001, Mantle flow at a slab edge: seismic anisotropy in the Kamchatka region, Geophys. Res. Lett., 28, 379–382.

Piana Agostinetti, N., and A. Amato, 2009, Moho depth and Vp/Vs ratio in peninsular Italy from teleseismic receiver functions, J. Geophys. Res., 114(B06303), doi:10.1029/2008JB005899.

Piana Agostinetti, N., M.S. Steckler, and F.P. Lucente, 2009, Imaging the subducted slab under the Calabrian Arc, Itlay, from receiver function analysis, Lithosphere, 1,3, 131-138.

Piromallo, C., and A. Morelli, 2003, P-wave tomography of the mantle under the Alpine-Mediterranean area, J. Geophys. Res., 108(B2), doi: 10.1029/2002JB001757.

Piromallo, C., T. W. Becker, F. Funiciello, and C. Faccenna, 2006, Three-dimensional instantaneous mantle flow induced by subduction, Geophys. Res. Lett., 33, L08304, doi: 10.1029/2005GL025390.

Plomerová, J., R. Arvidsson, V. Babuška, M. Granet, O. Kulhánek, G. Poupinet, and J. Šílený, 2001, An array study of lithospheric structure across the Protogine Zone, Varmland, south-central Sweden; signs of a paleocontinental collision, Tectonophysics 332, 1–21.

Plomerová, J., L. Margheriti, J. Park, V. Babuška, S. Pondrelli, L. Vecsey, D. Piccinini, V. Levin, P. Baccheschi, and S. Salimbeni, 2006, Seismic anisotropy beneath the Northern Apennines (Italy): mantle flow or lithosphere fabric?, Earth Planet. Sci. Lett., 247, 157–170.

Polet, J., P.G Silver, S. Beck, T. Wallace, G. Zandt, R. Ruppero, R. Kind, and A. Rudloff, A, 2000,

Shear wave anisotropy beneath the Andes from the BANJO, SEDA and PISCO experiments, J. Geophys. Res., 105, 6287–6304.

Poli, S., and M. W. Schmidt, 1995, H2O transport and release in subduction zones: Experimental constraints on basaltic and andesitic systems, J. Geophys. Res., 100, 22299-22314.

Pondrelli, S., C. Piromallo, and E. Serpelloni, 2004, Convergence vs. retreat in Southern Tyrrhenian
Sea: insights from kinematics, Geophys. Res. Lett., 31, L06611, doi:10.1029/2003GL019223.

Pozgay, S.H., D.A. Wiens, J.A. Conder, H. Shiobara, and H. Sugioka, 2007, Complex mantle flow in the Mariana subduction system: evidence from shear wave splitting, Geophys. J. Int., 170, 371–386.

Pozgay, S., D.A. Wiens, J.A. Conder, H. Shiobara, H. Sugioka, 2009, Seismic attenuation tomography of the Mariana subduction system: Implications for thermal structure, volatile distributions, and low spreading dynamics, Geochem Geophys Geosys., 10,4, doi:10.1029/2008GC002313.

Reyners, M., D. Eberhart-Phillips, G. Stuart, and Y. Nishimura, 2006, Imaging subduction from the trench to 300 km depth beneath the central North Island, New Zealand, with *Vp* and *Vp/Vs,* Geophys. J. Int., 165, 565–583.

Ribe, N. M., and Y. Yu, 1991, A theory for plastic deformation and textural evolution of olivine polycrystals, J. Geophys. Res., 86, 8325-8335.

Rychert, C. A., K. M. Fischer, D. G. A. Abers, T. Plank, E. Syracuse, J. M. Protti, V. Gonzalez, and W. Strauch. 2008, Strong along-arc variations in attenuation in the mantle wedge beneath Costa Rica and Nicaragua, Geochem. Geophys. Geosyst., 9, Q10S10, doi:10.1029/2008GC002040.

Rietbrock, A., 2001, P wave attenuation structure in the fault area of the 1995 Kobe earthquake, J. Geophys. Res., 106, 4141– 4154.

Rosenbaum, G, 2002), Reconstruction of the tectonic evolution of the western Mediterranean since the Oligocene, J. Virtual Explorer, 8, 107– 130.

Rosenbaum, G., and G. S. Lister, 2004, Neogene and Quaternary rollback evolution of the Tyrrhenian Sea, the Apennines and the Sicilian Maghrebides, Tectonics, 23, TC1013, doi: 10.1029/2003TC001518.

Rosenbaum, G., M. Gasparon, F. P. Lucente, A. Peccerillo, and M. S. Miller, 2008, Kinematics of slab tear faults during subduction segmentation and implications for Italian magmatism, Tectonics, 27, TC2008, doi:10.1029/2007TC002143.

Rossetti, F., B. Goffè, P. Monié, C. Faccenna, and G. Vignaioli, 2004, Alpine orogenic P–T–t deformation history of the Catena Costera area and surrounding regions (Calabrian Arc, Southern Italy): the nappe edifice of north Calabria revised with insights on the Tyrrhenian– Apennine system formation, Tectonics, 23, TC6011, doi:10.1029/2003TC001560.

Roth, E. G., D. A. Wiens, L. M. Dorman, J. Hildebrand, and S. C. Webb, 1999, Seismic attenuation tomography of the Tonga-Fiji region using phase pair methods, J. Geophys. Res., 104(B3), 4795–4809.

Rumpker, G., A. Tommasi, and J-M. Kendal, 1999, Numerical simulations of depth dependent anisotropy and frequency-dependent wave propagation effects, J. Geophys. Res., 104 (B10), 23141–23154.

Rüpke, L. H., J. P. Morgan, M. Hort, and J. A. D. Connolly, 2004, Serpentine and the subduction zone water cycle, Earth Planet. Sci. Lett., 223, 17–34, doi:10.1016/j.epsl.2004.04.018.

Russo, R.M., and P.G. Silver, 1994, Trench-parallel flow beneath the Nazca plate from seismic anisotropy, Science, 263, 1105–1111.

Salmon, M., S. Bannister, H. Bibby, M. K. Savage, and T. A. Stern, 2003, Attenuation and electrical resistivity in an asymmetric back arc extensional environment, Eos Trans. AGU, 84(46), Fall. Meet. Suppl., Abstract S22B-0450.

Sarker, G., and G. A. Abers, 1998a, Comparison of seismic body wave and coda wave measures of Q, Pure Appl. Geophys., 153, 665– 683.

Savage, M.K., 1999, Seismic anisotropy and mantle deformation: what have we learned from shear wave splitting? Rev. Geophys., 37, 65–106.

Schellart, W.P., 2004, Kinematics of subduction and subduction-induced flow in the upper mantle. J. Geophys. Res., 109, B07401, doi: 10.1029/2004JB002970.

Schellart, W. P., J. Freeman, D. R. Stegman, L. Moresi, and D. May, 2007, Evolution and diversity of subduction zones controlled by slab width, Nature, 446, 308-311, doi: 10.1038/nature05615.

Schellart, W. P., D. R. Stegman, and J. Freeman, 2008, Global trench migration velocities and slab migration induced upper mantle volume fluxes: Constrains to find an Earth reference frame based on minimizing viscous dissipation, Earth Sci. Rev., 118-144, doi: 10.1016/j.earscirev.2008.01.005.

Scherbaum, F., 1990, Combined inversion for the three-dimensional Q structure and source parameters using microearthquake spectra, J. Geophys. Res., 95, 12423–12438.

Shelly, D. R., G. C. Beroza, H. Zhang, C. H. Thurber, and S. Ide, 2006, High-resolution subduction zone seismicity and velocity structure beneath Ibaraki Prefecture, Japan, J. Geophys. Res., 111, B06311, doi:10.1029/2005JB004081.

Shito, A., S. Karato, K. N. Matsukage, and Y. Nishibara, 2006, Towards mapping the three-dimensional distribution of water in the upper mantle from velocity and attenuation tomography, in Earth's Deep Water Cycle, Geophys. Monogr. Ser., vol. 168, edited by S. D. Jacobsen and S. vanderLee, pp. 225–236, AGU, Washington, D. C.

Schurr, B., G. Asch, A.Rietbrock, R. Trumbull, and C. Haberland, 2003, Complex patterns of fluid and melt transport in the central Andean subduction zone revealed by attenuation tomography, Earth Planet. Sci. Lett., 215, 105–119, doi:10.1016/S0012-821X(03)00441-2.

Selvaggi, G., and C. Chiarabba, 1995, Seismicity and P wave velocity image of the Southern Tyrrhenian subduction zone, Geophys. J. Int., 121, 818–826.

Selvaggi, G., 2001, Strain pattern of the Southern Tyrrhenian slab from moment tensors of deep earthquakes: implications on the down-dip velocità, Ann. Geofis, 44, 155-165.

Silver, P.G., 1996, Seismic anisotropy beneath the continents: probing the depths of geology, Annu. Rev. Earth Planet. Sci., 24, 385–432.

Silver, P.G., and W.W: Chan, 1991, Shear-wave splitting and sub-continental mantle deformation, J. Geophys. Res., 96, 16429-16454.

Salimbeni, S., S. Pondrelli, L. Margheriti, J. Park, J., and V. Levin, 2008, SKS splitting measurements beneath Northern Apennines region: a case of oblique trench retreat, Tectonophysics, 462, 68–82.

Savage, M.K., 1999, Seismic anisotropy and mantle deformation: what have we learned from shear wave splitting? Reviews of Geophysics, 37(1), 65-106.

Shito, A., S. Karato, and J. Park, 2004, Frequency dependence of Q in Earth's upper mantle inferred from continuous spectra of body waves, Geophys. Res. Lett., 31, L12603, doi:10.1029/2004GL019582.

Schmid, C., S. Van Der Lee, and D. Giardini, 2004, Delay times and shear wave splitting in the Mediterranean region, Geophys. J. Int., 159, 275–290.

Schlotterbeck, B. A., and G. A. Abers, 2001, Three-dimensional attenuation variations in southern California, J. Geophys. Res., 106, 30719–30735.

Silver, P.G., and W.W. Chan, 1991, Shear wave splitting and subcontinental mantle deformation, J. Geophys. Res., 96 (B10), 16429–16454.

Silver, P.G., and M.K. Savage, 1994, The interpretation of shear-wave splitting parameters in the presence of two anisotropic layers, Geophys. J. Int., 119, 949–963.

Silver, P. G., and W. E. Holt, 2002, The mantle flow field beneath western North America, Science, 295, 5557: 1054-1058.

Smith, G.P., D.A. Wiens, K.M. Fischer, L.M. Dorman, S.C. Webb, and J.A. Hildebrand, 2001, A complex pattern of mantle flow in the Lau Backarc, Science, 292, 713–716.

Spakman, W., S. van der Lee, and R. van der Hilst, 1993, Travel-time tomography of the European- Mediterranean mantle down to 1400 km, Phys. Earth Planet. Inter., 79, 3-74.

Stachnik, J. C., G. A. Abers, and D. H. Christensen, 2004, Seismic attenuation and mantle wedge temperatures in the Alaska subduction zone, J. Geophys. Res., 109, B10304, doi:10.1029/2004JB003018.

Stampfli, G., and G. Borel, 2002, A plate tectonic model for the Paleozoic and Mesozoic constrained by dynamic plate boundaries and restored synthetic oceanic isochrons, Earth Planet. Sci. Lett., 196, 17–33.

Stegman, D. R., J. Freeman, W. P. Schellart, L. N. Moresi, and D. A. May, 2006, Influence of trench width on subduction hinge retreat in 3-D models of slab rollback, Geochem. Geophys. Geosyst., 7, Q03012, doi: 10.1029/2005GC001056.

Takanami, T., S. Sacks, and A. Hasegawa, 2000, Attenuation structure beneath the volcanic front in northeastern Japan from broad-band seismograms, Phys. Earth Planet. Inter., 121, 339–357.

Thurber, C. H., 1993, Local earthquake tomography: velocity and Vp/Vs theory, in Seismic Tomography: Theory and Practice, edited by H. Iyer and K. Hirahara, pp. 563– 580, CRC Press, Boca Raton, Fla.

Tommasi, A., D. Mainprice, G. Canova, and Y. Chastel, 2000, Viscoplastic self-consistent and equilibrium-based modeling of olivine lattice preferred orientations: implications for the upper mantle seismic anisotropy, J. Geophys. Res., 105, 7893–7908.

Trampert, J., and HJ van Heijst, 2002, Global azimuthal anisotropy in the transition zone. Science, 296, 1297–1299.

Tsumura, N., S. Matsumoto, S. Horiuchi, and A. Hasegawa, 2000, Three-dimensional attenuation structure beneath the northeastern Japan arc estimated from spectra of small earthquakes, Tectonophysics, 319, 241–260, doi:10.1016/S0040-1951(99)00297-8.

Yamazaki, D., and S. Karato, 2007, Lattice-preferred orientation of lower mantle materials and seismic anisotropy in the D" layer. In: Hirose K et al (eds) Post-perovskite: the last mantle phase transition. American Geophysical Union, Washington, DC, pp 69–78.

Zhang, A., and S. Karato, 1995, Lattice preferred orientation of olivine aggregates deformed in simple shear, Nature, 375, 774-777.

Vinnik, L.P., and R. Kind, 1993, Ellipticity of teleseismic S-particle motion. Geophys., J. Int., 113, 165–174.

Warren, L., and P. Shearer, 2000, Investigating the frequency dependence of mantle Q by stacking P and PP spectra, J. Geophys. Res., 105, 25,391– 25,402.

Winkler, K., and A. Nur, 1979, Pore fluids and seismic attenuation in rocks, Geophys. Res. Lett., 6, 1–4.

Winkler, K.W., and W.F. Murphy, 1995, Acoustic velocity and attenuation in porous rocks, in Rock Physics and Phase Relations: A Handbook pf Physical Constants, pp 20-34, ed. T.J. Ahrens, AGU, Washington, DC.

Wittlinger,G ., H. Haessler, and M . Granet, 1983, Three dimensional inversion of Qp, from low magnitude earthquakes analysis, Ann. Geophys., 6 , 427-438, 1983.

Wortel, M. J. R., and W. Spakman, 2000, Subduction and slab detachment in the Mediterranean Carpathian region, Science, 290, 1910-1917.